Evaluation of regional climate models for simulating sub-daily rainfall extremes

by

Virginia Edith Cortés Hernández

Thesis submitted to The University of Adelaide,
Faculty of Engineering, Computer & Mathematical Sciences,
School of Civil, Environmental & Mining Engineering
in fulfilment of the requirements for the degree of

Master of Philosophy

March, 2016

Table of Contents

List of Figures

List of Tables

Glossary

2-CC or super-CC	twice the Clausius-Clapeyron rate
4AR	the Fourth Assessment Report from the IPCC
AEP	annual exceedance probability
ARF	areal reduction factor
BMJ	the Betts-Miller-Janjić scheme
CAPE	the convective availability potential energy
C-C	the Clausius-Clapeyron rate
CFSR	Climate Forecast System Reanalysis
CMIP5	Coupled Model Intercomparison Project Phase 5
DC	the diurnal cycle
ESRL	Earth System Research Laboratory
ETCCDI	the Expert Team on Climate Change Detection and Indices
GCM(s)	General circulation model(s)
GEV	the Generalized Extreme Value distribution
GHGs	greenhouse gases
IPCC	Intergovernmental Panel on Climate Change
KF	the Kain-Fritsch scheme
MIROC 3.2	Model for Interdisciplinary Research on Climate version 3.2
MMM	Mesoscale and Microscale Meteorology Division
MSLP	mean sea level pressure
MTSR	mean of the temperature scaling rate
MYJ	the Mellor-Yamada-Janjić scheme
NARCCAP	North American Regional Climate Change Assessment Program
NARCliM	NSW/ACT Regional Climate Modelling
NCAR	National Center for Atmospheric Research
NCEP	National Centers for Environmental Prediction
NNRP	NCEP–NCAR reanalysis project
NOAA	the National Oceanic and Atmospheric Administration's
NWP	numerical weather prediction
OBS	the observations
PBL	the planetary boundary layer
PMF	probable maximum flood
PMP	probable maximum precipitation
Q-Q	the quantile-quantile plots
RCM(s)	Regional climate model(s)
RRTM	Rapid Radiative Transfer Model
SC	Seasonal cycle
WDM5	WRF Double Moment 5-class
WRF	Weather Research and Forecasting
YU	the Yonsei University scheme

Abstract

Over the last decade, observational and modelling studies have both indicated that the intensity and frequency of rainfall extremes have increased. This increase has been linked to the human emissions of greenhouse gases that cause the climate to warm. There is increasing evidence that the largest changes in rainfall extremes are likely to occur for short duration events (less than a day), enhancing the potential for flash flooding over urban catchments and fast responding rural catchments. The economic, social and environmental effects of flash flooding are often catastrophic, resulting in substantial damage to properties and fatalities due to its sudden onset with little or no warning.

The understanding of changes in sub-daily rainfall extremes is of paramount importance to help society in planning decisions about future flood risk resulting from climate change. Short duration rainfall is important for urban catchments where there is substantial investment in infrastructure. For instance, the design of urban water infrastructure for protection from stormwater requires information on rainfall extremes at short temporal (minutes to hours) and spatial (hundreds to thousands of meters) scales.

Although observational studies are valuable for exploring historical changes to extreme rainfall patterns, future projections are usually obtained through the use of climate models to explore how rainfall patterns will respond to future greenhouse gases concentrations. General circulation models (GCMs) are sometimes used for estimating the effect of climate change on the intensity and frequency of rainfall extremes under different greenhouse gases emission scenarios. However, their coarse resolution fails to capture regional features of rainfall extremes such as the size of convective storms (1-10 km^2) that are usually smaller than the spatial resolution of GCMs. By contrast, nested regional climate models (RCMs) are able to simulate the interactions between large-scale circulation systems and local scale weather patterns and topography. RCMs have proven to adequately simulate the statistical properties of rainfall extremes at daily and longer durations; while for sub-daily durations, model simulations are often improved by applying bias correction methods to match the observations. However, the evaluation of RCMs based on extreme rainfall statistics do not provide insight into whether the model gets the right answers (statistics of rainfall extremes) for the right reasons (correct representation of the underlying physical mechanism leading to rainfall extremes) and whether it is recommended to use the model simulations after applying any bias correction approach.

The purpose of the research reported in this thesis was to explore the use of physically meaningful metrics to evaluate the capacity of regional climate models to simulate sub-daily rainfall extremes. The research metrics will complement the standard suite of statistical metrics that are commonly used for model evaluation studies. The physically meaningful metrics focus on the skill of RCMs in reproducing (i) the diurnal cycle of rainfall extremes, (ii) the seasonal

cycle of extreme rainfall events and (iii) the observed relationship between sub-daily rainfall extremes with respect to the atmospheric temperature.

The research began with the evaluation of the capacity of three versions of the Weather Research and Forecasting (WRF) regional climate model to reproduce observed sub-daily rainfall extremes. First, the statistics of sub-daily rainfall extremes were estimated and compared with observations at 69 locations across the Greater Sydney region. The main results indicate underestimations in the intensity of rainfall extremes for 1-hour duration and overestimations in the intensity for longer durations (e.g. 3-hour, 6-hour and 12-hour), overestimations in the trend of the annual maxima of rainfall for sub-daily durations and overestimations in the annual maxima over high elevation areas and underestimations over coastal parts.

Despite these apparent biases, the ability of the three RCMs to reproduce the underlying physical processes of sub-daily rainfall extremes was reasonable. The diurnal cycle of hourly rainfall extremes was realistically captured by the RCMs with a late evening peak in agreement with the observations. The seasonality was also captured and better simulated for short durations (1-hour and 3-hour) and during summer months. The intensification of sub-daily rainfall extremes with temperature was well captured by the RCMs, particularly at hourly durations when rainfall extremes approximately followed the Clausius-Clapeyron scaling rate.

The overall capacity of the three RCMs provided the confidence to investigate likely changes in sub-daily rainfall extremes over Greater Sydney, considering two future periods in simulation (2020-2039 and 2060-2079) under the A2 emissions scenario of climate change. Future changes in sub-daily rainfall extremes were explored in (i) the intensity of sub-daily rainfall extremes, (ii) the diurnal cycle of rainfall extremes, (iii) the seasonality of sub-daily rainfall extremes, and (iv) the intensification of sub-daily rainfall extremes with temperature. The results from the two future periods were compared with the historical simulation period (1990-2009). The main findings indicated an overall increase in the intensity of rainfall extremes over inland areas for long durations (e.g. 6-hour and 12-hour), especially found in the long-term future period in the simulations.

No significant changes were found for future projections of the diurnal cycle of rainfall extremes, which was fairly consistent with the historical period. Surprisingly, the greatest changes were found in the seasonality of sub-daily rainfall extremes with an increase in the occurrence of sub-daily rainfall extremes during summer accompanied by a decrease during winter over the region. Future projections also indicated an intensification of rainfall extremes with temperature that followed a scaling rate close to the C-C rate for all sub-daily durations. In contrast, an analysis into the temperature scaling relationship revealed that the historical scaling relationship in simulations was not valid for future projections, with significant changes in the scaling rate. This has significant implications for the use of the Clausius-Clapeyron (C-C) scaling relationships for developing future climate projections, which are explored in the final part of this thesis.

Statement of Originality

I, Virginia Edith Cortes Hernandez, hereby declare that this work contains no material which has been accepted for the award of any other degree or diploma in any university or other tertiary institution and, to the best of my knowledge and belief, contains no material previously published or written by another person, except where due reference has been made in the text. In addition, I certify that no part of this work will, in the future, be used in a submission for any other degree or diploma in any university or other tertiary institution without the prior approval of the University of Adelaide and where applicable, any partner institution responsible for the joint-award of this degree.

I give consent to this copy of my thesis when deposited in the University Library, being made available for loan and photocopying, subject to the provisions of the Copyright Act 1968.

I also give permission for the digital version of my thesis to be made available on the web, via the University's digital research repository, the Library catalogue and also through web search engines, unless permission has been granted by the University to restrict access for a period of time.

Signature Date

Acknowledgements

I take this opportunity to gratefully acknowledge my principal supervisor Dr Seth Westra and co-supervisor Prof Martin Lambert for the opportunity to undertake my postgraduate study and for their effort in helping me to achieve my goal.

I would like to acknowledge the research scholarship provided by my supervisor through the Australian government.

I would like to also acknowledge to Feifei Zheng and Bree Bennett for their technical knowledge and constant help to improve my programming skills and statistical analysis during my studies.

I would also like to acknowledge Barbara Brougham for helping me to improve the writing and editing of my thesis.

I would like to thank to my husband Michael, his lovely family and my family and friends in Mexico for their unconditional love and support. I would also like to thank to my friends and colleagues in Adelaide for their support and motivation to complete my studies.

Finally and most importantly, I would like to thank to God for the gift of faith and love that accompanied me through this journey.

El Señor es mi pastor, nada me faltará.

Él me hace descansar en verdes praderas,

me conduce por aguas tranquilas y repara mis fuerzas;

me guía por el recto sendero, por amor a su nombre.

Aunque cruce por quebradas oscuras, no temeré ningún mal,

porque Él está conmigo y su vara y bastón me protegen.

Salmos 23

Chapter 1. Introduction

The increase of sub-daily rainfall extremes is of paramount importance in the assessment and management of future flood risk resulting from climate change. Evidence from observations (Mishra and Lettenmaier, 2011; Mishra et al., 2012b; Mishra et al., 2014; Sun et al., 2006; Westra et al., 2013) and climate models projections (Kharin et al., 2013; Sillmann et al., 2013) suggest an increase in the intensity of rainfall extremes as a result of increasing greenhouse gases (GHGs) emissions and the atmosphere temperature rising. This is because sub-daily rainfall extremes are expected to increase following the Clausius Clapeyron relationship (O'Gorman and Schneider, 2009; Trenberth, 2011), which implies that a warmer atmosphere can hold more moisture (if moisture is available), resulting in more extreme rainfall events.

An increased frequency and intensity of sub-daily rainfall extremes are the main cause of flash flooding (Alfieri and Thielen, 2015) over urban areas and rapid-responding rural catchments. The impact of flash floods is expected to increase with future rising sea levels and population growth and consequently increasing the future risk of failure of infrastructure. One example is in flood defence in urban areas. Moreover, the design of drainage systems in urban areas is controlled by the small response time of catchments to sub-daily rainfall extremes (Mishra et al., 2012a).

The changing nature of rainfall extremes along with limitations in the availability and quality of observational data, mean that an increasing number of important decisions for planning and designing for flood risk need to rely on climate models (Westra et al., 2014b). *General circulation models* (GCMs) are considered to be the primary source of information for likely changes in future climate variables, such as temperature, pressure and rainfall. However, their coarse spatial resolution with grid cells of hundreds of kilometres has always meant that rainfall projections from these models have been seen as unreliable for reproducing rainfall extremes (Christensen and Christensen, 2003).

Two approaches have therefore been developed to close the gap between the resolution of GCMs and the resolution needed for regional and local scale processes associated with rainfall extremes. Firstly, there is dynamical downscaling, which is able to simulate local conditions in greater detail by using output from the GCM to drive a nested regional numerical model to a higher spatial resolution. And, secondly, there is statistical downscaling, where a statistical relationship is

established between large scale variables, then subsequently used on the GCM data to obtain the relationship between local variables. For the purposes of the research described in this thesis, only dynamical downscaling was used.

Regional climate models (RCMs) produce a better representation of finer scales and are able to simulate the interactions between large-scale weather patterns and the local topography that are required to improve the intensity of rainfall at short durations (Gutowski et al., 2003).

Figure 1.1 illustrates the benefits of using a RCM to produce a higher spatial resolution of a localised area. The figure displays the result of using a 10-km horizontal resolution RCM to simulate the annual precipitation along southeast Australia during a defined period (Evans, 2012). Topographic and land-coast effects over the east coast are clearly seen in the RCM resolution (right panel) but not in the GCM (left panel).

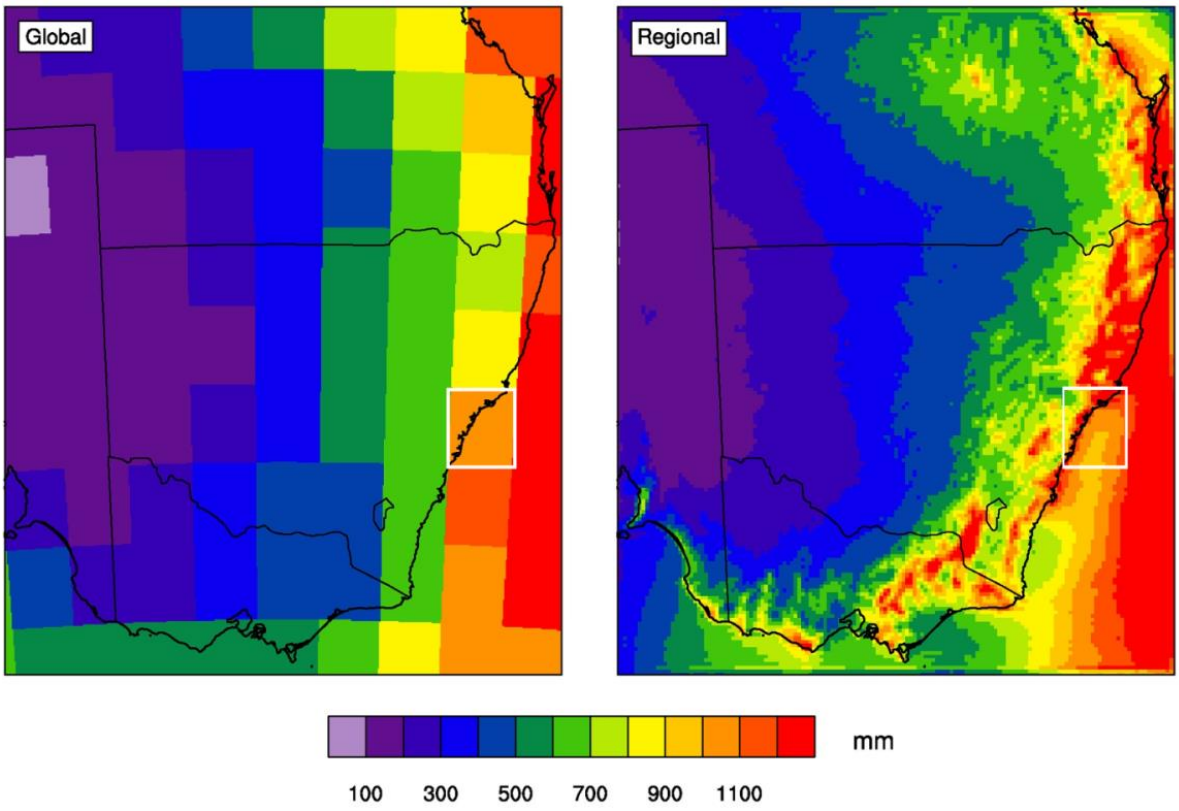

Figure 1.1 **Illustration of the differences in resolution of simulations between a GCM (left panel) and a RCM (right panel) over southeast Australia modified from Evans et al. (2012). The improved resolution in the RCM is able to simulate costal and topographic effects near to Sydney (white box) which are not captured by the coarse resolution of the GCM.**

RCMs have proved capable of simulating the observational features of rainfall extremes at daily durations (Chan et al., 2014; Durman et al., 2001; Fowler and Ekström, 2009; Frei et al., 2003).

However, it is yet to be determined whether such models can simulate the physical mechanisms that lead to the occurrence of sub-daily rainfall extreme events. RCM must realistically resolve the underlying physical processes that cause sub-daily rainfall extremes, before the RCM data can be used, for instance, in the assessment of future flood risk, which is required for robust decision and policy making.

The purpose of the research was, therefore, to evaluate the performance of RCMs by adding a set of metrics characterising the physical processes of rainfall extremes at short timescales to the standard statistical metrics and to investigate likely future changes in sub-daily rainfall using RCMs.

1.1 Objectives of the research

The main goal of the research reported in this dissertation was to evaluate the capacity of RCMs to simulate sub-daily rainfall extremes, and to capture the relevant physical mechanisms that lead to these extremes. To this end, the evaluation of climate models must include statistics and physical relationships relevant to temporal and spatial scales that influence sub-daily rainfall extreme mechanisms.

RCMs have proven reasonable in reproducing rainfall extremes in daily and longer durations but less effort has been devoted to evaluating rainfall produced by RCMs at short time-scales. Statistics applied to rainfall extremes, such as rainfall intensity-frequency-durations, are commonly used for model evaluation. However, the simulation of relevant physical processes by RCMs is yet to be tested.

The current research, therefore, sought to achieve three objectives:

- *to develop a strategy to evaluate regional climate models in reproducing sub-daily rainfall extremes by implementing a set of metrics that characterise the relevant physical processes;*
- *to apply these metrics to three versions of the Weather Research and Forecasting (WRF) RCM over the Greater Sydney region to assess whether the models are able to simulate sub-daily rainfall extremes; and*
- *to investigate the likely future response of sub-daily rainfall extreme events to climate change using each of the three WRF RCMs over the Greater Sydney region.*

The more detailed evaluation of the model results using the physically based metrics developed in the first objective will help determine the level of confidence that can be placed in projections of

future sub-daily extremes under a warmer climate. This can be used as valuable information in support of the assessment of future flood risk.

1.2 Outline of the thesis

Chapter 2 reviews the current understanding of sub-daily rainfall extremes intensification due to anthropogenic climate change. Sub-daily rainfall extreme events are of significant societal importance, as the main agent of flash-flood events in rapidly responding catchments. Extreme events in rainfall at fine spatial and temporal scales are an ongoing research interest, mainly for engineering design of flood protection infrastructure. A review of studies dealing with changes in rainfall extremes provides evidence that rainfall extremes are influenced by anthropogenic climate change, and the observed increase of rainfall intensities at short durations with surface atmospheric temperatures is conceptually governed by Clausius–Clapeyron equation at global scales, recognising that the intensity of rainfall is constrained by the atmospheric moisture availability over certain temperature ranges.

Current tools used for investigating rainfall extremes are climate models, particularly RCMs which better simulate the temporal and spatial scales dominated by convective generation mechanisms associated with extreme rainfall events. Although RCM are suitable for studying rainfall extremes, less effort has been devoted to evaluate their ability to reproduce the physical processes that lead to sub-daily rainfall extremes in terms of the diurnal and seasonal characteristics of rainfall extremes and the hypothesis for the intensification of rainfall intensity with temperature.

Chapter 3 introduces a strategy to evaluate the ability of RCMs to reproduce relevant physical aspects of sub-daily rainfall extremes. Observations from 69 weather stations across Greater Sydney and information from the CFSR reanalysis data are compared with three RCMs during 1990-2009. These RCMs were obtained from the *NSW/ACT Regional Climate Modelling* (NARCliM) project considering three different convective parameterisations in the *Weather Research and Forecasting* (WRF) model.

This strategy of RCM evaluation was compared with the diurnal cycle and seasonality of sub-daily rainfall extremes, the relationship between sub-daily rainfall extremes and temperature and the

observed statistics of sub-daily rainfall extremes (e.g. the annual maxima and the 1 in 10-year rainfall event) at Greater Sydney.

Chapter 4 explores projections of sub-daily rainfall extremes for near-term (2020-2039) and long-term (2060-2079) future periods in the three RCMs at Greater Sydney. Future projections correspond to three different configurations in the WRF model (described in Chapter 3) using as boundary conditions the GCM-MIROC 3.2 medres forced by the A2 emission scenario from the Intergovernmental Panel on Climate Change (IPCC).

Future changes associated to sub-daily rainfall extremes are investigated for:

- the diurnal cycle of hourly rainfall extremes
- the seasonality of sub-daily rainfall extremes at short-durations
- the relationship between sub-daily rainfall intensity and temperature
- the annual maxima of rainfall for sub-daily durations.

Chapter 5 summarises the major conclusions of the research, the research contributions and limitations and the recommendations for future work.

Chapter 2. Literature review

Changes in sub-daily rainfall extremes is an issue relevant to society, particularly in regions vulnerable to recurring flash flooding. The understanding and assessment of these changes are therefore integral to research in climate sciences and engineering hydrology, and in this context, a warming climate poses a challenge for prediction of rainfall extremes that involve complex interactions between large circulation and local weather systems. Future projections of sub-daily rainfall extremes require climate models that are able to reproduce the local scale and physical mechanisms that lead to the occurrence of rainfall extreme events at short time scales. These mechanisms include the diurnal and seasonal variability associated with convective rainfall, the spatial configuration of synoptic conditions associated with the most extreme rainfall events and the relationship between sub-daily rainfall extremes and temperature that have been poorly explored in RCMs.

2.1 Definitions of rainfall extremes

Extreme rainfall events are of interest to numerous disciplines and have different definitions that vary depending on the region, duration and type of analysis used (Jakob et al., 2011a, 2011b). These differences create difficulties in ensuring consistency when discussing extreme rainfall events. For instance, in climate science, rainfall extremes are defined by various extreme thresholds, such as the 90^{th}, 95^{th} or 99^{th} percentiles of a cumulative distribution function generally fitted to daily or longer rainfall durations. Alternatively, the annual maxima of rainfall are used for more extreme rainfall events (Groisman et al., 2001).

Other ways of identifying extreme rainfall include the use of indices for climate variability and extremes which are above or below specific physically-based thresholds. For instance, the Expert Team on Climate Change Detection and Indices (ETCCDI) (Zhang et al., 2011) developed 27 indices to define daily or longer duration extremes for different atmospheric variables, such as temperature and rainfall.

Table 2.1 outlines 10 of the ETCCDI indices that refer to rainfall extremes. These indices sample a wide variety of climates and include statistical definitions, such as the consecutive number of extreme events over the 95^{th} and 99^{th} percentile threshold – exceedance that is more evenly distributed in

space and meaningful for each area. However, the use of threshold definitions is subject to specific values that will be exceeded at different rates and in different locations.

Table 2.1 Definition of extremes in rainfall according to the ETCCDI indices (Zhang et al., 2011).

ID	Indicator	Definitions	Units
RX1day	Max 1-day precipitation amount	Monthly maximum 1-day precipitation	mm
RX5day	Max 5-day precipitation amount	Monthly maximum consecutive 5-day precipitation	mm
SDII	Simple daily intensity index	The ratio of annual total precipitation to the number of wet days (≥ 1 mm)	mm/day
R10	Number of heavy precipitation days	Annual count when precipitation ≥ 10 mm	days
R20	Number of very heavy precipitation days	Annual count when precipitation ≥ 20 mm days	days
CDD	Consecutive dry days	Maximum number of consecutive days when precipitation < 1 mm	days
CWD	Consecutive wet days	Maximum number of consecutive days when precipitation ≥ 1 mm	days
R95p	Very wet days	Annual total precipitation from days > 95th percentile	mm
R99p	Extremely wet days	Annual total precipitation from days > 99th percentile	mm
PRCPTOT	Annual total wet-day precipitation	Annual total precipitation from days ≥ 1 mm	mm

In flood hydrology, rainfall extreme events define high intensity rainfall at different durations that have an important role in catchment-scale runoff generation, water storage, floods and soil erosion. For flood estimation purposes, rainfall extremes refer to events with small probabilities (much rarer that in climate science) such as the 1% *annual exceedance probability* (AEP) events which occurs on average once in 100 years (Westra et al., 2014b). Also, events less frequent than 1% AEP are of increasing interest for flood risk management (Horsham, 2003).

Another definition is the *probable maximum precipitation* (PMP), which is the greatest accumulation of precipitation for a particular location, duration and time of year (WMO, 2009). PMP values have T-year return periods in the range 10^5 - 10^6, in order to ensure the design of long lifetime dams that may experience future climate change impacts (Kunkel et al., 2013). PMP values depend on meteorological conditions such as atmospheric moisture, transport of moisture into storms, upward motions and strong winds (Trenberth et al., 2003). Moreover, PMP events can be transformed to *probable maximum flood* (PMF) values that are typically used in the design of large engineering infrastructure.

Typical extreme rainfall consequences at short-duration: Flash flooding. Sub-daily rainfall extremes are the main cause of flash flooding in rapidly responding catchments, such as in some rural catchments and urban drainage areas. Flash floods are short-term events, mostly occurring within a few hours of heavy rain causing a rapid rise in streamflow with depths of water over low-lying areas (NOAA, 2014). Other causes include dam break, levee failure, snow melt and ice jams.

The Toowoomba flash flood in Queensland, Australia, provides an example of such a flood. This event was the result of the interaction of a low-pressure system and an upper level trough (van den Honert and McAneney, 2011), which delivered approximately 152 mm of rain in only half an hour. The cost of this extreme event was approximately AU$174M in material damages, with seven fatalities (Leonard et al., 2014). The effects of this extreme rainfall event were potentially exacerbated by the wet antecedent conditions since Queensland was at the time in the midst of a La Niña event (Figure 2.1).

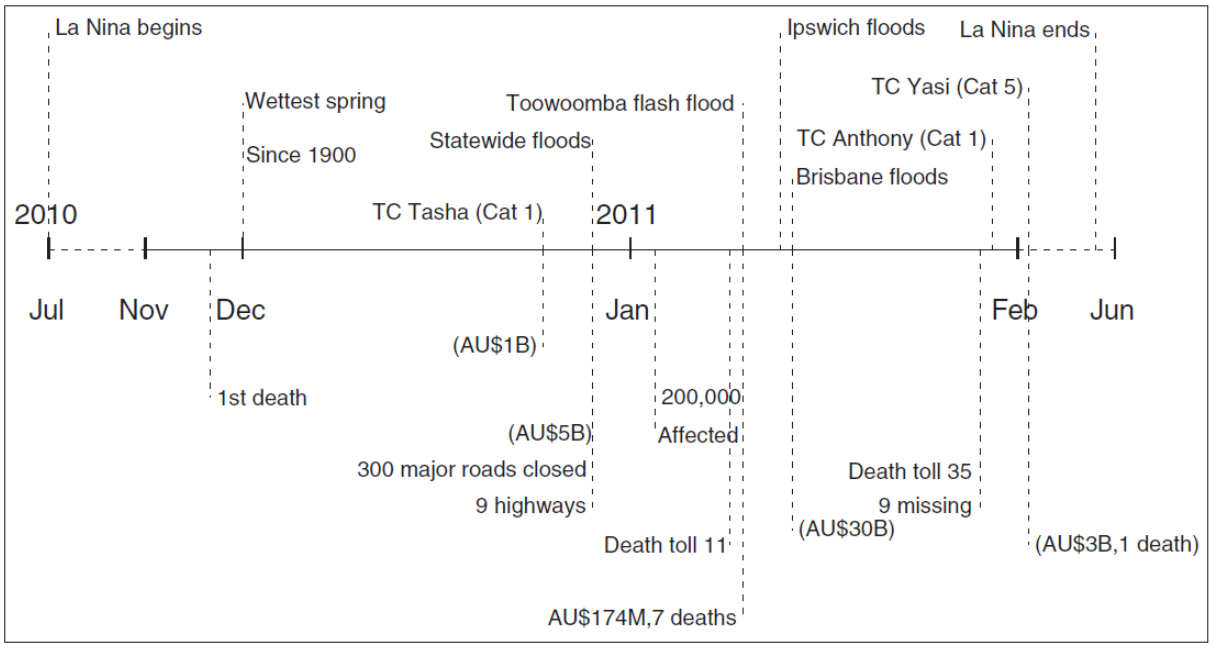

Figure 2.1 **Timeline of events related to the flood in Brisbane Australia during the wet season 2010-2011 (Leonard et al., 2014).**

Furthermore, during 2011, Typhoon Talas in Japan established a 72-hour rainfall record of 1625 mm and Korea experienced its wettest summer since 1908, and in 2012 flash floods generated by torrential rain swept the southern Russian Krasnodar Region causing 171 fatalities (Kotlyakov et al., 2013).

In the following year, 2013, seven hours of torrential rains flooded many regions of Buenos Aires, Argentina, with the hardest-hit area being the La Plata region, where 400 millimetres of rain fell in two hours, resulting in flash flooding and caused 86 fatalities (Aon, 2013). Finally, also during 2014, torrential rains caused flash flooding over several regions of Afghanistan and over the north of India and Pakistan, causing about 200 and 300 casualties, respectively (ADB, 2014).

During the last decade, in fact, flash flooding has caused severe damage or loss of property, infrastructure and environmental resources, together with injuries and hundreds of fatalities worldwide. Flash floods can be more dangerous than slower-onset floods due to the fact that their sudden nature allows little or no time for mobilising an emergency response (Ahern et al., 2005). According to the National Weather Service, flash floods are the number one weather-related killer in the US each year, and most fatalities happen in vehicles when people are swept away trying to cross flooded intersections (National Weather Service, 2010).

Urban areas are more susceptible to flash flooding due to impermeable surfaces which increase water runoff. The risk of such floods over urban and coastal areas is expected to increase in the future due to rising sea levels and increasing urbanisation. Moreover, climate change will lead to an increase in rainfall intensity at short durations with warmer atmospheric temperature and available moisture content (Willems et al., 2012). For this reason, investigation of changes in sub-daily rainfall extremes influenced by climate change is essential in order to support urban planning policies and to design engineering infrastructure for flood protection (Westra et al., 2014).

2.2 The response of rainfall extremes to a warming planet

The main changes in rainfall are observed in the intensity, frequency, duration and types of events (Trenberth, 2011; Trenberth et al., 2003). For instance, changes in annual average rainfall suggest a spatial variability tendency of wet regions to get wetter and dry regions to get drier (Allan and Soden, 2008; Allen and Ingram, 2002; Chou et al., 2013). However, changes in extremes might also increase in regions where annual averages decrease. This has already been observed in several regions worldwide (Dai, 2011), where a warmer climate is accelerating the evaporation of moisture over the land-surface. This increases atmospheric water vapour, which is concentrated in the lower troposphere and then transported by atmospheric winds to regions where storms are formed.

Increasingly moist weather systems favour more intense rainfall events, but may also reduce their duration and/or frequency (Trenberth, 2012).

Climate model projections also suggest that greenhouse gases may strongly influence rainfall extreme events, which are expected to become more intense and frequent in the future (Kao and Ganguly, 2011).

2.2.1 The influence of anthropogenic climate change on rainfall extremes

'Human influence on the Earth's climate is clear'. This affirmation is based on observational and climate model evidence that reflects increasing GHGs in the atmosphere, positive radiative forcing and observed climate warming (IPCC, 2013). Although natural variability is the main driver of the climate system, anthropogenic forcing has modified the natural bounds where the weather develops (Trenberth, 2012).

Most climate change impacts are perceived through changes in weather extremes, such as the heavy downpours mentioned in Section 2.1 that have caused major human fatalities and economic damage around the world during the past decade (Coumou and Rahmstorf, 2012). The IPCC in its Fourth Assessment Report (4AR) indicates that:

> *Generally, numbers of heavy daily precipitation events that lead to flooding have increased due to global warming (Solomon et al., 2007).*

Evidence of anthropogenic climate change. Evidence of anthropogenic climate change includes changes to the planetary and large scale circulation systems with increased surface temperature, atmospheric water vapour, evaporation and intensity of storms.

Temperature. The global land-ocean surface temperature is on average 0.85 °C (0.6 to 1.6°C) warmer since 1880 (IPCC, 2013). This rise in surface temperature has led to higher evaporation (mainly over oceans) which also has increased since late 1980's (Schlosser and Houser, 2007).

Atmospheric water vapour. The amount of water vapour in the atmosphere has increased since 1973 (Ross and Elliott, 2001), especially over regions where moisture is available. The specific humidity and total column water vapour content have increased globally at a rate of approximately 7%/°C (in agreement with the Clausius–Clapeyron rate) in response to changes in surface temperature (Allan et al., 2014). However, the relative humidity has declined over low latitude and mid-latitude land areas during the last decade, suggesting that this decrease may be due to limited

supply of water from the ocean. Possible implication of this decrease can mean less chance of precipitation because the threshold for condensation is reached less often (Simmons et al., 2010).

Changes in circulation patterns. The width of the tropical belt and associated changes in Hadley circulation patterns have caused the poleward migration of large-scale atmospheric circulation, such as jet streams and mid-latitude storm systems (Seidel et al., 2008). The intensity of tropical cyclones has also increased, with high wind speeds and heavy rainfall as a result of warmer tropical sea surface temperatures, while the occurrence, has decreased (IPCC, 2013; Solomon et al., 2007).

Changes in rainfall extremes. Empirical and modelling studies into extreme rainfall support the evidence of increasing intensity and frequency of rainfall extremes as global warming intensifies (Alexander et al., 2006; Coumou and Rahmstorf, 2012; Trenberth, 2012; Westra et al., 2013). The trend is global, with annual maximum daily rainfall intensity changing at a rate of 5.9-7.7%/°C with respect to averaged surface temperature (Westra et al., 2013).

These observations suggest a complex pattern of change, with regionally-specific changes in both atmospheric moisture availability and the atmospheric circulation patterns that draw moisture into a region. The changes also modify the atmospheric moisture recycling of local rainfall that results from moisture already in the atmosphere, convergence of the moisture brought in by the winds or evaporation of surface moisture into the atmosphere (Trenberth, 1999).

Similarly, GCMs adopted from the Coupled Model Intercomparison Project Phase 5 (CMIP5) (Taylor et al., 2011) indicate a global increase in daily rainfall extremes of about 6 % per °C and lower rates over extratropical land regions (Kharin et al., 2013). Most of these studies have focused on the daily timescale due to the availability of data and modelling outputs. However, the analysis of trends in sub-daily rainfall extremes remain limited due to the lack of sampling and poor quality in existing observations, as well as the lack of ability of coarse-resolution dynamical models to realistically simulate sub-daily rainfall (Chan et al., 2014). This has led to a recent focus on the observed relationship between sub-daily extreme rainfall and atmospheric temperature.

2.2.2 The relationship between rainfall intensity and temperature

Assuming a constant relative humidity, the actual atmospheric moisture content should increase at a rate referred to as the Clausius-Clapeyron rate of 7% per 1°C, which describes how a warmer atmosphere can hold more water (Trenberth et al., 2003). It has been suggested that the intensity of

extreme precipitation events will scale with the moisture available in the atmosphere; so that as a first approximation, it might be assumed that extreme precipitation will also scale at 7% per 1°C.

Considering typical atmospheric conditions, the saturation-specific humidity approximately increases by ~7% per degree at 0°C and ~6% per degree at 24°C for atmospheric pressure in the range of 850 mb and 700 mb (Trenberth et al., 2003).

The Clausius-Clapeyron relation is expressed as:

$$\frac{de_s}{dT} = \frac{Le_s}{RT^2} \qquad \text{(Eq. 2.1)}$$

where e_s is the vapour pressure (also called water holding capacity), T is the temperature, L is the latent heat (heat of transformation) of vaporization or condensation and R is the ideal gas constant (8.3144 J^{-1} mol K^{-1}).

The August-Roche-Magnus equation provides a good approximation of the water-holding capacity of the atmosphere under typical atmospheric conditions:

$$e_s(T) = 6.1094 \exp\left(\frac{17.625T}{243.04 + T}\right) \qquad \text{(Eq. 2.2)}$$

where e_s is the saturated vapour pressure which changes with T in ℃.

The rate of change of e_s with temperature is the Clausius-Clapeyron (C-C) temperature scaling. This scaling gives the fractional rates of changes of the column water vapour measured by satellite observations, which is the baseline for quantifying changes in the amount of water in the atmosphere (O'Gorman and Muller, 2010).

Although the Clausius-Clapeyron rate may be a convenient approximation for estimating how extreme rainfall will scale with temperature, changes in atmospheric large scale circulation patterns, thermodynamics of the atmosphere and clouds and limitations in moisture increase can induce deviations in the C-C scaling. Furthermore, changes in moisture content can be modified by additional latent heat release which enhances the low-level moisture convergence, leading to an increase in rainfall (O'Gorman and Schneider, 2009; Trenberth, 2005).

Extremes scaling with atmospheric temperature. A number of empirical studies have been conducted to determine how rainfall extremes scale with atmospheric temperature. Observational studies in Europe and Australia have found that approximately the 99th percentile of sub-daily rainfall follows the C-C rate (Hardwick Jones et al., 2010; Lenderink and van Meijgaard, 2008). In addition,

studies of hourly rainfall extremes have also reported increases in extremes at about twice (~14%/°C) the C-C scaling rate (also termed 2-CC or super-CC) for high temperatures up to 22°C (Berg et al., 2013; Lenderink and van Meijgaard, 2008; Lenderink and Van Meijgaard, 2010; Mishra et al., 2012b; Utsumi et al., 2011). Moreover, convective rainfall is considered to be the dominant rainfall type associated to super-CC scaling rates found at 10-minute and hourly rainfall intervals (Berg et al., 2013; Loriaux et al., 2013).

Climate modelling studies have also reported on the ways in which extreme rainfall might scale with temperature. Two studies using a cloud-resolving model in the tropics indicated that rainfall extremes increase approximately in line with the C-C scaling (Muller et al., 2011; Romps, 2010). In another study using an idealised squall line for mid-latitudes, a super-CC scaling at sub-hourly time scales was found (Singleton and Toumi, 2013). A recent study using the convective-permitting mesoscale model with 2.5 km horizontal resolution, Harmonie, found for 11 intense (convective) rainfall cases a scaling rate of 11%-14% per degree (Attema et al., 2014).

Results from the aforementioned studies have contribute to the understanding of potential changes to sub-daily rainfall extremes following either the C-C and super-CC. However, the interpretation of the observed scaling rates is complex and requires a better understanding of the interaction between atmospheric variables and physical processes that influenced on the scaling (Westra et al., 2014b).

Temperature, atmospheric moisture and rainfall extremes. Increasing observational and climate modelling studies have investigated the relationship between atmospheric temperature and rainfall intensity as a basis for projecting changes in sub-daily rainfall extremes, arguing that the intensity should increase following either the CC rate or 2 C-C over certain ranges of temperature and availability in moisture. For example, a study by Hardwick Jones et al. (2010) showed that hourly rainfall extremes increase with temperature up to 24°C (Figure 2.2a), approximating the C-C rate for several regions across Australia. However, the scaling decreases at higher temperatures and becomes negative (also known as the inflection point of the temperature scaling).

The decrease in rainfall intensity at higher temperatures has been associated with a deficit in atmospheric moisture content, but this relationship is yet to be understood. Some studies have plotted the relative humidity and associated temperature (Figure 2.2b), finding a clear agreement between the temperature when the scaling occurs and when the relative humidity begins to decline (Hardwick

Jones et al., 2010; Lenderink et al., 2011; Shaw et al., 2011; Utsumi et al., 2011). In addition, results by Hardwick Jones et al. (2010) suggest a need to investigate not only the moisture holding capacity of the atmosphere, but also the moisture content available at the time of observation.

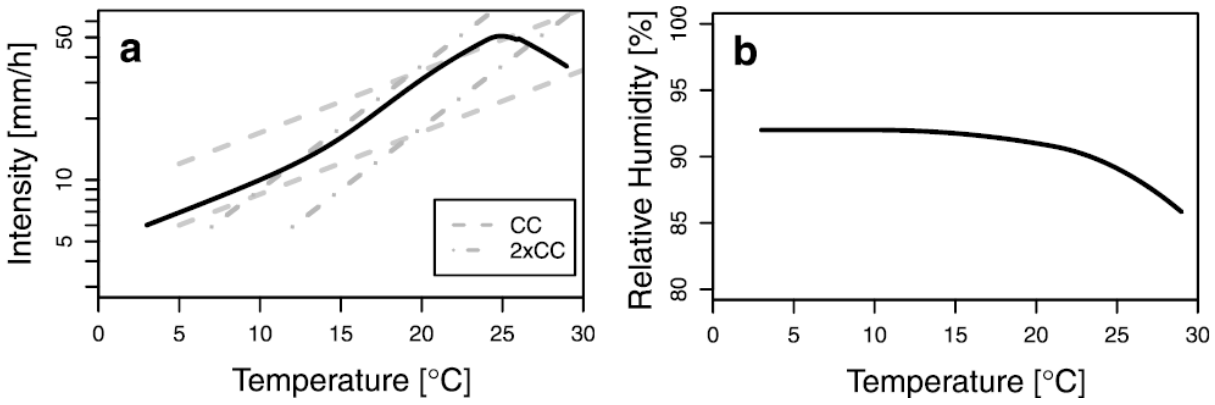

Figure 2.2 **Relationship between surface temperature and rainfall extremes based on empirical studies by Westra et al. (2014b). (a) Black line represents the observed increase in rainfall intensity with temperature following approximately the C-C scaling (long-dashed black lines) below 12°C. For temperatures from 12°C to 24°C, the increase of rainfall intensity follows the super-CC scaling (dot-dashed black lines); whereas for temperatures higher than 24°C, the scaling becomes negative. (b) Observed behaviour of relative humidity decreasing at higher temperatures.**

Berg et al., (2009) suggest that results obtained from the relative humidity do not necessarly imply the same decrease for the total moisture content. Thus, dew point temperature T_d is the temperature at which the air is fully saturated and is considered as a direct measure of atmospheric absolute humidity (Lenderink and Van Meijgaard, 2010). Dew point temperature represents the actual absolute specific humidity q_v of the atmosphere, expressed by:

$$q_{sat}(T_d) = q_v(T) \qquad \text{(Eq. 2.3)}$$

where q_{sat} is the saturation specific humidity as function of drew point temperature (T_d) (omitting the dependency of q_{sat} on pressure) and q_v is the actual specific humidity (or moisture content) of the air.

The difference between temperature and the dew point temperature ($T - T_d$) is commonly referred to as the *dew point depression*, which is a direct measure of relative humidity (Lenderink and Van Meijgaard, 2010). As a first approximation, constant dew point depression implies no changes in relative humidity for most temperature ranges (since q_{sat} is approximately an exponential function of T). Despite the fact that dew point temperature is a better indicator of humidity, the use of surface air

temperature gives a better representation of the peak in rainfall intensity over a certain temperature, because a decline from 24°C cannot be observed using dew point temperatures.

2.2.3 Evidence of increase in sub-daily rainfall extremes

Most studies have identified an increase in rainfall extremes over land since 1950 based on daily observational data at large regional (Groisman et al., 2012; Hartmann et al., 2013; Skansi et al., 2013; van den Besselaar et al., 2013) and global scales (Alexander et al., 2006; Donat et al., 2013; Groisman et al., 2005; Westra et al., 2013). For example, Groisman et al. (2005) identified a widespread increase in daily rainfall extremes (defined by the upper 0.3%) over mid-latitudes while Alexander et al. (2006) reported a significant increase in the intensity and frequency of global observed daily rainfall extremes (rainfall above the 95^{th} and 99^{th} percentiles) between 1951 and 2003. In fact, rainfall extremes observed in the northern hemisphere have become more intense (Min et al., 2011), particularly in 30% of the main urban areas across the USA, which recorded a statistically significant increase for the period 1950-2009 (Mishra and Lettenmaier, 2011). Westra et al. (2013) also found a global increasing trend in annual maximum daily rainfall intensity at a rate of 5.9-7.7%/°C with averaged surface temperature.

Furthermore, climate model projections applied during the CMIP5 suggest a global increase in daily rainfall extremes as the climate warms by about 6% per 1°C, with lower rates over extratropical land regions (Kharin et al., 2013; Sillmann et al., 2013). However, findings from Westra et al. (2014b) suggest that trends in rainfall extremes from daily scales might not be reflected in sub-daily time scales.

The few existing trend studies of sub-daily rainfall extremes mainly focus on single sites (i.e. urban catchments) or small regions (Beuchat et al., 2011; Fujibe, 2013; Jakob et al., 2011b) with some considering large scale regions and long term trends (Hartmann et al., 2013). However, the main findings agree that rainfall intensity increases even at sub-hourly durations (Chan et al., 2013; Westra and Sisson, 2011).

According to a recent regional assessment by Westra et al. (2014b), there is a scarcity of literature related to sub-daily rainfall extremes in many parts of the world. This is mainly attributed to incomplete sampling in rain gauge stations, poor-quality data at sub-daily intervals (Nicholls and Alexander, 2007) and non-homogeneous spatial distribution in the observations.

The lack of high quality and long sub-daily rainfall records is a major limitation to project changes in sub-daily rainfall extremes under a future climate. Therefore, climate models with fine temporal

and spatial scales are used to complement the existing gaps in the observations and to generate projections of sub-daily rainfall extremes under future climate change.

2.3 Climate models

2.3.1 General circulation vs regional models

General circulation models. GCMs are global in their focus and have coarse resolutions of hundreds of kilometres (with ~100-km grid spacing) that simulate reasonably well the large-scale time-averaged rainfall patterns, but fail to reproduce the spatio-temporal distribution of rainfall or small-scale regional features (Tripathi and Dominguez, 2013), such as persistence (Johnson and Sharma, 2011). These models have also proved limited in terms of reproducing rainfall extremes. Although the frequency is relatively well simulated, the intensity of rainfall is underestimated (Dai, 2006; Sun et al., 2006). Moreover, the coarse horizontal resolution of GCMs cannot accurately represent the distribution of extreme events at short scales (Chen and Knutson, 2008).

The underestimation of the occurrence of heavy rainfall with a poor representation of moist physical processes is another disadvantage of GCMs (Kang et al., 2014). Sub-daily rainfall extreme events are mainly related to convective processes (Haerter and Berg, 2009; Hand et al., 2004; Mishra et al., 2012a) which occur on fine temporal and spatial scales that GCMs cannot resolve. Indeed, most urban hydrology studies require rainfall intensities at short durations because of the focus on the behaviour of urban drainage systems.

Figure 2.3 illustrates the temporal and spatial scales of atmospheric processes, the range of scales covered by the GCMs and the fine-scale resolution required in climate models to simulate sub-daily rainfall extreme for urban hydrology studies.

Regional climate models. RCMs are often used to resolve this mismatch. They can be nested into a GCM to represent the atmospheric physics at a fine horizontal grid resolution (spacing from 2km to 50 km). RCM can help address important research questions in urban hydrology by downscaling global climate models into regional scales of high temporal (10 min to few hours) and spatial resolutions (~10 km or less) at which decision makers and stakeholders operate (Berne et al., 2004; Fowler et al., 2007).

Indeed, RCMs offer a better representation of the local scale features, such as topography, coastline and land cover, required to investigate rainfall patterns (Chan et al., 2013; Evans and McCabe, 2013).

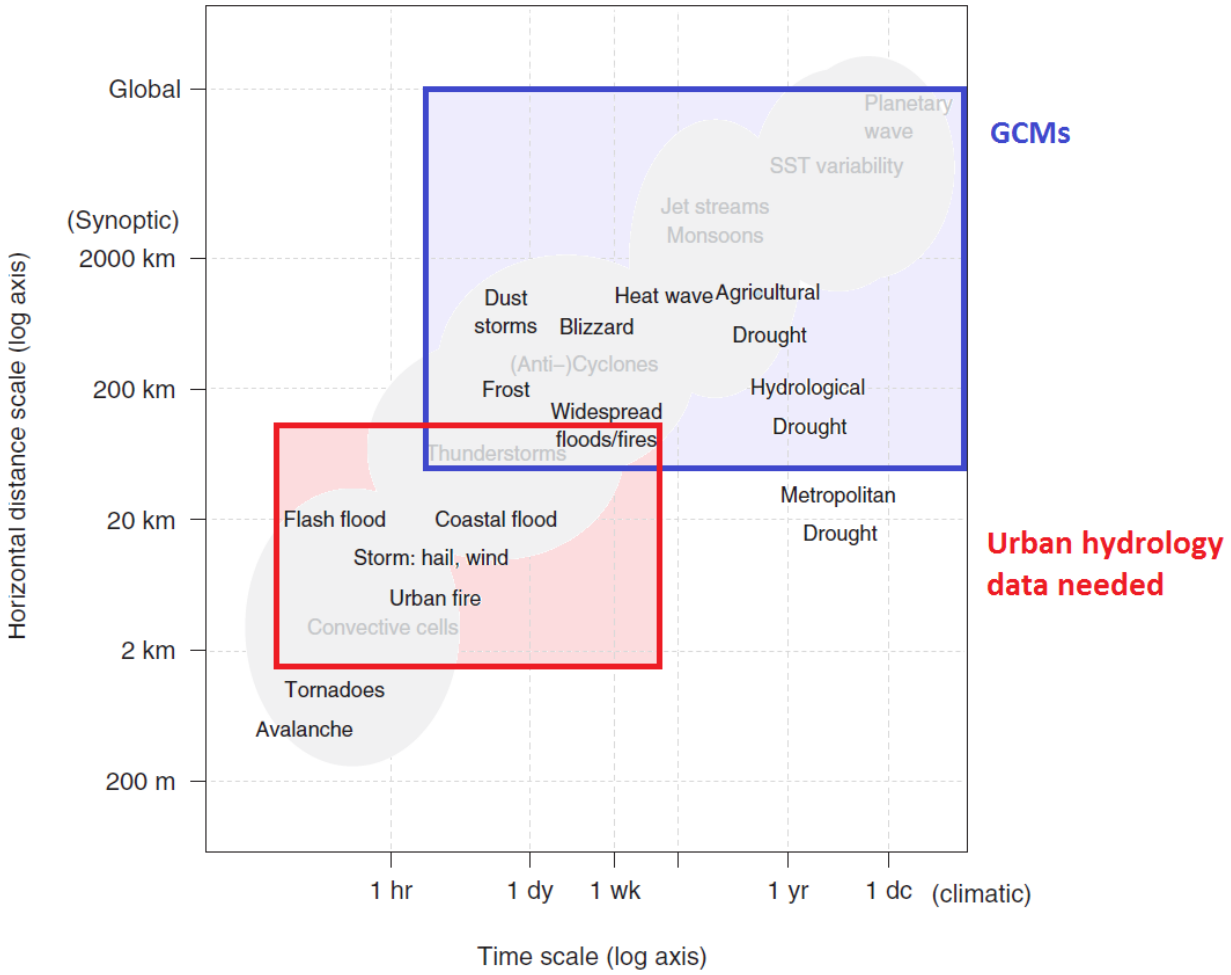

Figure 2.3 **Temporal and horizontal spatial scales of atmospheric processes (in grey circles), the range of scales represented in GCMs (blue square) and the resolution needed for urban hydrology (red line) adapted from Di Luca et al. (2012) and Leonard et al. (2014).**

Some differences between the main GCMs and RCMs are listed in Table 2.2. These differences are found in the temporal and spatial resolutions and in the parameterisation schemes and the lateral boundary conditions selected. For instance, GCMs are coupled atmosphere-ocean models covering horizontal resolutions that are typically greater than 100 km, while RCMs are pure atmospheric models without a couple ocean component and run at higher resolutions ($\leq$ 50 km).

Another major difference between GCMs and RCMs is the lateral boundary condition in RCMs, which can be provided by a GCM, a global (re-)analysis or from another RCMs when using a double nesting technique (Wibig et al., 2015).

Table 2.2 Comparison of the spatial and temporal resolutions of two typical GCMs and two typical RCMs.

Model	Name	Spatial resolution	Temporal resolution	Description
GCM	CSIRO-Mk3.0	1.875°× 1.875° (~200 km)	Monthly, daily and six-hourly	CSIRO-Mk3.0 is a coupled atmosphere–ocean model with dynamic sea-ice and also has a soil–canopy scheme with prescribed vegetation properties
	HadCM3	2.5° × 3.75° (~300 km)	Daily and six-hourly	HAdCM3 is a coupled atmosphere-ocean (sea ice model) general circulation model without the need for the flux adjustments (flux quantities connecting the atmospheric and oceanic systems)
RCM	PRECIS (HadRM3P)	0.44°× 0.44° (~50 km) or 0.22°× 0.22° (~25 km)	hourly	PRECIS is a hydrostatic atmospheric and land surface model of limited area using physical parameterisations, boundary conditions, initial conditions and spin-up. It also contains an atmospheric sulphur cycle
	WRF	0.1°× 0.1° (~10 km)	hourly	WRF is a non-hydrostatic mesoscale, primitive-equation model with different physical schemes and boundary conditions

Advantages and disadvantages. The advantages and disadvantages of GCMs and RCMs are outlined in Table 2.3. It can be seen that RCMs are highly dependent on GCM boundary conditions and are highly sensitive to the physical parameterisation (e.g. convection scheme, cloud microphysics scheme, planetary boundary layer scheme and longwave and shortwave radiation schemes) used.

The added value provided by the regionalisation of spatial and temporal resolutions in these models has encouraged the use of RCMs for understanding changes in rainfall extremes. However, most studies have investigated rainfall extremes for seasonal or daily simulations, and for regional or larger scales (Fowler et al., 2005; Gutowski et al., 2010; Salathé et al., 2010; Wehner et al., 2010). For instance, the magnitude of extreme regional rainfall for daily and multi-daily durations during winter has been skilfully simulated by 13 RCMs across the UK (Fowler and Ekström, 2009).

Table 2.3 Summary of main advantages and disadvantages of climate models for rainfall extremes.

Climate mode	Advantages	Disadvantages
GCMs	• Consistent representation of the physical processes that interact at global and regional scales • Able to reproduce rainfall extremes at daily and longer time scales	• Expensive and intensive computation cost • Operate at spatial scales too coarse and for long time periods • Poor performance of rainfall extremes at short-durations
RCMs	• Higher temporal and spatial resolution than GCMs • Better representation of local scale features such as topography, land-sea contrasts and changed surface cover • Better representation of atmospheric physics that lead to sub-daily rainfall extreme events • Good performance of daily rainfall extremes	• Expensive and intensive computation cost • Nested within a global climate model that provide boundary layer conditions • Highly dependent to convective parameterizations • Simulate individual extreme events over limited areas • Prone to bias

In other studies, five RCMs simulated quite well the 1-day rainfall extreme events when compared to radar data across the Netherlands (Hanel and Buishand, 2010); and RCMs used in the North American Regional Climate Change Assessment Program (NARCCAP) demonstrated a satisfactory performance in reproducing the historical season of occurrence, mean, and variability of 24-hour precipitation extremes for 100 urban areas across the United States (Mishra et al., 2012a). However, a general conclusion suggests that RCM simulations depend greatly on the region, season, intensity and duration of the rainfall event considered (Maraun et al., 2010).

2.3.2 The use and assessment of regional climate models

Simulating sub-daily rainfall extremes. A few recent studies have looked at sub-daily rainfall extremes using RCMs. For instance, Lenderink and van Meijgaard (2008) investigated changes in hourly rainfall maxima over Europe using the 25 km resolution RCM, and found a good agreement in the increase of hourly rainfall extremes with temperature between the observed climate and the modelled climate change signal.

Other studies include RCMs with a 10 km horizontal resolution which are able to capture reasonably well the spatial scale of 3-hour rainfall extremes (Tripathi and Dominguez, 2013) and the diurnal cycle of sub-daily rainfall (Evans and Westra, 2012). However, Hanel and Buishand (2010) found that the intensity of 1-hour rainfall maxima in eight 25-km RCM simulations was too low compared

with radar observations. The finding is consistent with Mishra et al. (2012a) who found that the intensity of 3-hour rainfall extremes is underestimated. It was also found that with high spatial resolution, the capacity of RCMs in rainfall extreme simulations decreases.

RCMs usually perform poorly when dealing with convection with high time and space variability, generating a bias in terms of rainfall extremes (Argueso et al., 2013). This is due to the scale-separation approximation that is introduced by the convective parameterisations (Li et al., 2012), where moist physical processes (e.g., convective, cloud, and rain processes) that trigger rainfall extremes are poorly simulated (Evans and Westra, 2012). Parameterisation schemes used in RCMs are a known source of uncertainties and errors in simulation of Australian regional conditions because most RCMs are primarily developed for the tropics and for coarser resolution (50–100-km) GCMs (Hohenegger et al., 2008).

Convective-permitting models

Alternatives for investigating sub-daily rainfall events are *convective-permitting models.* Convective-permitting models are very high-resolution models (~1-km grid resolution) that display realistic model dynamics and a better representation of convection without the need for parameterisation schemes (Kendon et al., 2012). Some advantages of using convective-permitting models can be observed in the intensity of the most extreme rainfall (Prein et al., 2013) and the realism (spatial and temporal structure) of hourly rainfall extremes (Chan et al., 2014; Kendon et al., 2012). However convective-permitting models are computationally very expensive which limits their implementation.

The need for a physical basis in the evaluation of RCMs. There is considerable confidence in the ability of climate models to project future climate change, especially at global scales and for projections of some climate variables (e.g. temperature) than for others (e.g. precipitation) (Randall et al., 2007). This confidence is based on the fact that the models can reproduce observed features of past and current climate based on physical principles (Solomon et al., 2007).

The capacity of RCMs to predict climate change at the local level has been investigated by comparing simulations with observations. Typically, the model evaluation approaches consist of *indices* and *metrics* that evaluate statistics of rainfall extremes for daily and longer durations.

Indices are used to characterise the properties of the data, for example the number of days exceeding the 99th percentile threshold. Indices such as this therefore allow the spatial comparison of the probability distribution of rainfall across different regions (Alexander et al., 2006; Moberg et al., 2006; Zhang et al., 2011).

Metrics, on the other hand, characterise model performance and its sensibility to observational uncertainties, spatial scales, domain and the period of the simulation. Usually, metrics are scalar measurements used to directly compare model outputs with observations, for example, in the estimation of statistical measures, such as the mean error, root-mean square error, correlation and variance (Gleckler et al., 2008; Holtanová et al., 2012).

Direct measures of extreme rainfall in RCMs. Several studies have examined rainfall extremes in climate models (Benestad, 2010; Gregersen et al., 2013; Nguyen et al., 2010). Rainfall extremes have been evaluated by different indices that characterise the tail of the distribution of rainfall. Examples of indices commonly used are:

- The STARDEX (Haylock et al., 2006) and ETCCDI (Zhang et al., 2011) rainfall indices
- the threshold exceedance indices, such as the 95th or 99th percentiles of a probability distribution function (Benestad, 2010)
- the maximum rainfall in a day or in a specific number of consecutive days (Beniston et al., 2007; Groisman et al., 2001)
- T-year return periods of rainfall at different durations (Fowler and Ekström, 2009; Frei et al., 2006)
- the intensity-duration(-area)-frequency (ID(A)F) relationship (Nguyen et al., 2010; Olsson et al., 2012).

The performance of extreme rainfall indices in climate models is also quantified by metrics. According to Sunyer et al. (2013), these metrics can be separated into two main categories:

- metrics that evaluate the performance of climate models at model grid level or regional average (Hanel and Buishand, 2010; Lenderink et al., 2011). These metrics analyse the bias for one or more indices, the properties of empirical distributions, and the confidence intervals of return levels (Frei et al., 2006)
- metrics that examine the ability of models to represent the spatial distribution of rainfall (Fowler and Ekström, 2009; Lenderink and Van Meijgaard, 2010). These metrics focus on

semi-variograms (Zolina et al., 2013) and principal components analysis (Ngongondo et al., 2011).

Typical metrics applied in the climate sciences are the Taylor diagram, which illustrates the model bias and the spatial pattern and variability of the root mean square error (RMSE).

Other studies have used a combination of different metrics. For example, Lenderink et al. (2011) applied the bias and the spatial variance using the 99.9^{th} percentile of rainfall intensity between the RCM output and the observations. In addition, Sunyer et al. (2013) considered a set of indices for extreme rainfall (i.e. 90^{th}, 95^{th}, 97.5^{th} and 99^{th} percentiles of the wet days precipitation amount) and two metrics (bias and RMSE).

In addition to the direct metrics of evaluation based on statistics, there is another set of metrics applied in meteorological and climate research that accounts for inconsistencies and systematic errors in climate models (Trenberth et al., 2003). These types of metrics evaluate the representation of the physical processes that regulate moist convection and the influence of large-scale circulation systems that favour the onset of rainfall extremes events.

The diurnal cycle of sub-daily rainfall extremes. The diurnal cycle has also been used to investigate the amplitude, timing of the maximum rainfall intensity and the frequency of rainfall occurrence in RCMs (Evans and Westra, 2012). The cycle is caused by diurnal variations of solar radiation and associated atmospheric variables, such as pressure, wind, temperature and humidity (Dai and Trenberth, 2004); and is an important characteristic of rainfall over regions dominated by topographical features and synoptic systems. The cycle can be expressed in terms of frequency and intensity of rainfall as a function of the time of day (Trenberth et al., 2003) or can be characterised by the diurnal composites and harmonic analysis. For example, the harmonic phase displays the timing of the maximum rainfall amount and frequency, which greatly depend on the region (Ai-Juan et al., 2008).

Several studies have been conducted to characterise the diurnal cycle of rainfall for many regions worldwide. For instance, in the tropics, the timing of maximum rainfall intensity is linked to the destabilisation of the boundary layer due to the daytime insolation that is observed during the afternoon over land areas; while in regions of complex terrain and predominant sea-breeze circulation, the peak of maxima intensity is observed from midnight to early morning (Nesbitt and Zipser, 2003). Several studies indicate that the afternoon peak of rainfall is caused by convective rainfall (i.e., generated by mesoscale convective systems or complexes) over continental regions

while the night-time peak is caused by light rainfall in maritime climates (Dai and Trenberth, 2004; Hitchens et al., 2010; Jeong et al., 2011).

It was concluded from the current study that the diurnal cycle of 3-hour rainfall events, the probability of rainfall occurrence, the intensity of rainfall per occurrence and the amplitude were reasonably well reproduced by a RCM over southeast Australia (Evans and Westra, 2012). However, the intensity of observed sub-daily rainfall events was often underestimated while the occurrence was overestimated.

Seasonal variability of sub-daily rainfall extremes. The occurrence of extreme events is associated with background conditions that favour the formation of clouds and subsequent rainfall. Rainfall extremes have a strong thermodynamic component in relation to seasonal changes that are associated with the variability of tropical circulation patterns. For example, the Hadley circulation over the tropics has a strong seasonal cycle that favours upward air motion with positive anomalies of moisture convergence and cloud formation over the summer hemisphere (Trenberth et al., 2000).

Rainfall extremes also have a strong temporal component, and are associated with the rainy season that typically occurs during the wet and/or summer months (Chou and Lan, 2011). The monsoon in South Asia, for example, is responsible for most of the summer rainfall in the tropics. Rainfall extremes during the monsoon are the result of a reversal of the prevailing surface winds that are strongly seasonal due to thermal differences between land and ocean surface during the wet season (Kitoh et al., 2013).

The seasonality of rainfall extremes has been used in the past to evaluate RCMs. For instance, Fowler and Kilsby (2003) identified significant seasonal and regional changes in the intensity of rainfall extreme events for the UK. Other studies have concluded that RCMs are able to reproduce the seasonality of rainfall extremes at daily durations (Maraun et al., 2011).

In addition, Schindler et al. (2012) evaluated the performance of 14 RCMs being used in the ENSEMBLES project simulating the annual cycle of daily rainfall extremes across the UK using extreme value distribution. They found that most RCMs failed in the representation of the amplitude of the annual cycle, especially in regions with strong peaks that typically occur during summer (such

as in East Anglia), although they performed better in the timing of maxima occurrence and spatial pattern, especially during winter months.

Studies of the diurnal cycle of rainfall have also focused on the season of the year, for example, the warm season when most rainfall events occur (Carbone and Tuttle, 2008). Li et al. (2008) investigated the diurnal cycle of rainfall in China for all of the seasons. They found there are significant differences in the prevailing wind and water vapour supply between the warm and cold season that are influenced by the East Asian monsoon.

A study in the UK suggested that the shape of the harmonic of the seasonal cycle of monthly maxima in rainfall is strongly dependent on the region where the rainfall extremes occurred, predominantly during the summer months when convective rainfall extremes are prevalent (Maraun et al., 2009). Also a recent study by Zheng et al. (2015) in the Greater Sydney region showed that the seasonal variability of rainfall extremes for storm-burst durations from 5 to 15 minutes and from 6 to 48 hours increased during summer months when convective rainfall extremes typically occurred.

2.4 Research gaps

Climate models can facilitate the projection of sub-daily rainfall extremes in the future climate, but GCMs are coarse in resolution and fail to capture the local scale of rainfall extremes. In contrast, RCMs are run at much finer temporal and spatial resolutions, which are more suitable for investigating changes in sub-daily rainfall. However, it is yet to be determined if the ability of RCMs to reproduce different aspects of sub-daily rainfall extremes that match the available observations.

The ability of RCMs to simulate sub-daily rainfall extremes requires a strategy of evaluation based not only on direct measures of whether RCMs match the statistics of extremes, also provide the right representation of the physical processes, such as the interaction between large-scale circulation systems and local scale thermodynamics which ultimately lead to the occurrence of sub-daily rainfall extremes over tropical and subtropical regions.

To evaluate the capacity of RCMs in reproducing sub-daily rainfall extremes, relevant physical processes must be correctly simulated (Westra et al., 2014b):

- The diurnal cycle of sub-daily rainfall extremes in terms of the timing of the maxima occurrence, which can provide insight about the key-rainfall generating mechanisms of rainfall

extremes such as local moist convection, land-sea breeze circulation, orographic forcing and tidal variations in surface pressure.

- The seasonal cycle of sub-daily rainfall extremes in terms of the season of the year of the maxima occurrences that corresponds to the dominant synoptic atmospheric conditions. For instance, convective rainfall commonly takes place during summer months while stratiform rainfall occur during months at which large circulation systems (i.e. fronts) are predominant.
- The configuration of synoptic mean conditions associated with the most extreme events in model simulation. For instance, the configuration of troughs, convergence and divergence patterns and zones of prevailing winds and shear associated to the most rainfall extreme events.
- The relationship of atmospheric temperature with the intensity of sub-daily rainfall extremes at sub-daily time scales, which is compared between the observations and model simulations to indicate under which conditions this empirical relationship holds or is exceeded. For example, changes in the scaling rate associated with the latent heat released within the storm or changes from stratiform rainfall to convective rainfall.

There is therefore a critical need to evaluate RCMs using this larger diversity of metrics, which is the focus of the following chapter.

Chapter 3. Evaluation of regional climate models in simulating observed sub-daily rainfall extremes

3.1 The need for a strategy to evaluate the capacity of RCMs to simulate sub-daily rainfall extremes

To understand the changes in sub-daily rainfall extremes, high resolution RCMs are more suitable than GCMs because of their better representation of smaller-scale topographic features (Gutowski et al., 2010). In order to quantify the reliability of RCM-derived projections, metrics or indices are often used to statistically compare the differences between model outputs and observations (Sunyer et al., 2013).

Although some previous studies have implemented RCMs to investigate statistics of rainfall extremes, few studies have investigated the capacity of RCMs to capture the physical mechanisms associated with the observed sub-daily rainfall extremes (Westra et al., 2014). These mechanisms are especially important, for instance, during summer when precipitation over land is often convective and exhibited a clear diurnal cycle (Dai and Trenberth, 2004). For instance, Evans and Westra (2012) investigated the ability of a RCM to simulate the diurnal cycle of 3-hour rainfall extremes over southeastern Australia. In other studies, Mishra et al. (2012a) evaluated the ability of a RCM to reproduce the seasonality of 3 and 24-hour rainfall extremes across the United States and Tripathi and Dominguez (2013) evaluated the ability of a RCM to reproduce individual extreme rainfall during summer and winter months.

Additionally, the thermodynamic basis of the Clausius-Clapeyron relationship has been used to explain potential increases in rainfall extremes with warm temperatures using climate projections and historical rainfall observations. For instance, some studies are usually compared the C-C relation which provides a hypothetical increase of the water holding capacity of the atmosphere with surface temperature, but additional effects on temperature due to vertical fluxes contribute to a shift from C-C to about 2-CC rates (Lenderink and van Meijgaard, 2008; Lenderink and Van Meijgaard, 2010; Trenberth, 2011). These previous studies have significantly contributed to build

knowledge for evaluating the representation of the physical mechanisms associated with short-duration rainfall extremes in RCMs simulations.

This study therefore recommends implementing evaluation metrics characterising the physical processes of sub-daily rainfall extremes in RCMs. The use of only the statistics of rainfall extremes (e.g. the annual maxima of rainfall) to evaluate RCMs do not provide enough evidence for demonstrating that the skill of RCMs corresponds to the right representation of the underlying physical processes triggering sub-daily rainfall extremes and do not provide confidence that the RCMs can be used for investigating climate projections (especially in the future) of such extremes. Therefore, a strategy to assess the physical processes that produce sub-daily rainfall extremes and analyse the statistics of extreme rainfall events is needed, and is outlined in Figure 3.1.

The physical processes contributing to sub-daily rainfall extremes are first examined through the timing of the diurnal (DC) of rainfall extremes to determine the performance of the selected RCM. If the performance is satisfactory, the RCM is able to correctly capture the convective pattern and then considered for the next condition. However, the RCM is recommended to be discarded if the performance is insufficient. The second condition is the seasonality (or seasonal cycle (SC)) of rainfall extremes. The adequate performance indicates that the RCM was driven by the right convective environment condition and therefore it can be assessed in the next condition. The third condition is the temperature scaling (TS) of sub-daily rainfall extremes. If the capability of the RCM is satisfactory, the RCM was able to simulate the expected intensification of rainfall extremes with high temperatures according to either the C-C or 2-CC rate.

The range of conditions evaluated in the RCM provides guidance to determine the suitability of the RCM prior to recommending its use to investigate sub-daily rainfall extremes. However, the last stage to be considered is that even if these metrics are adequately simulated by the RCM, there may still be some errors in the RCM that can be amended by a post-processing statistical correction method (e.g. bias correction). Once the RCM has been bias corrected, outputs from the RCM can be used, for instance, as input of hydrological models in the estimation of flood risk.

In the case that the RCM fails to reproduce these metrics, the main recommendation it is not to use the RCM to produce projections of rainfall extremes. Rather, efforts should be devoted to understanding the reason for the RCM's poor reproduction of the selected metrics, and where possible identify alternative approaches for simulating extremes (e.g. alternative RCM structures or

statistical downscaling approaches that do not depend on modelled rainfall data) that better capture the key physical processes that lead to the extremes.

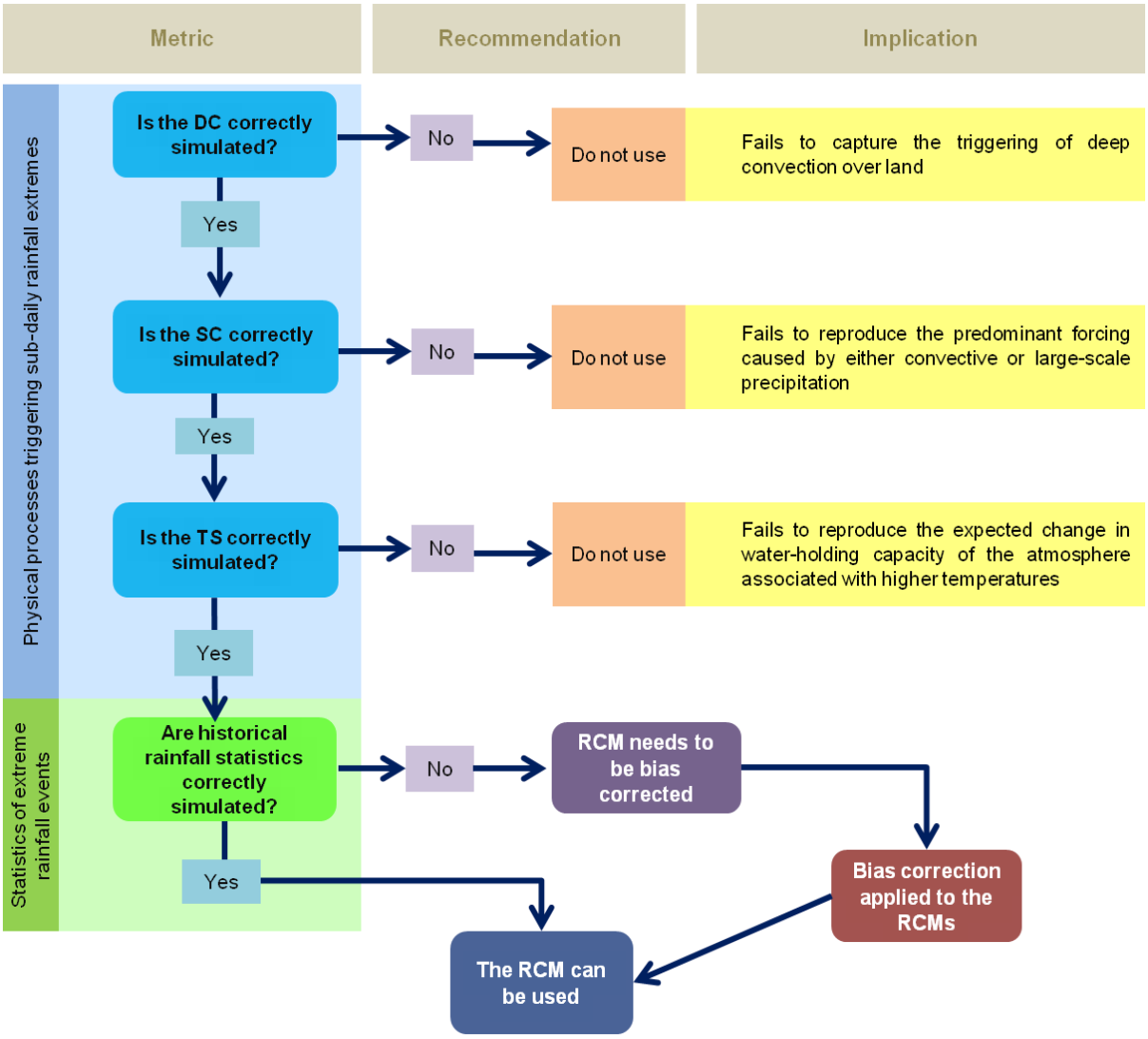

Figure 3.1 **Flow chart that provides guidance to decide whether a RCM can be used to evaluate sub-daily rainfall extremes based on the representation of physical processes relevant to the occurrence of such extremes. These processes included the diurnal cycle (DC), the seasonal cycle (SC) and the temperature scaling (TS) of sub-daily rainfall extremes.**

3.2 Applying the model evaluation strategy to assess the capacity of three RCMs to simulate sub-daily rainfall extremes in the Greater Sydney region

This chapter applies the strategy to evaluate RCMs in reproducing different aspects of sub-daily rainfall extreme events based on the framework described in Figure 3.1. This strategy focused on the ability of the RCMs to simulate:

- the diurnal cycle of rainfall extremes
- the seasonal cycle of extreme rainfall events
- the relationship between sub-daily rainfall extremes and surface temperature
- the observed annual maxima of sub-daily rainfall

The model evaluation was applied to three different configurations of the WRF model (R1, R2 and R3). Simulations were compared with observations for 1-hour, 3-hour, 6-hour and 12-hour durations at 69 weather locations across Greater Sydney during 1990-2009.

In addition, composite maps associated with the 10 most extreme rainfall events between the reanalysis data and model outputs are shown in Appendix 2.

3.2.1 Data from Greater Sydney

Greater Sydney covers all of the Sydney metropolitan area that accounts for around 46 percent of New South Wales population and represents an area of major natural flooding risk since the 1810s (INSW, 2012).

Observational data. Two different sets of data from 1990-2009 were used in the evaluation of RCM simulations. These were:

- Observational records of rainfall and surface temperature at sub-hourly durations from 69 weather stations across Greater Sydney (Figure 3.2) were obtained from the Australian Bureau of Meteorology. The selected datasets consider records with more than 90% of completeness after removing missing or accumulated data and were aggregated into sub-daily durations.
- Datasets of mean sea level pressure and wind (u and v components) fields were obtained from the Climate Forecast System Reanalysis (CFSR) database (Saha et al., 2010) and for selected days associated with the 10 most extreme rainfall events at Sydney Airport (station number 066037) weather station during 1990-2009. Gridded data from the CFSR were extracted for

the 3-hour temporal resolution and 0.5° latitude x 0.5° longitude grid spatial resolution covering the Greater Sydney domain.

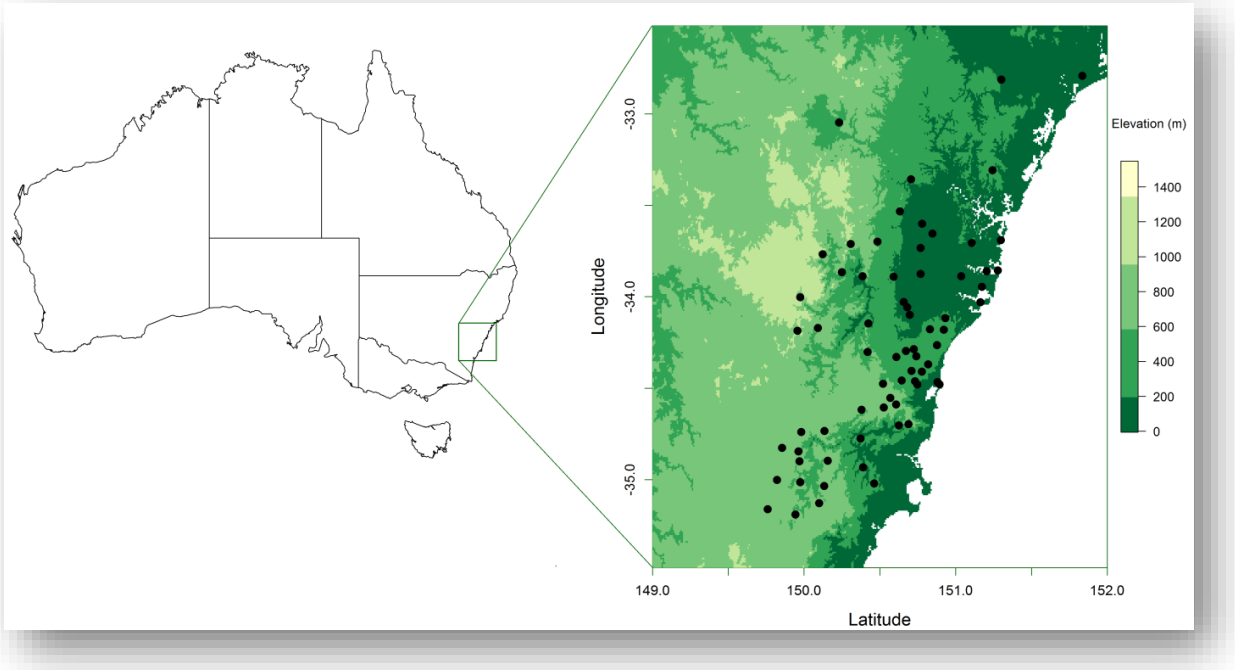

Figure 3.2 Elevation map of Greater Sydney. Black dots indicate the location of 69 weather stations.

3.2.2 Simulations from three RCMs

High-resolution climate modelling datasets from the WRF model (Skamarock et al., 2008) covering Greater Sydney were obtained from the NARCliM project (Evans et al., 2014).

The NARCliM project is a collaboration project between the New South Wales and Australian Capital Territory governments to generate present and future regional climate projections for the CORDEX-Australasia and southeastern Australian regions (domain 1 and domain 2 in Figure 3.3). The latter domain has been of significant interest in the simulation of east-coast lows (Evans and McCabe, 2010; Evans and McCabe, 2013; Evans et al., 2011) that strongly influence the rapid development of storm systems, resulting in heavy rain over southeastern Australia (Speer et al., 2009).

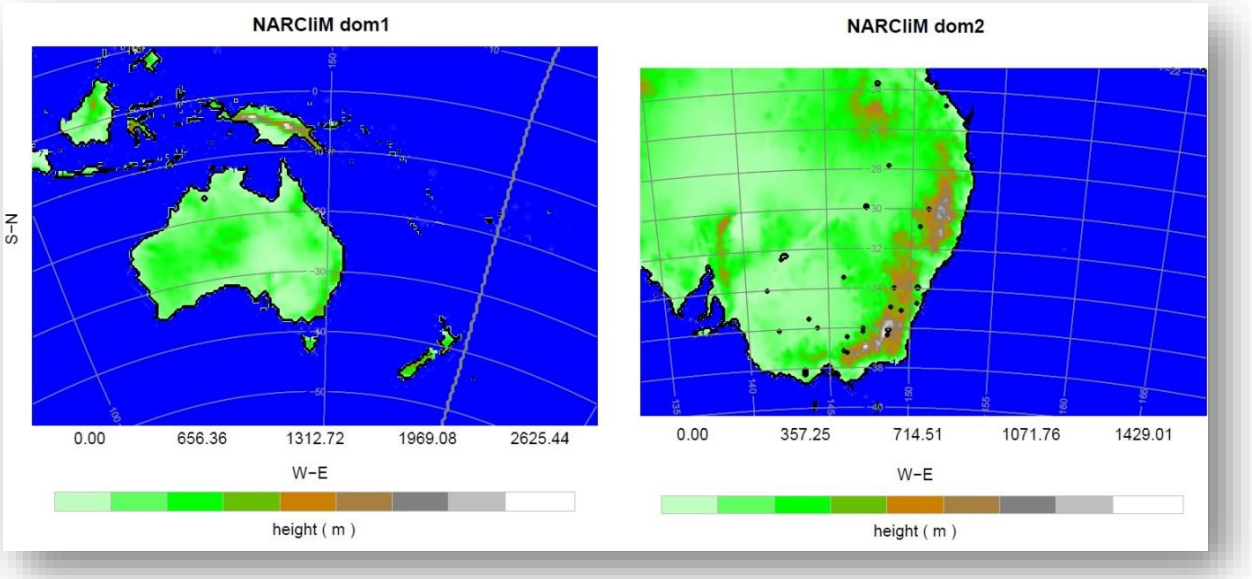

Figure 3.3 **Maps showing the NARCliM domains (Evans et al., 2014). Domain 1 with an outer 50-km-resolution nest (left panel) and domain 2 with an inner 10 km-resolution nest (right panel).**

As part of the NARCliM project four GCMs were selected to be downscaled: MIROC-medres 3.2; ECHAM5; CGCM 3.1; and CSIRO mk3.0. This selection was based on their independence ranking in simulating past and actual climate over southeastern Australia using different climate variables, such as temperature, precipitation, MSLP and 10-metre wind fields, and metrics, such as bias, RMSE, mean absolute error (MAE) and spatial correlation (R). Consideration was also given to their performance in covering the largest range of plausible future climates in Australia (Evans et al., 2014). Moreover, three different configurations of the WRF-RCM were used for the dynamical downscaling of the four GCMs from coarse resolution (~100–300 km) to regional resolution (50km-10 km).

For each RCM, three periods of 20 years were defined:

- historical record (1990-2009)
- near-term prediction (2020-2039)
- long-term projection (2060-2079).

Simulations of the historical record used the 6-hour boundary conditions from the NCEP–NCAR reanalysis project (NNRP) (Evans and Westra, 2012), whereas for future climate projections each of the four selected GCMs provided the boundary condition in the RCMs, under the A2 emission scenario of the IPCC (IPCC, 2007).

Configurations of the WRF model. The advanced WRF model version 3.3 was used for the dynamical downscaling of the GCMs participating in the NARCliM project. The WRF model is a numerical weather prediction (NWP) system suitable for operational weather forecasting and numerous atmospheric research applications (Skamarock et al., 2008). The WRF model was developed by a multi-agency effort of the National Center for Atmospheric Research's (NCAR) Mesoscale and Microscale Meteorology (MMM) Division, the National Oceanic and Atmospheric Administration's (NOAA) National Centers for Environmental Prediction (NCEP) and Earth System Research Laboratory (ESRL), along with other research agencies and organisations (Skamarock et al., 2008).

The WRF model allows the use of multiple combinations of physics and dynamics configurations in the model that make it flexible for use with specific applications, locations and timescales. Another characteristic associated with convective parameterisation is that convection in the WRF model is easily triggered, which does not allow time for the production of the degree of convective energy required for more intense rainfall (Evans and Westra, 2012; Stephens et al., 2010; Sun et al., 2006).

Three different configurations of the WRF model were chosen as the three RCMs studied: R1, R2 and R3. The parameterisations in these models have demonstrated good performance in simulating the historical record of rainfall and other climate variables, such as temperature, pressure and 10-m wind over southeastern Australia (Evans and McCabe, 2010; Evans and Westra, 2012; Evans and McCabe, 2013; Evans et al., 2011).

Table 3.1 describes the three different parametrisations used in the configurations of the WRF. These include the physical schemes for the planetary boundary layer (PBL), cumulus convection, cloud microphysics and radiation used for the three configurations of the WRF model, which differed mainly in the PBL and cumulus convection schemes:

- R1 and R3 used the **Kain-Fritsch** (KF) cumulus convection scheme (Kain, 2004). This scheme triggers convection in an adjacent 60hPa air parcel that generates positive buoyancy and ascends. Thereafter, the updraft, downdraft and entrainment fluxes increase gradually until 90% of the convective availability potential energy (CAPE) is removed. Deep convection is activated when the updraft flux rises upwards until it reaches 3 to 4 km cloud depth.

- R2 used the **Betts-Miller-Janjić** (BMJ) scheme which triggers deep convection using empirically based quasi-equilibrium thermodynamic profiles instead of moist adiabatic conditions (Betts and Miller, 1993). The construction of the profiles and the specification of the relaxation timescale are adjusted for different convective regions, depending on cloud efficiency. This scheme is mainly used to model tropical convection.
- R1 and R2 used the **Mellor-Yamada-Janjić** (MYJ) planetary boundary layer (Janjić, 1994) scheme. This is a one dimensional prognostic turbulent kinetic energy scheme with local vertical mixing that seems to be appropriate for all stable and slightly unstable flows (Mellor and Yamada, 1982).
- R3 used the **Yonsei University** (YU) scheme which is a non-local-K scheme with an explicit entrainment layer and parabolic K profile in the unstable mixed layer (Hong et al., 2006). This type of nonlocal scheme is more applicable to convective-unstable boundary layers.

Table 3.1 The three most independent/best performing configurations for the WRF model over south-east Australia according to Evans et al. (2014).

RCM	Planetary Boundary Layer scheme	Cumulus convection scheme	Cloud microphysics scheme	Short and long-wave radiation schemes
R1	Mellor-Yamada-Janjic (MYJ)/ Eta similarity	Kain-Fritsch (KF)	WRF Double Moment 5-class (WDM5)	Dudhia / Rapid Radiative Transfer Model (RRTM)
R2	Mellor-Yamada-Janjic (MYJ)/ Eta similarity	Betts-Miller-Janjić (BMJ)	WRF Double Moment 5-class (WDM5)	Dudhia / Rapid Radiative Transfer Model (RRTM)
R3	Yonsei University (YSU) / MM5 similarity	Kain-Fritsch (KF)	WRF Double Moment 5-class (WDM5)	NCAR Community Atmosphere (CAM) / CAM

These three different configurations of the WRF model were used to produce a number of key climate variables – rainfall, temperature, MSLP, 10-m wind – at hourly time steps.

3.3 Methods

Testing the capacity of the RCMs to evaluate sub-daily rainfall extremes was undertaken in two parts. The first part compared the metrics characterising the physical processes associated with sub-daily rainfall extremes between RCM simulations and observations. The second part compared the statistics of sub-daily rainfall extremes, such as the annual maxima and 1 in 10-year rainfall event between RCM simulations and observations.

For each of the 69 point locations taken from the observations, the closest grid point (tcg) in the RCM was estimated as:

$$tcg = \min\left[\sqrt{(lat_{obs} - lat_{\mathrm{mod}})^2 + (lon_{obs} - lon_{\mathrm{mod}})^2}\right] \quad \text{(Eq. 3.1)}$$

where min is the minimum of the difference between the latitude (*lat*) and longitude (*lon*) for the observations and RCMs outputs.

Compared to GCM results, the spatial resolution of 10 km in the RCM (grid point) is much closer to the the resolution for each weather location in the observations (Evans and Westra, 2012), there are still likely to be differences in the intensity of extreme rainfall at point locations compared to those at 10km resolution grids. This can be seen by considering areal reduction factors (ARFs) (Stensmyr et al., 2014), which show how the intensity of area-averaged rainfall decreases with increasing area. Nevertheless, the majority of the analysis in this chapter focuses on metrics such as the diurnal cycle, seasonality and temperature scaling, and these issues are less likely to be affected by the modelling resolution.

The processing and statistical analysis of both observations and RCM outputs were carried out within the R environment (http://www.r-project.org).

3.3.1 The diurnal cycle of sub-daily rainfall extremes

Several studies have used the diurnal cycle of rainfall as a test bed for evaluating physical parameterisations in GCMs and RCMs (da Rocha et al., 2009; Evans and Westra, 2012; Jeong et al., 2011; Sato et al., 2009; Walther et al., 2013; Wang et al., 2011). In fact, the diurnal cycle for regional scales in which land-sea and mountain-valley circulation are important needs to be well represented as part of simulating the key processes that lead to precipitation (Nesbitt and Zipser, 2003).Some of the typical characteristics of the diurnal cycle such as its shape, presence of a peak and its timing were examined using the 1-hour annual maxima for both the observations (OBS) and the three RCMs. The diurnal cycle of hourly annual maxima rainfall events (referred to herein as rainfall 'extremes') was estimated) for the entire study region (69 locations across Greater Sydney region) and period (1990-2009), with 1380 events in total for the 20 year period. Thereafter, the number of extreme events occurring at each time of day, OD(t), was calculated using equation 3.2.

The occurrence of extreme rainfall events at time t = 01:00, 02:00… 24:00 hr day, represented as $OD(t)$, is expressed as:

$$OD(t) = \sum_{i=1}^{n} I(T(E_i), t) \quad \text{(Eq. 3.2)}$$

where $T(E_i)$ is the time of occurrence of the i^{th} (i=1, 2,…,n) extreme rainfall event (E_i), n is the total number of extreme events of hourly durations and I is the indicator function:

$$I(T(E_i), t) = \begin{cases} 1 & T(E_i) = t \\ 0 & \text{otherwise} \end{cases} \quad \text{(Eq. 3.3)}$$

where the variation in the value of OD(t) is defined as the diurnal cycle.

This algorithm was applied to examine the diurnal variability of extreme rainfall events from the 69 locations across the study region during 1990-2009 and results are presented in terms of the time of occurrence.

3.3.2 The seasonality of sub-daily rainfall extremes

Rainfall extremes at short duration have a dominant convective origin and often occur during the summer months (warm and wet season). As in the diurnal cycle, the seasonality of rainfall extremes can be used to evaluate the shape and timing of the number of extreme occurrences. The number of extreme events at 1-hour, 3-hour, 6-hour and 12-hour durations was estimated for each season: summer (December–February), autumn (March–May), winter (June–August), and spring (September–November). The seasonality is denoted as OS(s) and is expressed as:

$$OS(s) = \sum_{i=1}^{n} I(S(E_i), s) \quad \text{(Eq. 3.4)}$$

where $s \in$ |spring, summer, autumn, winter|. I is the indicator function as in equation 3.2 and $S(E_i)$ is the season of the occurrence.

The seasonality was estimated for the OBS and the R1, R2 and R3 simulations at 69 locations across Greater Sydney during 1990-2009.

3.3.3 The relationship between sub-daily rainfall extremes and temperature

The methodology of Lenderink and van Meijgaard (2008) was adapted to examine the temperature dependence scaling of sub-daily rainfall extremes. This relationship assumes that the intensity of rainfall extremes increases with warmer surface temperatures following the Clausius–Clapeyron

relation (~7%/°C), assuming that relative humidity is approximately constant and there is not a significant change in the large-scale circulation patterns (Trenberth et al., 2003).

The scaling rate was estimated through the Clausius–Clapeyron equation (Eq. 2.2) for both the observations (OBS) and the three RCM simulations (R1, R2 and R3) during 1990 to 2009. For 1-hour, 3-hour, 6-hour and 12-hour durations, the maximum intensity of rainfall events on each wet duration (defined as rainfall depth > 0.1 mm) was paired with the mean daily temperature. The rainfall-temperature pairs were sorted from low to high temperature and then split into 12 bins, with the same number of elements for each bin.

Both the 99th and 99.9th percentile of rainfall intensity at sub-daily durations and the median temperature (considered as the representative temperature) were estimated for each bin. Then, an exponential regression was applied by fitting a least-square linear regression to the logarithm of the 99th and the 99.9th percentiles of rainfall for sub-daily durations. Accordingly to Hardwick Jones et al. (2010), the rainfall depth is related to the change in temperature ΔT as follows:

$$P_2 = P_1(1+\alpha)^{\Delta T} \qquad \text{(Eq. 3.5)}$$

where P is the rainfall depth and α is the regression parameter equal to 0.068 which is equivalent to the C-C scaling rate (6.8%/°C) at 25°C, obtained from the August-Roche-Magnus approximation (Eq. 2.2).

The regression parameter α, also known as the scaling rate, sets a scale for increasing rainfall extremes about the same rate as the moisture increase with temperature (Trenberth et al., 2003). This regression assumes a constant scaling across temperature, and the slope of the linear regression represents the temperature scaling of sub-daily rainfall extremes, which will be closely examined in the results section.

3.3.4 Statistics of sub-daily rainfall extreme events

The mean of the annual maxima rainfall and the 1 in 10-year rainfall event for 1-hour, 3-hour, 6-hour and 12-hour durations were estimated for both observations and the whole domain in the RCM from 1990 to 2009. The 1 in 10-year rainfall events were estimated by fitting a generalized extreme value (GEV) distribution to the annual maxima.

The R software package '*ismev'* was used for estimating the GEV family of distributions, this function can be expressed as:

$$G(z) = \exp\left\{-\left[1+\xi\left(\frac{z-\mu}{\sigma}\right)\right]^{-1/\xi}\right\} \qquad \text{(Eq. 3.6)}$$

where μ is a location parameter, σ is a scale parameter and ξ is a shape parameter, defined on the set $[z : 1 + \xi(z - \mu)/\sigma > 0]$, where the parameters satisfy $-\infty < \mu < \infty$, $\sigma > 0$ and $-\infty < \xi < \infty$.

The parametric form of the GEV encompasses that of the Gumbel, Frechet and Weibull distributions, including generalized linear modelling of each parameter (see more details in Coles (2001).

The spatial variation in temporal trends for the mean annual maxima of rainfall at sub-daily durations for both observations and RCM simulations was also estimated. The mean annual maxima were fitted to a linear model using the linear regression function *lm* in the R software (http://www.r-project.org).

The use of quantile-quantile plots for the annual maxima of rainfall at sub-daily durations for selected locations in both observations and RCM simulations was also estimated in the R software.

3.4 Results

3.4.1 Is the observed diurnal cycle of sub-daily rainfall extremes realistically reproduced by RCMs?

The number of extreme occurrences expressed as a function of the time of day (given as the local time) was estimated at 69 locations across the Greater Sydney region during the period 1990-2009. Figure 3.4 illustrates the diurnal cycle of the total number of hourly rainfall extremes estimated from the OBS (black line) and the R1(blue), R2(red line) and R3 (purple line).

The occurrence of sub-daily rainfall extremes in the OBS exhibits a clear diurnal cycle which reaches a late afternoon peak (around 5:00 pm local time).

Previous work by Evans and Westra (2012) over southeastern Australia (where Greater Sydney is also included) identified that the diurnal cycle of rainfall as mainly driven by low level thermal convection (generated from surface heating or evaporation), atmospheric instability (energy

available for convection) and low-level (700 hPa) convergence of moisture (feeding moisture into the storm).

When results from R1, R2 and R3 outputs were compared with the OBS, it was found that:

- The peak of extreme occurrences was underestimated around 25% by R1 and occurs one hour later than in the OBS. Moreover, the number of extreme occurrences was overestimated from early night to the noon hours.
- R2 overestimated up to 15% of the peak number of extreme occurrences, and estimated activity occurring two hours later than in the OBS. The number of occurrences in R2 fluctuated; they were underestimated from afternoon to late evening and overestimated until midnight.
- Two peaks of extreme occurrences were found in R3. However, the higher peak underestimated the number of extreme occurrences by approximately 14% and the peak was found up to three hours later than the OBS.

The results overall indicate that R1, R2 and R3 were able to capture reasonably well the observed diurnal cycle of rainfall extremes over the region, with a realistic representation of the amplitude and phase of the diurnal variability of rainfall extremes and timing in the peak of rainfall extreme occurrence. However, some discrepancies in the amplitude of the diurnal cycle and in the delay of timing of the peak occurrence can be attributed to the three different parameterisation schemes used in the configuration of the WRF model (Table 3.1). For instance, the YSU PBL scheme in combination with the KF scheme may influence in the late activation of convection that caused a 3-hour delay in the timing of the peak of rainfall occurrence found in R3.

The total number of wet events (rainfall amount higher than 0.1mm/hour) was also analysed (not shown) for each model simulation and results indicated that the total number of wet events were more frequent than in the observations but less intense. This finding also agrees with a well-known issue in climate models when investigating wet events and it is identified as the “drizzling effect” where climate models tend to overestimate the frequency of light precipitation (0.1mm – 1 mm) and underestimate the intensity of heavy precipitation (Dai, 2006).

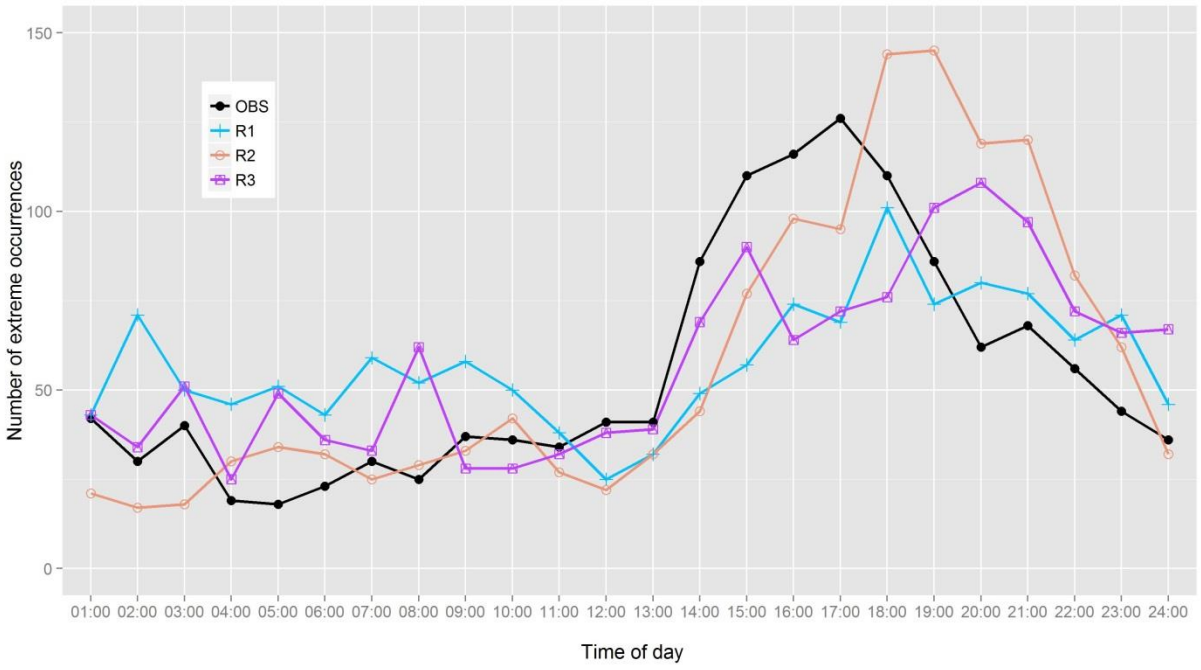

Figure 3.4 **Diurnal cycle of hourly rainfall extremes in the observations (black line) and the R1 (blue line), R2 (red light) and R3 (purple line) simulations for 69 locations across Great Sydney during 1990-2009.**

3.4.2 Is the observed seasonality of sub-daily rainfall extremes realistically reproduced by RCMs?

The seasonal variability or seasonality of the number of extreme rainfall events at sub-daily durations was estimated in the observations (OBS) and RCM simulations at 69 locations across Greater Sydney during 1990-2009. Figure 3.5 shows the seasonality of rainfall extremes at 1-hour, 3-hour, 6-hour and 12-hour durations for both the OBS (black bar) and the R1 (blue bar), R2 (red bar) and R3 (purple bar) simulations.

A recent work by Zheng et al. (2015) suggests that observed hourly rainfall extremes over the same region (Greater Sydney) are mainly of convective origin and summer-dominated, but that for longer duration rainfall extremes are mainly driven by large-scale circulation patterns, such as frontal systems that occur during winter months and along the Australian east coast. In agreement with the previous study, the seasonal distribution of sub-daily rainfall extremes in the observations was characterised by a peak of maxima occurrence during summer months for all durations and the minima occurrence during winter for short durations and during autumn for long durations. When comparing the seasonality of sub-daily rainfall extremes in three RCM-simulations with the OBS, it was found that:

- For the 1-hour duration, the observed peak of maxima occurrence during summer and the minima occurrence during winter is overall well reproduced by all the RCMs. R1 has the best performance in the seasonality of hourly rainfall extremes.
- For the 3-hour duration, the observed peak of maxima occurrence in summer was better simulated by R1; while the minima occurrence in winter was better captured by R3.
- For the 6-hour and 12-hour durations, the observed peak of maxima occurrence in summer was better simulated by R3; while the minima occurrence in autumn was better reproduced by R2.

The results showed that the seasonality of rainfall extremes for short durations was reasonably simulated by R1 and R3. Therefore, it is suggested that the KF convective scheme used in both R1 and R3 was able to capture the dominant thermal convection during summer months. For longer durations, this scheme was also able to simulate the synoptic and mesoscale convergence over the east coast lows during winter months.

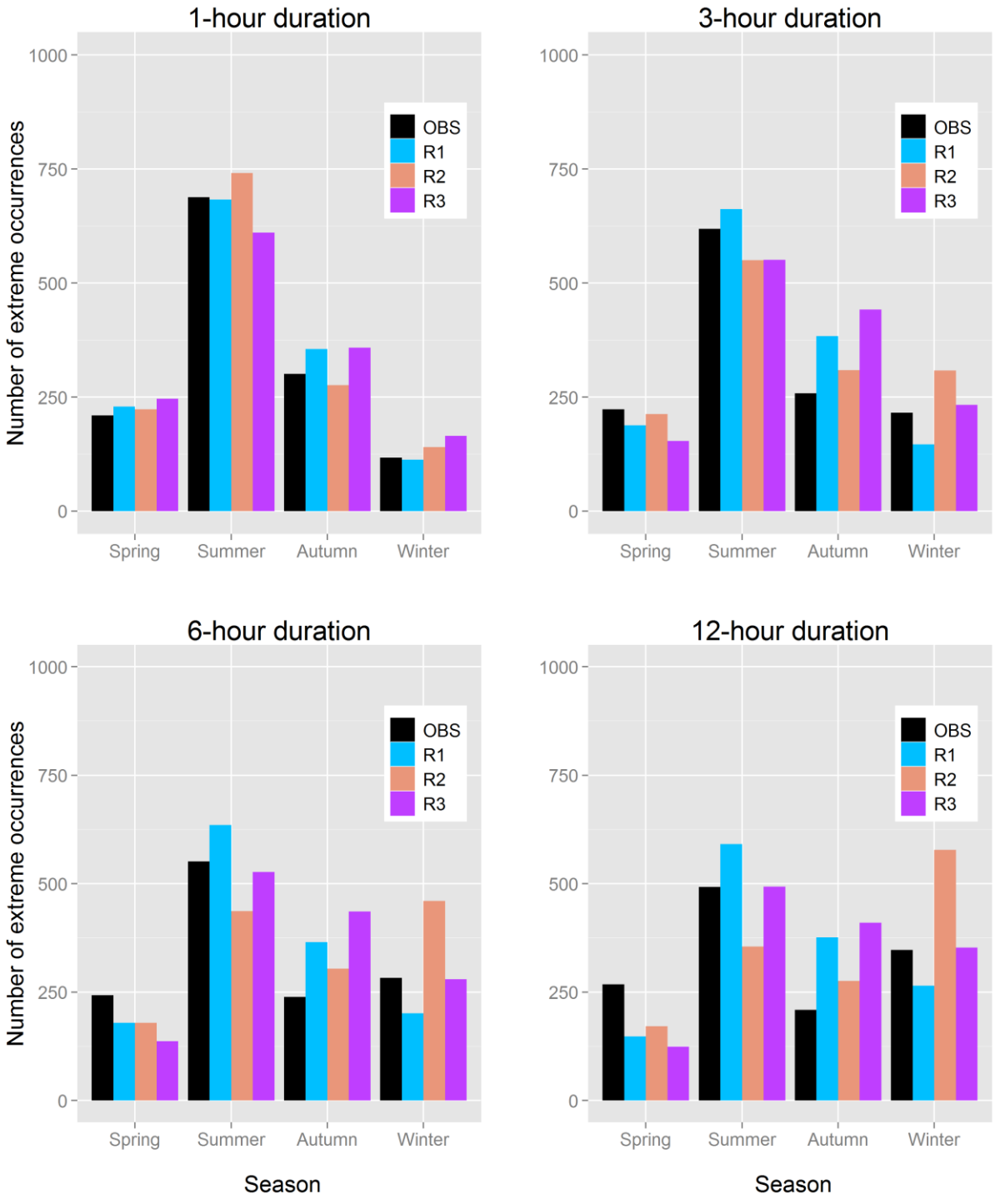

Figure 3.5 **Seasonality of sub-daily rainfall extremes in the observations (black bars) and R1 (blue bars), R2 (red bars) and R3 (purple bars) simulations for 69 locations across Greater Sydney during 1990-2009.**

3.4.3 Is the observed relationship between sub-daily rainfall extremes and temperature reproduced by RCMs?

The exponential regression between the 99th and 99.9th percentiles of sub-daily rainfall and surface temperature was estimated in the OBS and R1, R2 and R3 simulations at 69 locations across Greater Sydney during 1990-2009.

Figure 3.6 illustrates the scaling relationship between 1-hour, 3-hour, 6-hour and 12-hour rainfall extremes and daily mean temperature for both observations (the OBS) and R1, R2 and R3 outputs.

Exponential regression (α) was used to characterise the scaling of rainfall extremes with temperature and then identified scaling rates following the Clausius-Clapeyron principle. Results in the OBS suggest that at hourly durations most locations across Greater Sydney increased following the C-C relationship (~7%/°C) for temperature ranges up to 20°C. This concurs with a previous study by Hardwick Jones et al. (2010) which had found that over the eastern region of Australia the 99th percentile of hourly rainfall intensity scales with the mean temperature.

When the temperature scaling was compared with the OBS, the results indicated that:

- For hourly durations, scaling rates were roughly consistent with the observed C-C rate for R2 and R3 and slightly different in R. These rates approximately followed the C-C rate for temperature ranges up to 16°C, and after this range the scaling relationship decreased with higher temperatures ranges.
- For durations greater than 1-hour, the scaling of sub-daily rainfall extremes was not found in agreement with the OBS.

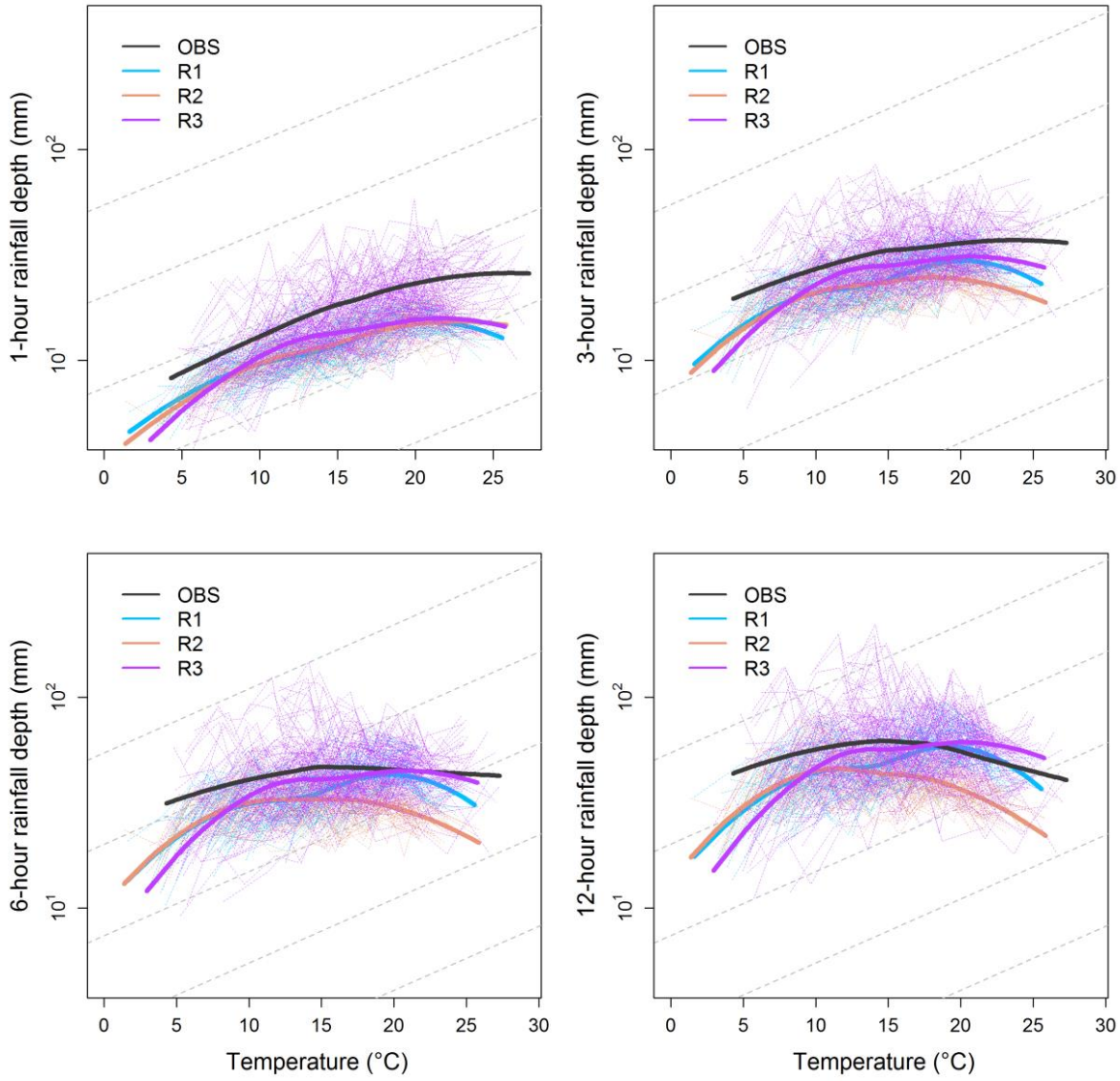

Figure 3.6 **Exponential regression between the 99th percentile of sub-daily rainfall and the surface temperature for both the OBS (black line) and R1 (blue line), R2 (red line) and R3 (purple line) outputs across Greater Sydney region during the period 1990-2009. Dashed grey lines correspond to the C-C rate (6.8%/°C).**

The temperature scaling for the 99.9th percentile was found to be much closer to the C-C scaling rate. Figure 3.7 illustrates the scaling relationship between 1-hour, 3-hour, 6-hour and 12-hour rainfall extremes and daily mean temperature for both observations (the OBS) and R1, R2 and R3 outputs. When the temperature scaling was estimated and compared with the OBS, it was found that:

- The best performance is found at hourly durations for temperature ranges up to 23°C. This scaling is consistent with the observed C-C rate, especially for R3.
- For durations greater than 1-hour, the scaling rates decreased but model simulations were still consistent with observations.

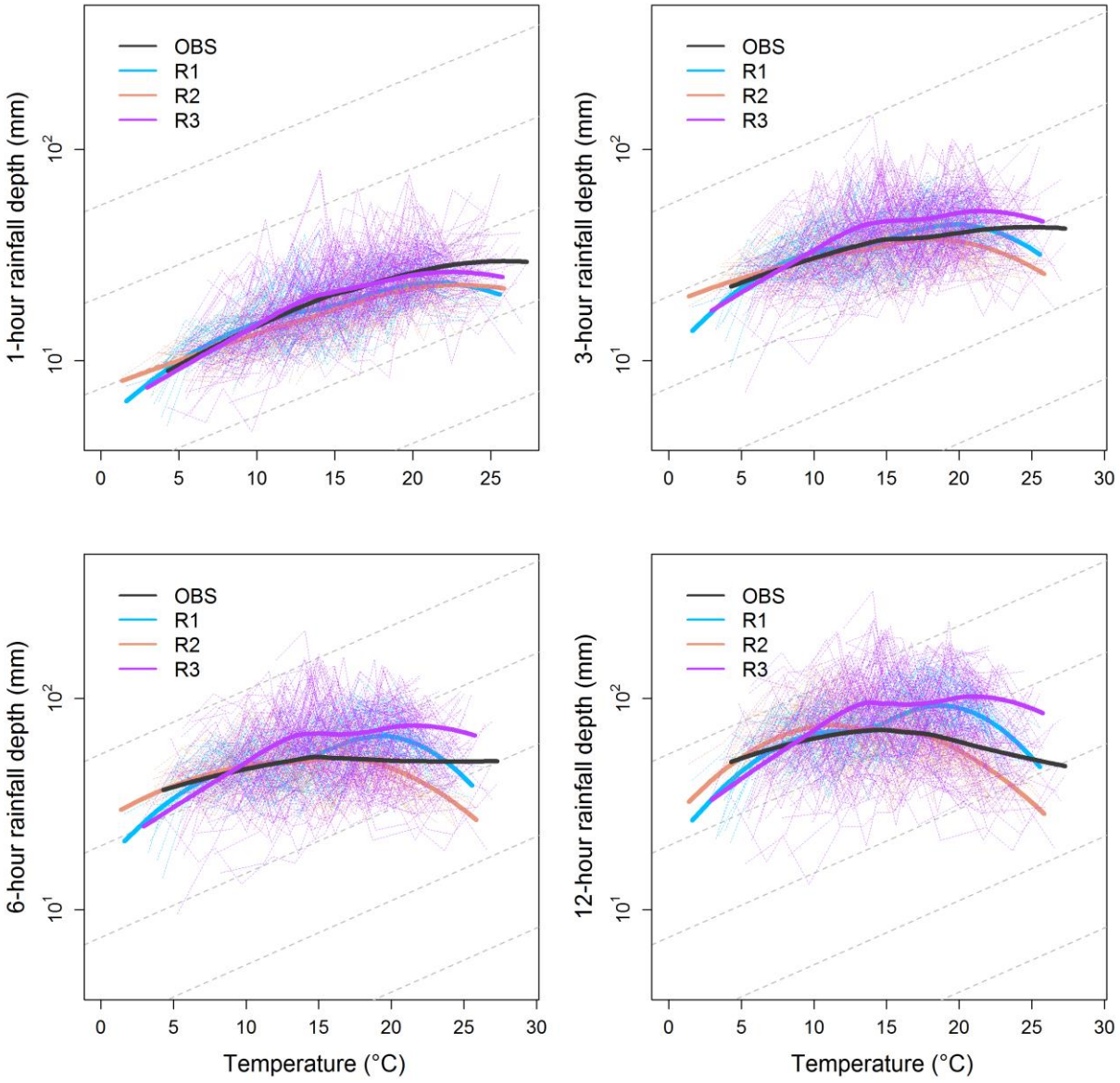

Figure 3.7 **Exponential regression between the 99.9th percentile of sub-daily rainfall on wet days and the surface temperature for both the OBS (black line) and R1 (blue line), R2 (red line) and R3 (purple line) outputs across the Greater Sydney region during the period 1990-2009. Dashed grey lines correspond to the C-C rate (6.8%/°C).**

The scaling parameter (α) in Eq. (3.5) was estimated at 69 point locations in the OBS and the whole Greater Sydney region for R1, R2 and R3 simulations during the period 1990-2009. Figure 3.8 shows the spatial variability of α for 1-hour, 3-hour, 6-hour and 12-hour durations for both observations (circles) and R1, R2 and R3 outputs.

Results in the OBS fitted α values about the C-C rate, particularly over the northern part of Greater Sydney, mainly observed at short durations. For longer durations, the α values declined and also became negative, particularly near the coastline.

Comparing results in the OBS with the fitted α values from R1, R2 and R3, it was found that:

- Noticeable spatial differences were found among the three outputs. Results from R2 and R3 indicated an increase of α values that was also found for longer durations, whereas R1 exhibited the lowest α values over the northern Greater Sydney region.
- For hourly durations, R2 and R3 better represented the spatial variability of the observed α values, particularly over inland areas, while α values were underestimated by R2.
- For longer durations than 1-hour, α values decreased in R1, R2 and R3 as had been found in the observations. However, results in R2 and R3 pointed to an increase in α values along the northern and central inland.

The scaling parameter was approximately reproduced by R2 and R3 for hourly durations. However, at long durations most of the models slightly overestimated but captured the decrease of α values along the coastline.

Results from R1, R2 and R3 suggest that the intensity of rainfall extremes, particularly at hourly durations approximately increased with temperature following the C-C scaling rate, in agreement with a previous study by Hardwick Jones et al. (2010). Although scaling rates close to 2-CC (~14%/°C) were found from 3-hour to 12-hour durations over north inland and ocean parts in R2, the scarcity of observations over those regions limited the evidence to support the simulated 2-CC scaling rate.

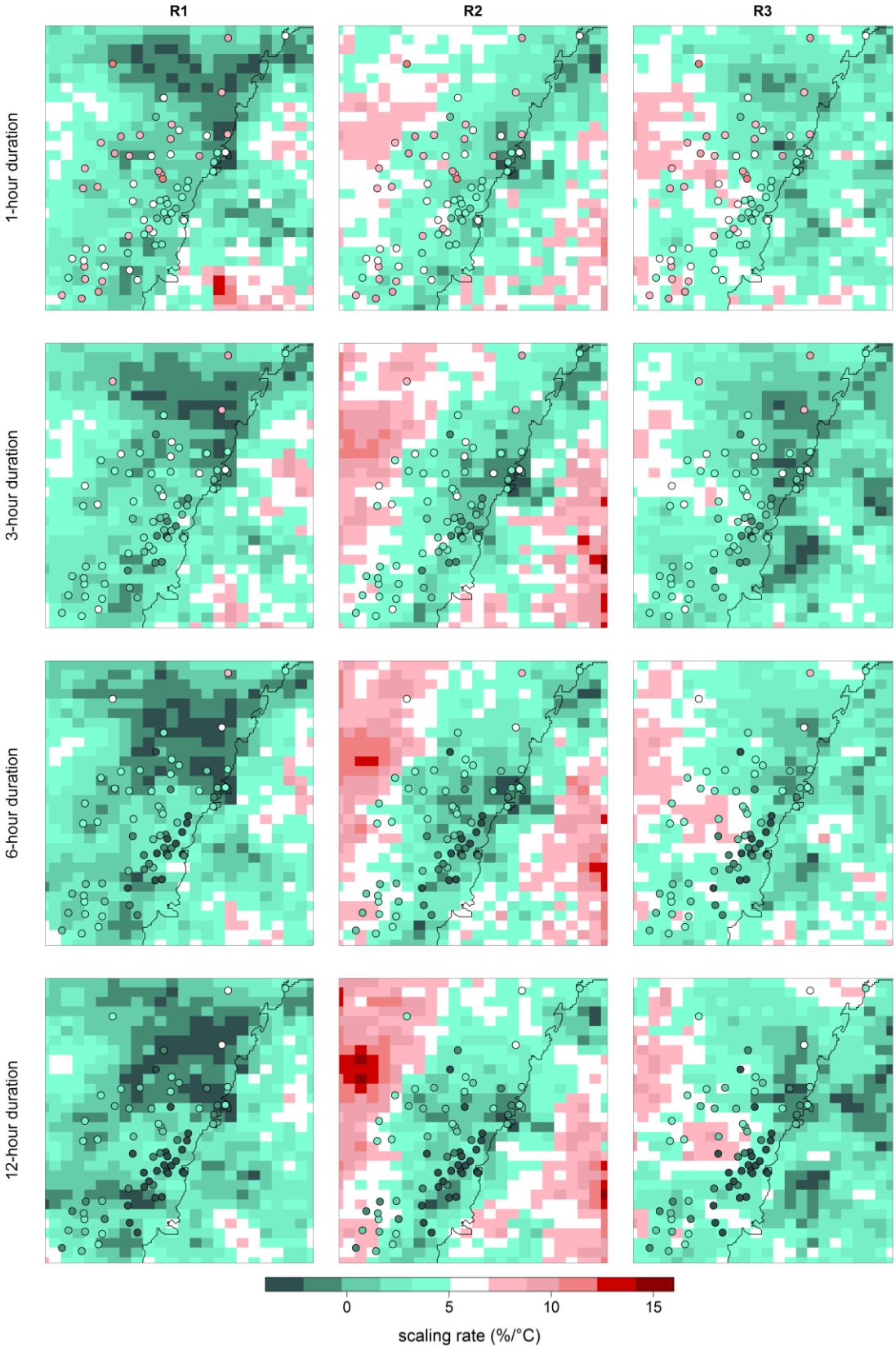

Figure 3.8 **Spatial variability of the exponential regression fitted to 1-hour, 3-hour, 6-hour and 12-hour rainfall extreme between observations (circle) and R1, R2 and R3 outputs. Scaling ranges in green colour indicate values lower than the C-C rate(< 7%/°C), while rates approximately the C-C (~7%/°C) are in white and rates higher than the C-C rate (>7%/°C) are in red.**

3.4.4 Are the statistics of observed sub-daily rainfall extremes correctly reproduced by the three RCMs?

The mean of the annual maxima of rainfall for sub-daily durations in observations at 69 locations across Greater Sydney region was compared with simulations in R1, R2 and R3. Figure 3.9 shows a set of spatial maps of the mean of the annual maxima (rainfall depth in mm) for 1-hour, 3-hour, 6-hour and 12-hour durations in both the observations (circles) and the R1, R2 and R3 outputs during 1990-2009.

Results in the observations showed high rainfall depths near to the coastline (particularly in the centre) and low values over inland regions (especially over the south and centre parts) for most of the durations. When the mean of the annual maxima in the observations was compared with R1, R2 and R3, it was found that:

- The hourly rainfall depth was overall underestimated by the RCMs; R1 and R2 underestimated it by up to 45% and R3 by up to 40%.
- The mean of the annual maxima at 3-hour duration was underestimated by R2 up to 40%, but overestimated by R1 and R3 up to 50%.
- For the 6-hour duration, the rainfall depth was overestimated by R1 and R3 up to 70% but underestimated by R2 up to 40%.
- The mean of the annual maxima at 12-hour duration was overall overestimated for the three RCMs, particularly in R3 and over inland part where the rainfall depth was overestimated more than twice the observations.

The observed mean of the annual maxima was overall underestimated along the coastline and for hourly durations by the three RCMs. R1 and R3 had better spatial consistencies along the coastline; while R2 was able to reproduce the spatial consistency over inland parts for most of the durations.

The mean of the annual maxima of rainfall in the observations was underestimated for short durations (e.g. 1-hour to 3-hour) and mainly overestimated for longer durations (e.g. 6-hour to 12-hour) by the three RCMs. These findings also show that none of the three RCMs was able to fully reproduce the observed sub-daily rainfall extremes over Greater Sydney.

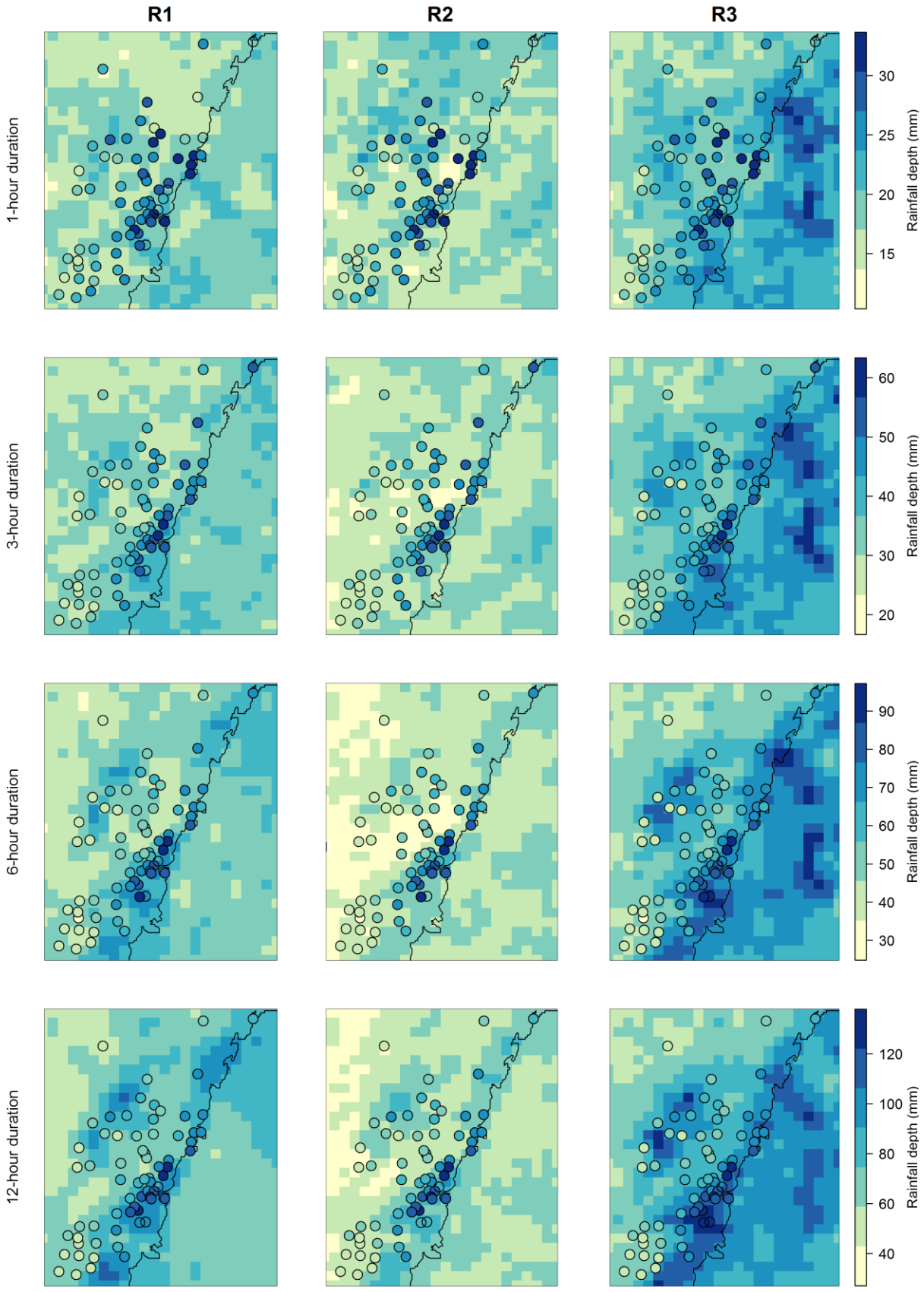

Figure 3.9 **Map showing the mean annual maxima of rainfall for 1-hour, 3-hour, 6-hour and 12-hour rainfall durations from the observations (circles) and R1, R2 and R3 across the Greater Sydney region from 1990 to 2009.**

To provide further insight into the capacity of the three RCMs to capture the IFD relationships, a more detailed investigation into six different sites across Greater Sydney was undertaken by using quantile-quantile (Q-Q) plots.

For six selected sites across Greater Sydney, Figure 3.10 shows a set of Q-Q plots of the annual maxima of rainfall (rainfall depth in mm) for 1-hour, 3-hour, 6-hour and 12-hour durations in R1(blue round points), R2 (red square points) and R3 (purple triangle points). Three sites are located near low-elevation coastal regions (right plots); whereas the other three sites are over inland and two of them are in high elevation parts (left plots).

The magnitude of the annual maxima in the three RCMs was compared using the 45-degree reference black line constructed from the observations at each site. Results showed that rainfall depths were mainly underestimated in low elevation coast parts for most of the durations, especially evident in R2. In contrast, rainfall depths were mainly overestimated for high elevation inland parts and for longer durations, especially evident in R3. The results of the annual maxima of rainfall also suggest that the performance of the different RCMs varied depending on the location (e.g. coastal or inland parts) and duration considered. For instance, the best performance found over low-elevation coastal parts was in R3 for short duration and R1 for longer durations; whereas for inlands part was in R2.

The influence of elevation, latitude and longitude in the spatial properties of sub-daily rainfall extremes are presented and detailed in Section 2.4 of the Appendix. Results from the spatial properties indicated that simulations from R1 had the best performance in capturing the spatial correlation of observed sub-daily rainfall extremes across Greater Sydney.

Additionally, the fitted GEV was scaled at each location by the mean annual maxima over the 20 year period for both the OBS and the three RCMS and then compared with the 1 in 10 year estimate in the growth curve (Supplementary Figure 3 and Supplementary Figure 4).

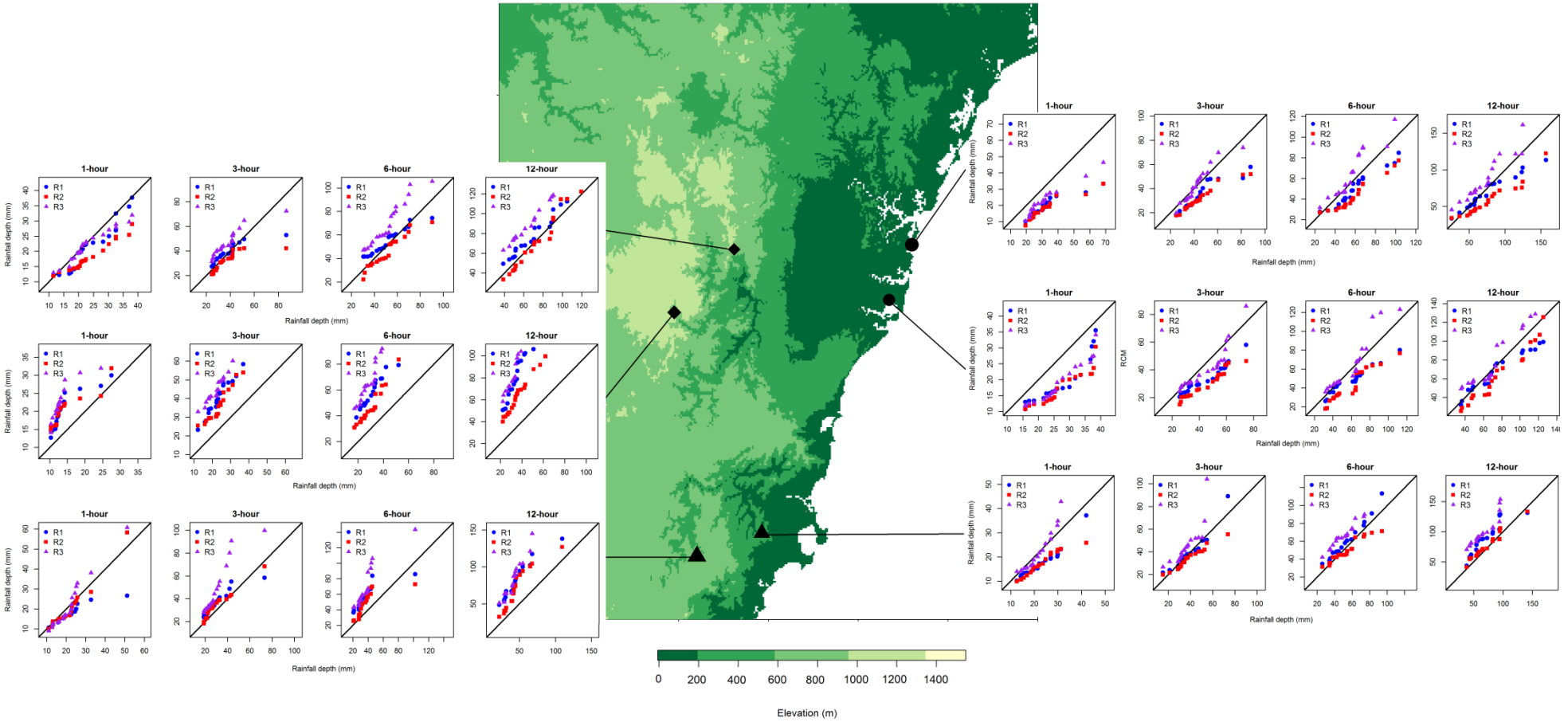

Figure 3.10 **Quantile-quantile plots of the annual maxima of rainfall for 1-hour, 3-hour, 6-hour and 12-hour durations for R1 (blue points), R2 (red points) and R3 (purple points) simulations at six locations across Greater Sydney during the period 1990-2009. The diagonal in the QQ plot represent the normal line in the observations.**

The annual maxima of rainfall for sub-daily durations were fitted to the GEV distribution to estimate the 1 in 10-year rainfall event for 1-hour, 3-hour, 6-hour and 12-hour durations for both the observations and the three RCMs over Greater Sydney. Figure 3.11 shows the spatial distribution of the 1 in 10-year rainfall event (also rainfall depth in mm) in the observations (circles) and the R1, R2 and R3 outputs over Greater Sydney region during 1990-2009.

Results in the observations showed high rainfall depths near to the coastline (particularly over the centre parts) and low rainfall depths over south and centre inland parts. When the observed rainfall depths for the 1 in 10-year rainfall event were compared with simulations in R1, R2 and R3, it was found that:

- For 1-hour duration, rainfall depths were overall underestimated by the three RCMs. R1 and R2 underestimated the rainfall depth up to 60% along the coastline, whereas R3 underestimated it up to 40% over inland parts.
- For 3-hour duration, rainfall depths were overestimated by R1 and R3 up to 60% over inland parts and underestimated by R2 up to 40% along the coast.
- For 6-hour duration, the intensity of the 1 in 10-year rainfall event was overestimated by R1 and R3 and underestimated by R2. R3 overestimated the intensity of rainfall up to 65%, whereas R2 underestimated it up to 45% over inland parts.
- For 12-hour duration, the intensity of the 1 in 10-year rainfall event was mainly overestimated by R3 and R1 and slightly underestimated by R2. R3 overestimated the intensity of rainfall for most locations and up to 80% over inland parts, whereas R2 underestimate the intensity of rainfall up to 30% along the coastline.

The rainfall depth for the 1 in 10-year rainfall event was overall underestimated by the three RCMs for hourly durations but overestimated for longer durations. R2 tended to underestimate the 1 in 10-year rainfall events over coast parts for all durations; while R3 tended to overestimated rainfall depths near the coastline for most of the durations. Similar to the mean of the annual maxima, these finding indicate that none of RCMs over-performed the observed sub-daily rainfall extremes over the region.

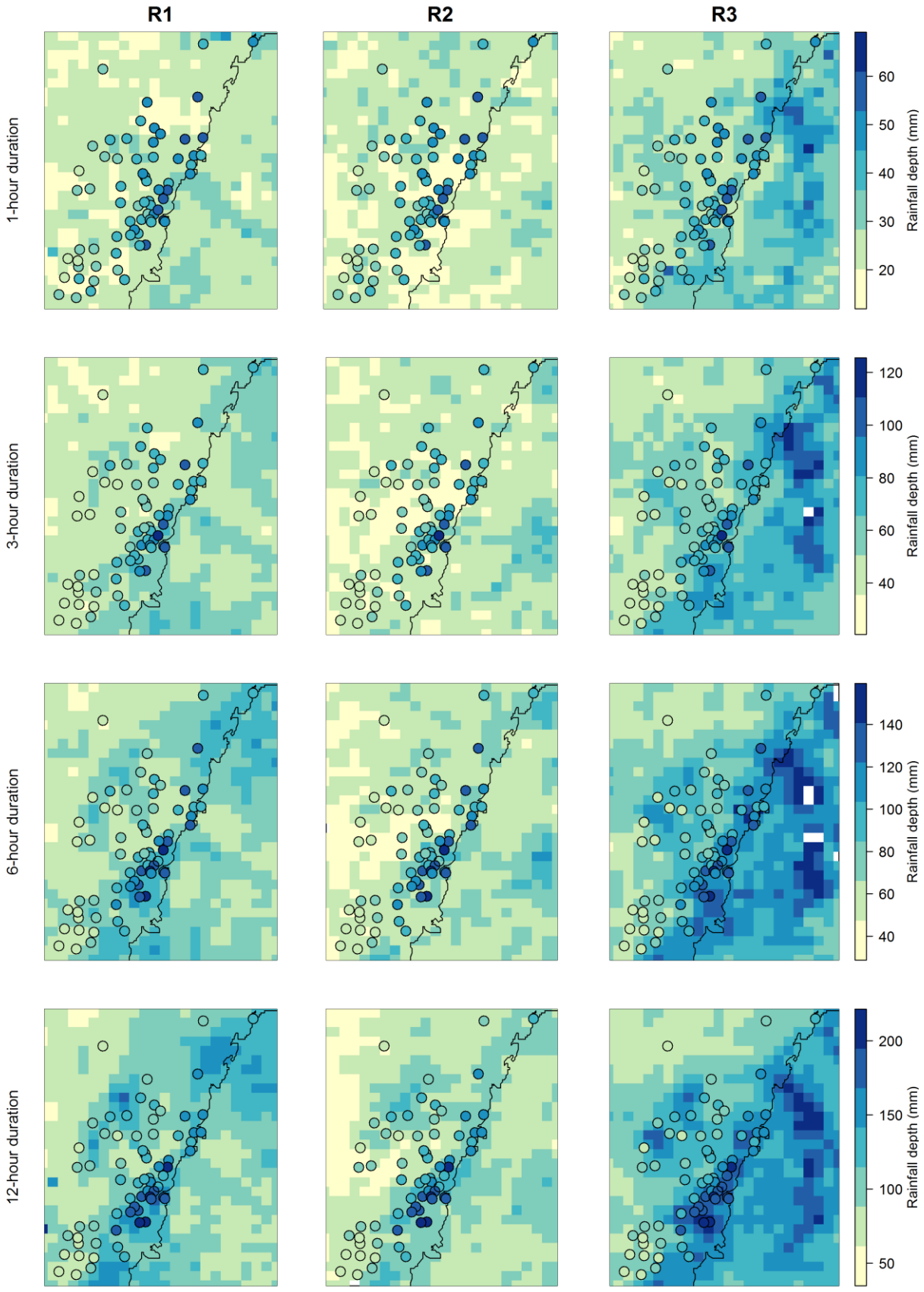

Figure 3.11 **Map showing the 1 in 10-year extreme rainfall event estimated by fitting the GEV distribution to the observations (circles) and to simulations for the R1, R2 and R3 over Greater Sydney region from 1990 to 2009.**

The annual maxima of rainfall for 1-hour, 3-hour, 6-hour and 12-hour durations were also fitted by a linear regression, in which the slope of the fitting was used for characterising the trend of annual maxima in the observations (circles) and in simulations for the three RCMs during 1990-2009 over Greater Sydney region, as shown on a spatial map in Figure 3.12.

Results in the observations showed that the trend of annual maxima of sub-daily rainfall was mostly positive, particularly over inland parts and for short durations (e.g. 1-hour and 3-hour); while the trend was negative for longer durations (e.g. 6-hour and 12-hour), particularly in the centre coast parts. These results also agreed with a previous study by Zheng et al. (2015) in which the trend of the annual maximum decreased for durations longer than 3 hours.

When the spatial trend in the observations was compared with the three RCMs, it was found that:

- The trend of annual maxima of rainfall at hourly durations and for most locations was mainly underestimated by R1 and R2. The observed trend was overall positive and better reproduced by R2 and R3, especially along the coastline.
- The trend of annual maxima at 3-hour durations was underestimated by R1 and overestimated by R2 and R3, particularly in the centre coast. The observed trend was mainly positive over inland parts (captured by R2 and R3) and negative along the coastline (captured by R1).
- The trend of the annual maxima at 6-hour duration was mainly overestimated by the three RCMs, especially near to the coastline. The negative trend of the annual maxima along the coastline was mostly captured by R1.
- The trend of the annual maxima at 12-hour duration was overall overestimated by all RCMs. R1 and R3 overestimated the negative the trend along the coastline and R2 significantly overestimated the trend over centre inland and coast parts.

The results in the three RCM showed spatial variation in the trend of annual maxima with mostly overestimations for 3-hour to 12-hours durations. The observed negative trend along central and south costal parts and for longer durations was captured by R1 and R3 but not reproduced by R2, which instead tended to highly overestimate the trend. Moreover, when the trend of annual maxima of rainfall extremes in the RCMs was closely examined, results indicated that the linear trend was only significant for approximately eight sites across Greater Sydney (not shown).

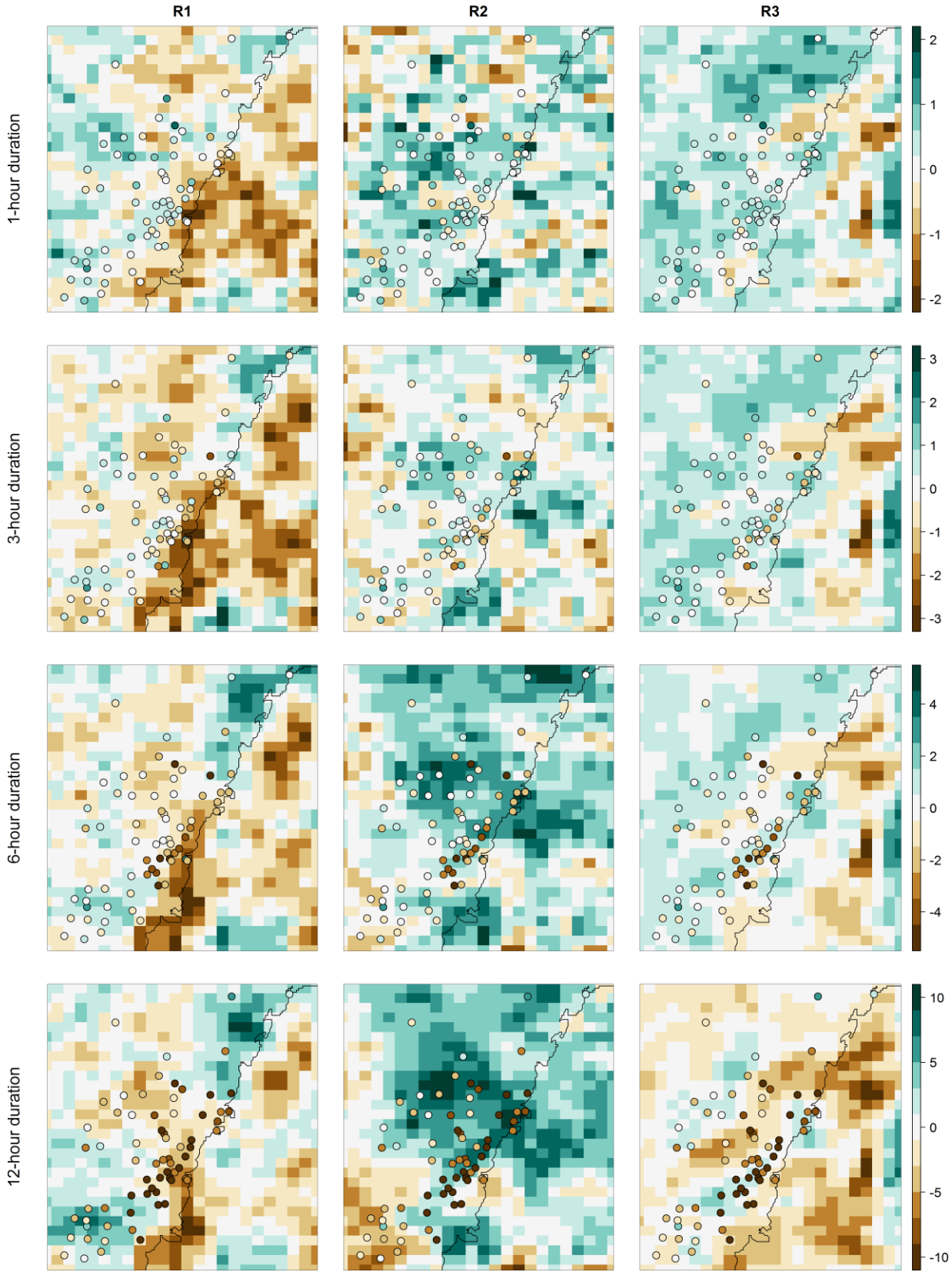

Figure 3.12 **Trend of annual maxima for 1-hour, 3-hour, 6-hour and 12-hour durations for the observations (circles) and R1, R2 and R3 simulations at Greater Sydney during the period 1990-2009.**

Overall, these results indicate that the duration and location considered significantly influenced the performance of RCMs, with some models performing better for certain parts and durations. However, the statistics applied to sub-daily rainfall extremes did not provide insight into whether the RCMs are getting the intensity of rainfall extremes due to the right representation of the underlying physical processes that lead to the occurrence of such extremes or whether RCMs outputs are suitable for predicting future changes in sub-daily rainfall extremes. For this reason, the implementation of evaluation metrics characterising the relevant physical processes of sub-daily rainfall extremes is presented in the following section.

3.5 Summary and conclusions

A strategy to evaluate RCMs in simulating sub-daily rainfall was described in this chapter. This strategy was used to evaluate different aspects of sub-daily rainfall extremes using three different configurations of the WRF model (R1, R2 and R3) over Greater Sydney during 1990-2009.

This chapter explored the performance of WRF in simulating sub-daily rainfall extremes using both direct statistical measures of sub-daily rainfall, and indirect measures (i.e. the diurnal cycle, seasonal cycle, temperature scaling and large-scale synoptic patterns) that indicate whether the model correctly simulates the physical processes that lead to the climate extremes. Commencing with the direct measures, the results are summarised as follows:

- The observed magnitude of the mean annual maxima of rainfall and the 1 in 10-year rainfall event was underestimated for short durations by the three RCMs. However, for longer durations the observed rainfall depth was better reproduced along the coastline by R3.
- The change from positive to negative in the observed trends of annual maxima was partially captured and mainly overestimated by the three RCMs. However, the negative trend for longer durations was better simulated by R1.
- The use of Q-Q plots for the annual maxima showed significant differences in the performance of the different RCMs, which depended on the location and duration considered.
- The overall statistics of sub-daily rainfall extremes were partially reproduced by the RCMs, although none of the RCMs was superior for all the durations and analysis considered.

Applying the flow chart articulated in Figure 3.1, the generally poor performance in simulating the direct statistics of sub-daily extremes would suggest that bias correction would be necessary in order to use the extremes data for developing future projections; however, this should only be undertaken

provided that the model shows sufficient performance in the set of physically based metrics described in Section 3.1.

The outcomes of the analysis are as follows:

- The observed diurnal cycle of hourly rainfall extremes was overall well captured by the three RCMs with a late evening peak of rainfall extreme occurrence, although the timing of the peak was delayed up to three hours.
- The observed seasonality of rainfall extremes was overall well simulated by the three RCMs, particularly for short durations. However, the RCMs failed in capturing the highest occurrence of rainfall extremes during winter and the lowest during summer across Greater Sydney.
- The temperature scaling rate was overall reproduced, particularly at hourly durations when the temperature scaling in the observations was clear. Moreover, the temperature scaling in hourly simulations became closer to the observations when the 99.9th percentile of sub-daily rainfall was analysed. The scaling rate from the RCMs approximated the CC rate for hourly durations, whereas scaling rates much lower than the C-C rate were found for longer durations.

Based on these results, it can be concluded that although R1, R2 and R3 performed differently for the statistics of sub-daily rainfall extremes, with mainly underestimations at short durations and overestimations at longer durations, the underlying physical processes were overall realistically simulated by these models. This suggests that the RCM simulations might remain useful for investigating potential changes in sub-daily rainfall extremes, as will be explored in the following chapter.

Chapter 4. Exploring future changes in sub-daily rainfall extremes using RCMs over Greater Sydney

There is growing scientific evidence that global warming resulting from high emissions of GHGs, has contributed to the increase in the intensity and frequency of rainfall extremes, particularly at short durations (Hanel and Buishand, 2010; IPCC, 2013; Lenderink and van Meijgaard, 2008). Indeed, this increase is expected to continue with a future warmer climate, enhancing the flood risk in small urban and rural catchments susceptible to flash flooding, with devastating socio-economic and environmental impacts.

Long term projections of short-duration, flood-producing extreme rainfall events represent an important source of the types of information that are required for informing decisions related to mitigation and adaptation to climate change (Kendon et al., 2008). Long term projections of extreme weather events, such as severe rainfall, are vital to the development of meaningful rural and urban planning policies, for example the design of flood defences and general engineering infrastructure (Maraun et al., 2010).

However, the large uncertainties associated to future changes on GHGs, population growth and development and land use, represent a big challenge for projecting changes to flood risk based only on historical records. Therefore, it is important to consider results from observational, modelling and theory studies, with a focus on the physical processes, in order to understand how the intensity of sub-daily extreme rainfall might respond to a warmer climate (Westra et al., 2014b).

4.1 Future changes in rainfall extremes: Temperature, season and region

As temperature increase, the risk of flooding due to short-duration extreme burst rainfall is expected to increase with future climate (Conrad and Ashish, 2015; Hurkmans et al.). Given the short and intense nature of these bursts, convective rainfall such as summer downpours are the dominant rainfall type in relation to urban flooding, as revealed by high resolution RCMs (Gregersen et al., 2013; Kendon et al., 2014).

RCMs are like to remain the main source of information for future projections of changes in sub-daily extreme rainfall and therefore it will be required to study not only quantities and trends but also

to explore different aspects of sub-daily rainfall extremes associated to the physical mechanism and theories that can provide insight about likely changes, as found in the previous chapter.

4.1.1 The response of rainfall extremes to increased temperature

The relationship between rainfall intensity and atmospheric temperature provides a theoretical basis for the intensification of rainfall extremes with future changes in climate (Allen and Ingram, 2002; Trenberth, 2011). Rainfall extremes are expected to increase with higher atmospheric temperature because a warmer atmosphere can hold more moisture, which will eventually fall as rain. Two mechanisms are commonly thought to be important in determining future changes to extreme rainfall – the water-holding capacity of the atmosphere, and the dynamics of storm-generating systems:

- The water-holding capacity of the atmosphere will increase at the rate of approximately 7%/°C, predicted by the Clausius–Clapeyron (C-C). It is commonly assumed that the rainfall rate will increase in proportion to this rate, at least under conditions when the influence of dynamics and precipitation efficiency are not significant (Trenberth et al., 2003).
- Rainfall extremes can also increase more rapidly than the C-C rate, with rates up to double the C-C rate (super C-C) due to increases in precipitation efficiency with warming (Singh and O'Gorman, 2014). Changes in the dynamics of the atmosphere and the convective cloud, the size of the convective cloud, and the moist adiabatic temperature profile will also contribute to extreme rainfall events (Trenberth et al., 2003, O'Gorman and Schneider, 2009).

The notion that the C-C rate might constrain future changes in rainfall extremes (particularly at short duration) has assumed similar atmospheric conditions to the present climate, such as fairly constant relative humidity and no significant changes in the large-scale atmospheric circulation, but with higher temperatures and specific humidity values (Lenderink and van Meijgaard, 2008). By contrast, Lenderink and van Meijgaard (2008) found that hourly rainfall extremes increase by about twice the C-C rate in some regions in central Europe because the increase in latent heat release appears to intensify low-level moisture convergence in convective rainfall, giving rise to the greater C-C rate.

This accords with a recent study from Harding and Snyder (2015) indicating that in regions and seasons governed by dynamically derived convective rainfall, changes in rainfall extremes cannot be solely predicted by the general thermodynamic contribution, because at mid-latitudes in summer,

extratropical rainfall extremes from mesoscale convective systems (i.e., cyclones and fronts) predominate; therefore, the contribution of the scaling is less significant (O'Gorman, 2015).

4.1.2 Future changes in rainfall extremes with significant regional and seasonal variations

Future predictions from climate models suggest changes in the intensity and frequency of rainfall extremes associated with differences in the duration, location and season of the year. For example, a very high resolution model suggests a future intensification of hourly rainfall extremes during summer, which are expected to increase at the end of the 21st century over the UK (Kendon et al., 2014).

Results from model simulations also indicate that more intense rainfall extremes might be related to the early onset of convection in spring (warm season) over tropical regions (Trenberth, 2011). However, this early onset can enhance the chance of drought in early summer (August–September) in regions such as the North Central US (Harding and Snyder, 2014).

The frequency of extreme rainfall is expected to increase in high latitudes and tropical regions and in winter in the northern mid-latitudes (IPCC, 2012). For example, future scenarios of daily rainfall extremes, based on the HadCM3 and ECHAM5 GCMs over Sweden, show a general increase in the frequency of wet days during winter and a decrease in summer, using the 90th percentile of rain day amounts (Chen et al., 2015).

High resolution climate models. RCMs are one of the primary tools for investigating changes in rainfall extremes in the future because they have demonstrated the capacity to reproduce past records at daily (Buonomo et al., 2007; Durman et al., 2001; Fowler et al., 2005; Frei et al., 2006) and sub-daily durations (as shown in the previous chapter), and this has increased confidence in their use for future projections (Chan et al., 2014; Gregersen et al., 2013).

However, the ability of RCMs to reproduce past and present records may not be a sufficient indicator of the capacity of RCMs to operate effectively in a period of climate change in the future. Therefore, both the thermodynamic contribution and regional and seasonal changes are important features for providing insight into possible future changes in sub-daily rainfall extremes. The validity of such features in the circumstances of future climate change using RCMs is the focus of this chapter.

4.2 Future changes in sub-daily rainfall extremes using RCMs

Results from the three different configurations of the WRF model (R1, R2 and R3) demonstrated an overall reasonable performance in reproducing the physical processes of sub-daily rainfall extremes over Greater Sydney, as described in Section 3.4. This capability in model simulations was considered satisfactory to use RCMs projections to explore future changes in sub-daily rainfall extremes, although it was anticipated that some discrepancies in the models will remain for future projections, for example negative bias in the intensity of rainfall extremes, and therefore historical simulations were compared with two future simulated periods within the model domain.

RCM simulations of the future climate were obtained from the NARCliM project (Evans et al., 2014) and forced by the GCM-MIROC under the A2 high emission scenario of the IPCC (IPCC, 2007). Future simulations correspond to the near-term prediction (*2020-2039*) and long-term projection (*2060-2079*) periods that were also compared with the historical period (*1990-2009*) in model simulations over Greater Sydney.

4.2.1 Data

As in the previous chapter, hourly model outputs for Greater Sydney were obtained from the NARCLIM project (Evans et al., 2014), for the near-term and long-term future periods. R1, R2 and R3 also correspond to three different physics scheme configurations of the WRF model as described in Table 3.1.

For future projections, the lateral boundary condition for the three RCMs was provided by the GCM Model for Interdisciplinary Research on Climate (MIROC) version 3.2. The MIROC 3.2 is one of five GCMs participating in the NARCliM project, and was chosen for use in this current study because of its high independence ranking when simulating past climate records over south-east Australia (Evans and Ji, 2012).

The historical period in the RCMs. Hourly outputs of temperature and rainfall from R1, R2 and R3 during 1990-2009 over Greater Sydney, described in Section 3.2.4, were used as a baseline.

Future projections in RCMs. Hourly simulations of temperature and rainfall in R1, R2 and R3, but for the near-term prediction (2020-2039) and long-term projection (2060-2079) periods under the A2 emission scenario of climate change, were used for investigating potential future changes in sub-daily rainfall extremes over Greater Sydney.

The main differences between the historical period and both future periods in the three RCM simulations are outlined in Table 4.1.

Table 4.1 Differences between the historical, near-term and long-term future simulations in the RCMs

Period	Period name	Lateral boundary condition in the three RCMs	Future GHGs emission scenario
1990-2009	historical	NNRP	NA
2020-2039	near-term future	MIROC 3.2-medres	A2 emission scenario
2060-2079	long-term future	MIROC 3.2-medres	A2 emission scenario

For each RCM (R1, R2 and R3), model simulations were named accordingly to the simulated period (e.g. R1 1990-2009).

4.3 Methods

The potential influence of future climate change in some of the well-established features of sub-daily rainfall extremes reproduced by the three RCMs during the historical period are investigated for the near-term and long-term future periods, and these include:

- the diurnal cycle of hourly rainfall extremes
- the seasonality of sub-daily rainfall extremes
- the intensification of sub-daily rainfall extremes with temperature
- the annual maxima of sub-daily rainfall extremes.

These features that are associated to changes in sub-daily rainfall extremes were also investigated for 69 locations across Greater Sydney (Figure 3.2) and for the entire domain in the simulations (only for the temperature scaling and the annual maxima of rainfall extremes).

4.3.1 Future changes in the diurnal cycle of sub-daily rainfall extremes

In Chapter 3, it was reported that the occurrence of hourly rainfall extremes over Greater Sydney exhibits a clear diurnal cycle with a late afternoon peak as a result of thermal convection and this feature was mostly captured by the three RCM simulations, although the timing of the peak occurrence was offset up to 3 hours later than in observations in one of the RCMs. Despite this, the overall performance of the RCMs is considered sufficient to investigate the influence of future climate change on the diurnal cycle of hourly rainfall extremes.

The diurnal cycle of hourly rainfall extremes was explored for the near-term prediction and the long-term projection periods and compared with the historical period at 69 grid points (corresponding to the same location of observations used in Chapter 3) across Greater Sydney.

The annual maxima of hourly rainfall extremes were distributed in terms of the time of day to estimate the total number of extreme occurrences, as in Eq. 3.3 (Section 3.3.1). For each RCM, the diurnal variability and peak of rainfall extreme occurrence were analysed during the near and long-term future projections and then compared with the historical period in simulations.

4.3.2 Future changes in the seasonality of sub-daily rainfall extremes

Observations of the seasonality of the sub-daily rainfall extremes in Greater Sydney during 1990-2009 revealed the highest occurrence of extremes during the warm summer season, likely resulting from convective thunderstorms over the region.

This seasonal feature was better captured by hourly simulations than by longer durations in R1, R2 and R3 during the historical simulated period. Therefore, the three RCMs were considered as tools to investigate the likely influence of future climate change on the seasonality of sub-daily rainfall extremes over Greater Sydney.

The seasonality of rainfall extremes for future simulations was estimated as in Section 3.3.2 The annual maxima of rainfall extremes at sub-daily durations were distributed by season (i.e., summer, autumn, winter and spring) in order to estimate the total number of extreme occurrences in each season for 69 locations across Greater Sydney, as in Eq. 3.4. The seasonality of sub-daily rainfall

extremes for the near-term and long-term future periods was compared with the historical period for the three RCMs.

4.3.3 Future changes in the scaling of sub-daily rainfall extremes with temperature

The increase of sub-daily rainfall extremes with temperature found in observations of weather in Greater Sydney is considered to be a robust concept by which to investigate future likely changes in sub-daily rainfall. This relationship was estimated for the near-term prediction and long-term projection periods at 69 grid points across Greater Sydney for R1, R2 and R3.

The scaling rate and exponential regression were estimated as in Section 3.3.3. The exponential regression was fitted to both the 99th and 99.9th percentile of sub-daily rainfall and the mean daily temperature using Eq. 3.5. Then, the α fitting was again used to characterise the scaling rate during the future simulated periods, and then to compare them with values obtained during the historical period in three RCMs.

4.3.4 Future projections in the annual maxima of sub-daily rainfall extremes

The mean annual maxima of rainfall for 1-hour, 3-hour, 6-hour and 12-hour durations were estimated in the R1, R2 and R3 simulations for the entire domain of Greater Sydney, for near-term and long-term future periods. Then, the ratio of the magnitude of the mean of the annual maxima of rainfall between both *future* periods and the *historical* period was estimated as:

$$ratio = \frac{mean \quad annual\max_{future}}{mean \quad anual\max_{historical}} \qquad \text{(Eq. 4.1)}$$

The ratio was also estimated for each grid point in the model and then compared with the historical period using simulations (baseline) for the near-term future period and the long-term future period in the three RCMs.

4.4 Results

4.4.1 Is the diurnal cycle of rainfall extremes for future projections changing from the historical period in simulations?

The diurnal cycle of hourly rainfall extremes was estimated for the near-term and the long-term future periods, and then compared with the historical period in three RCMs. Figure 4.1 shows the simulated diurnal distributions of the total number of extreme rainfall events at 69 locations across Greater Sydney for the historical period, the near-term and the long-term future periods.

The results from the three RCMs and for the three simulated periods indicated that:

- Extreme rainfall events exhibited a strong diurnal variability, but usually with a late afternoon peak, which agreed with results from the observations shown in the previous chapter.
- The R1 simulations exhibited a late afternoon peak with the highest diurnal peak reached by the long-term future period (Figure 4.3 top panel).
- The R2 and R3 simulations also exhibited a late afternoon peak but with the highest diurnal peaks reached during the near-term future periods (Figure 4.3 middle and bottom panels).
- Comparing the diurnal cycle of hourly rainfall extremes for future and past simulations, it was found that there were no significant changes in the shape or amplitude of the diurnal cycle for the two future simulated periods (2020-2039 and 2060-2079) in comparison with the past period (1990-2009).

The results suggest that the strong diurnal cycle of rainfall extremes found in the simulations was not influenced by the increase of GHGs emissions in future periods, and according to results from the three RCMs, local rainfall extremes might still be dominated by convective rainfall with a late afternoon peak of rainfall extremes occurrences for the region of Greater Sydney.

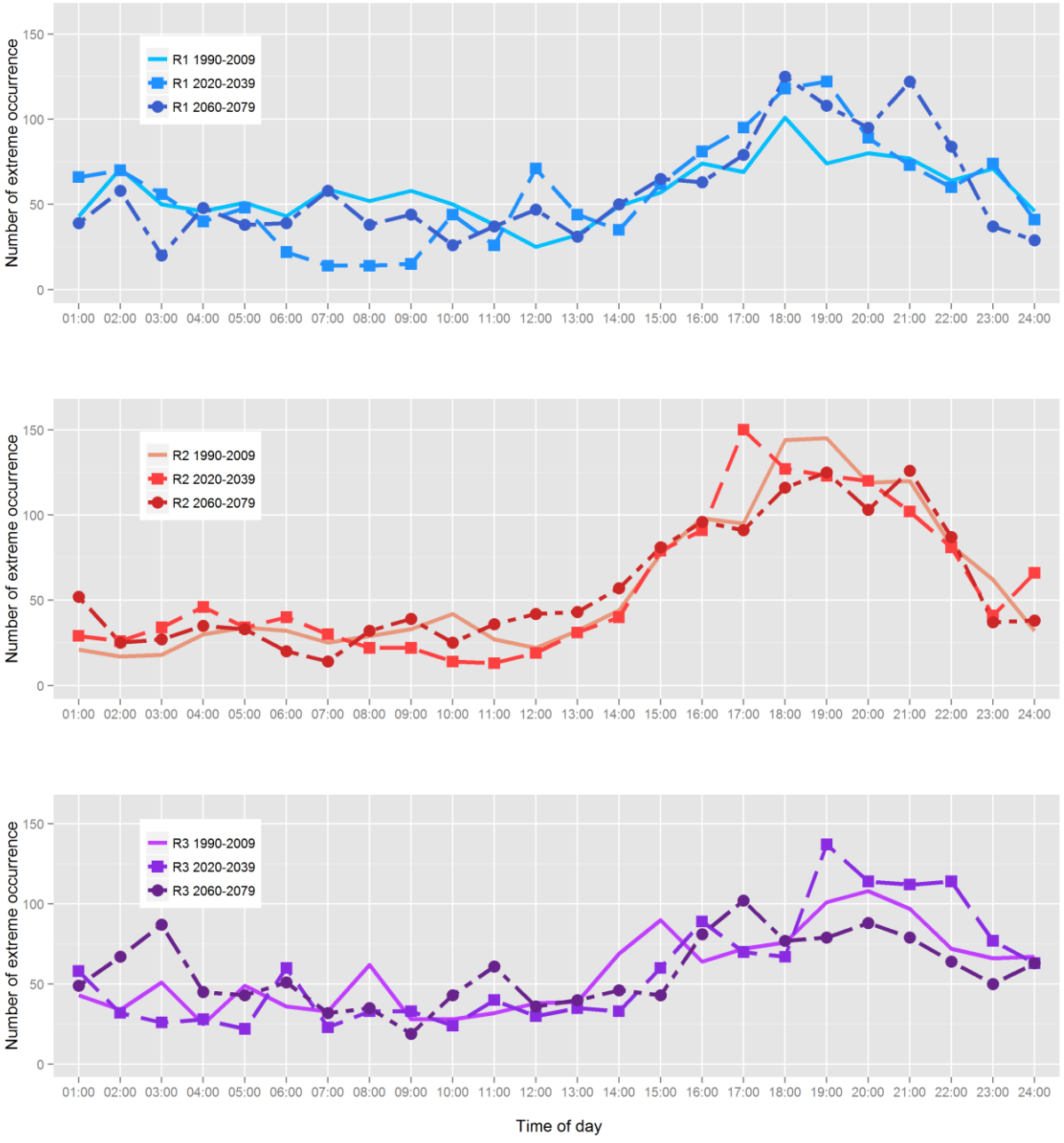

Figure 4.1 **Diurnal cycle of extreme rainfall occurrences for 69 locations across Greater Sydney obtained from R1 (blue lines), R2 (red lines) and R3 (purple lines) simulations for the historical (light colour lines), near-term future (medium colour lines) and long-term future (dark colour lines) periods.**

4.4.2 Is the seasonal cycle of sub-daily rainfall extremes in future projections changing from the historical period in simulations?

The seasonal cycle of sub-daily rainfall extremes was estimated for the near-term and the long-term future periods and then compared with the historical period in the R1, R2 and R3 simulations. Figure 4.2 shows the seasonal distributions of the total number of extreme rainfall events for 69 locations across Greater Sydney for the historical period (bars in light colour), the near-term future period (bars in medium colour) and the long-term future period (bars in dark colour) for R1 (blue), R2 (red) and R3 (purple) simulations.

For the historical period, the seasonal distribution of rainfall extremes was characterised for short rainfall durations by maxima in summer and minima in winter, whereas for long durations, the occurrence varied for each model, with the peak mostly happening in summer (except for R2) and the minima in spring.

When both simulated future periods were compared with the historical period, it was found that:

- R1 exhibited a clear seasonality with an increase in extreme rainfall events during summer months and a decrease during autumn and winter months for all durations, with this increase being more evident for the long-term future period.
- R2 showed seasonality in the occurrence of extreme rainfall events, with events taking place mainly during the summer and falling off in the winter. For the near-term period, the occurrence of rainfall extremes was greater than for the late future period for the autumn months, but less extreme during winter.
- R3 indicated a more extreme near future period with main increase during summer and spring and decrease during winter months. For both future simulated periods, the main occurrence of extreme events was found during summer, whereas the minima in winter.

The results from R1, R2 and R3 recorded an overall increase in the number of extreme occurrences during summer months and a decrease for winter months when compared to the historical simulations, although for the near future in R2 and R3 these changes seemed to be more extreme than for the long-term future.

Results for future changes in the seasonality of sub-daily rainfall extremes over Greater Sydney indicated that in a future climate, most extreme rainfall events can be expected in the summer with fewer occurring in the winter months. Therefore, it was concluded that the seasonality of sub-daily rainfall extremes over Greater Sydney will remain influenced by summer convective rainfall, with the maxima occurrence was particularly observed during warm and wet (summer) months.

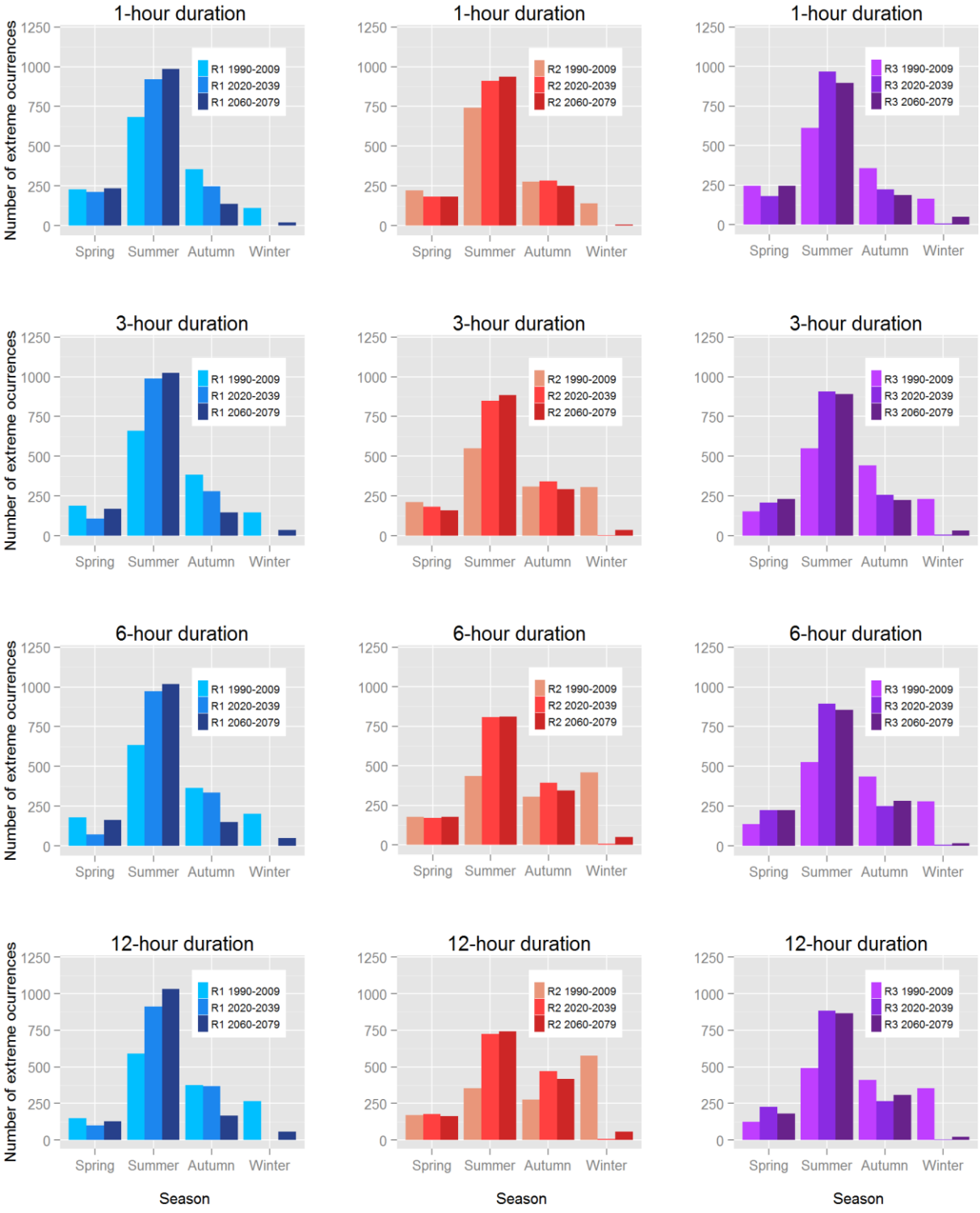

Figure 4.2 **Seasonality of sub-daily rainfall extremes estimated from R1 (blue bars), R2 (red bars) and R3 (purple bars) simulations at 69 selected grid points across Greater Sydney during the historical (1990-2009), the near-term prediction (2020-2039) and long-term projection (2060-2079) periods.**

4.4.3 Is the relationship between sub-daily rainfall extremes and atmospheric temperature valid for future projections in RCMs?

The scaling relationship between the 99th percentile of sub-daily rainfall and mean temperature was investigated for the near-future prediction and the long-term future periods in simulations from R1, R2, and R3 and then compared with the historical simulations considering only 69 grid points across Greater Sydney region. Figure 4.3 illustrates the scaling of sub-daily rainfall extremes with temperature for R1 (blue), R2 (red) and R3 (purple) simulations for the historical period (lines in light colour), the near-term future period (lines in medium colour), and the long-term future period (lines in dark colour).

When the scaling relationship between sub-daily rainfall extremes and temperature in the RCMs for future projections was compared with the historical simulations, it was found that:

- R1 showed scaling rates that approximated the C-C rate, particularly for 1-hour and 3-hour rainfall extremes and for temperature ranges from 2°C to 23°C. For longer durations, rainfall extremes also increased close to the C-C rate for temperatures up to 21°C.
- R2 also followed the C-C rate for temperatures up to 23°C for short durations and for long durations for temperatures up to 20°C.
- R3 also showed a temperature scaling rate close to the C-C rate for temperatures up to 24°C for short rainfall durations and up to 22°C for long rainfall durations.

The scaling rates in future projections of the RCMs approximate the C-C scaling rate, particularly for 1-hour and 3-hour durations and for temperatures up to 23°C. For 6-hour and 12-hour durations, the scaling relationship of rainfall extremes with temperature showed scaling rates different to the C-C rate for temperatures up 21°C. Indeed, for temperatures higher than these ranges the scaling relationship decreases and the scaling rate becomes negative.

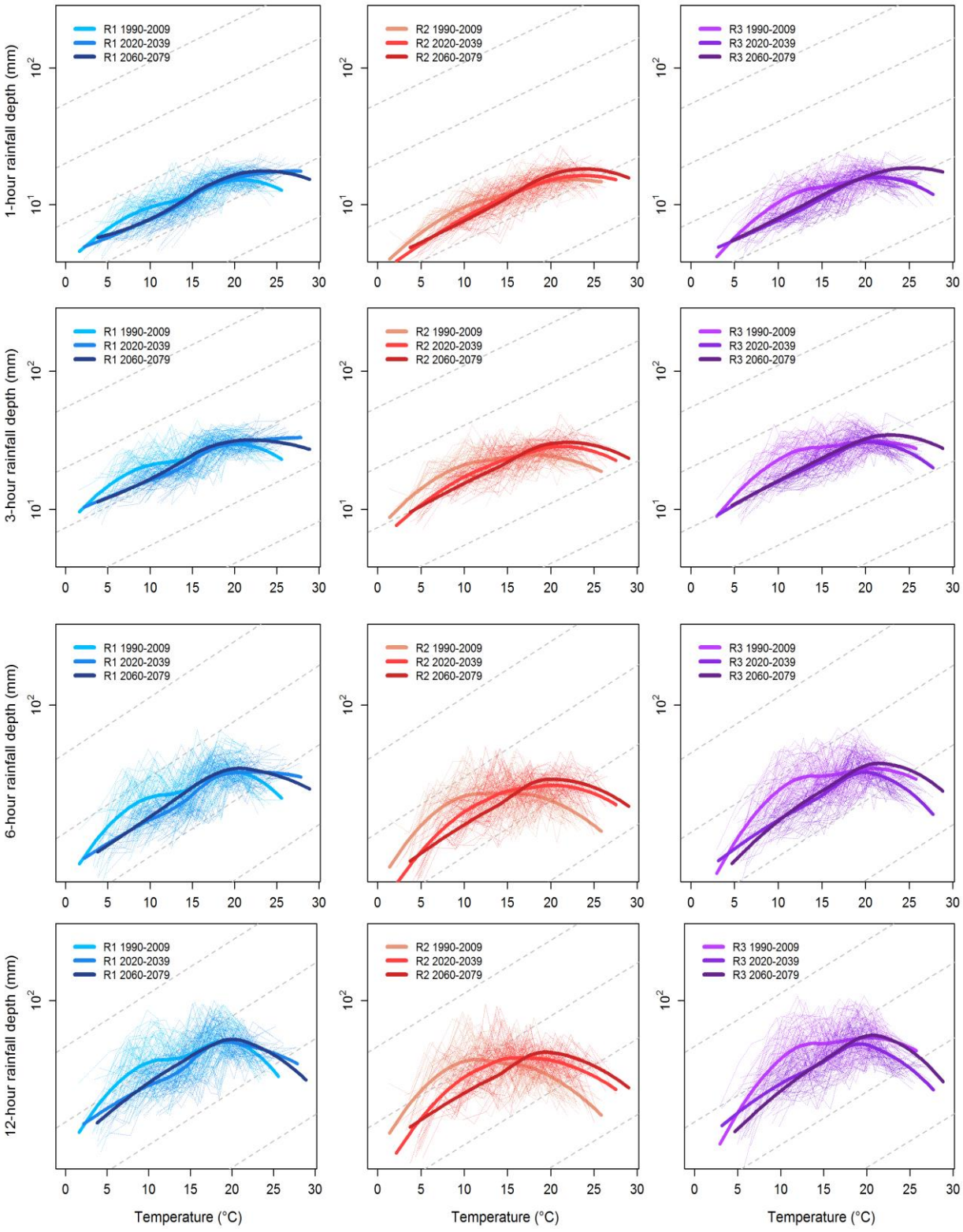

Figure 4.3 **Increase of the 99th percentiles of rainfall intensity at sub-daily durations with surface temperature for R1 (blue), R2 (red) and R3 (purple) simulations. An exponential regression is fitted to 69 grid cells for the: (i) historical period (light colour lines), (ii) near-term future projection (medium colour lines) and (iii) long-term future projections (dark colour lines). Dashed lines correspond to the C-C rate (~7%/°C).**

The relationship between the 99.9th percentile of sub-daily rainfall and surface temperature was also investigated for the near-future prediction and the long-term future periods in R1, R2, and R3. Figure 4.4 illustrates the temperature scaling estimated at 69 grid-point locations across Greater Sydney in R1, R2 and R3 simulations during the historical period, the near-term future period and the long-term future period.

Comparing the temperature scaling in each RCM and simulated period, it was found that:

- R1 closely followed the C-C rate for temperatures up to 23°C for most sub-daily durations and for both the near-future and long-term future periods.
- R2 approximated the C-C rate for temperatures up to 24°C for most sub-daily durations and for both the near-future and the long-term future projections.
- R3 also followed the C-C rate for temperatures 24°C for most sub-daily durations and for both future projections.

The scaling temperature ranges obtained from the 99.9th percentile of hourly rainfall in both the near-term future and long-term future projections approximated the C-C rate. These temperature scaling rates were found for temperature ranges higher than the historical period.

The results for future projections for both the 99th and 99.9th percentiles of rainfall indicated that the intensification of hourly rainfall extremes with temperature approximately followed the C-C rate for temperatures no higher than 24°C. Moreover, the temperature scaling for future projections was found for temperature ranges higher than the historical simulated period for most durations. However, for a given temperature, the intensity of rainfall extremes (either the 99th or 99.9th percentiles of rainfall) in the historical period was higher for the future period in simulations, especially for long duration.

Simulations of three RCMs for the historical period found that the temperature scaling was like the C-C rate only for hourly durations, while for future projections, the temperature scaling tended to approximate to the C-C rate, especially for the long-term future.

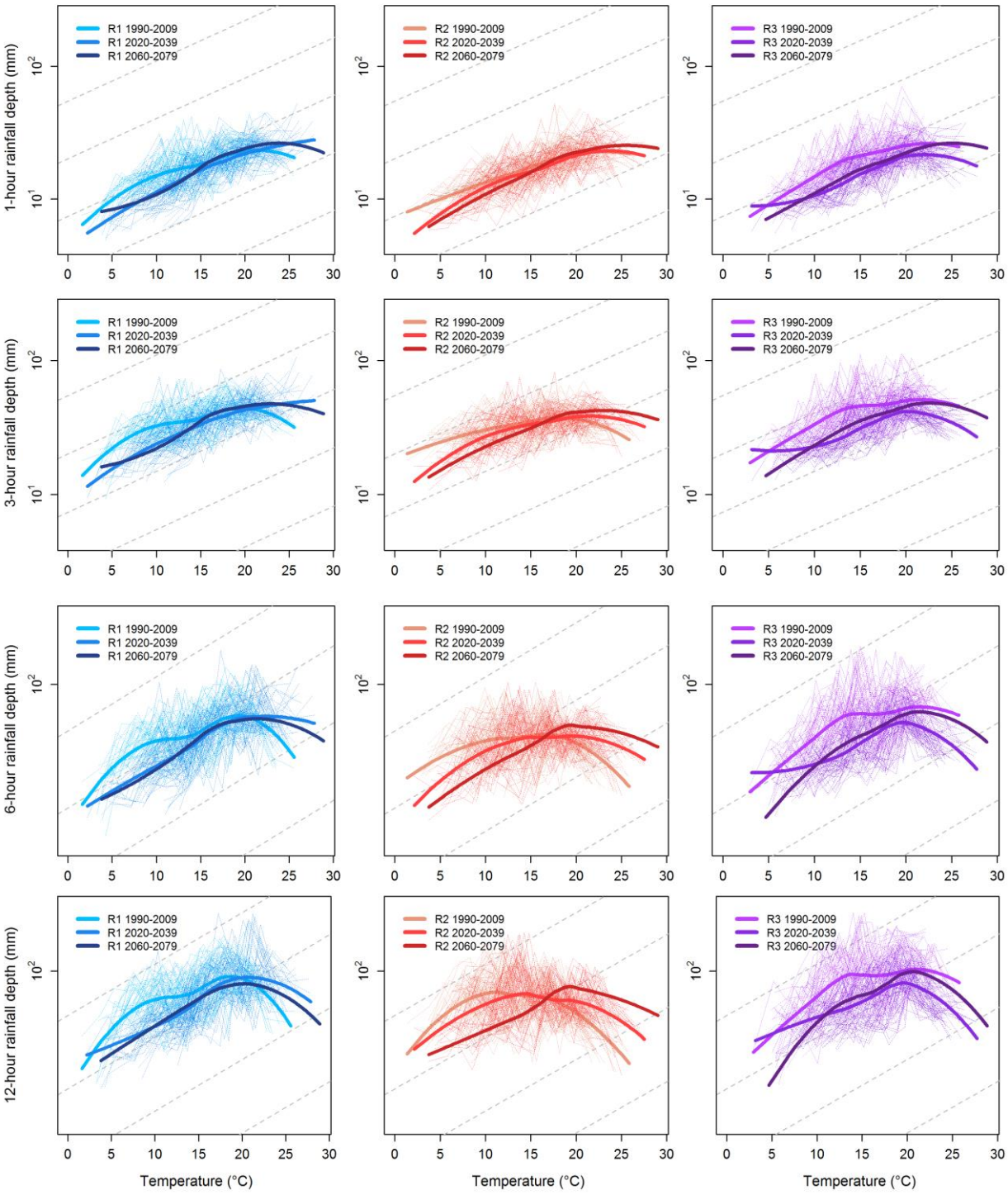

Figure 4.4 **Increase of the 99th percentiles of rainfall intensity at sub-daily durations with surface temperature for R1 (blue), R2 (red) and R3 (purple) simulations. An exponential regression is fitted to 69 grid cells for the: (i) historical period (light colour lines), (ii) near-term future projection (medium colour lines) and (iii) long-term future projections (dark colour lines). Dashed lines correspond to the C-C rate (~7%/°C).**

The mean of the temperature scaling rate (mtsr) at 69 point locations across Greater Sydney was also estimated for the historical period, the near-term future and the long term future periods. The mtsr was also compared between the 99th and the 99.9th percentiles of hourly rainfall intensity.

Table 4.2 outlines the mtsr estimated for the 99th percentile and the 99.9th percentile of houly rainfall intensity for the three simulated period and for the three RCMs. The mtsr is presented in terms of percentage per 1°C of temperature in order to be comparable with the C-C rate (7%/°C).

The results indicate that the mtsr estimated for the 99.9th percentile of rainfall intensity were overall higher than those for the 99th percentile, especially for the long-term future period in the simulations from all three RCMs. The magnitude of the mtsr varied from the lowest 4.35%/°C rate (found in R3) to the highest 6.28 %/°C rate (found in R1), with mtsr values slightly below the C-C rate over Greater Sydney.

Table 4.2 The mtsr for the 99th and 99.9th percentile of hourly rainfall for the three simulated periods and for the three RCMs across Greater Sydney.

RCM	Period	TS from the 99th percentile (%/°C)	TS from the 99.9th percentile (%/°C)	Comparison between the 99.9th and the 99th percentile
R1	1990-2009	4.58	4.62	higher
	2020-2039	6.10	6.28	higher
	2060-2079	5.73	6.28	higher
R2	1990-2009	4.76	4.84	higher
	2020-2039	5.82	5.25	lower
	2060-2079	6.18	5.98	lower
R3	1990-2009	4.35	5.46	higher
	2020-2039	5.47	5.32	lower
	2060-2079	5.79	5.88	higher

The magnitude of the mtsr found for the simulated periods agreed with the temperature scaling rate close to the C-C rate and with no evidence for super C-C rates over the region, as also found in the previous chapter in observations.

The findings presented in Figures 4.3 and 4.4 and Table 4.2 suggested that hourly rainfall extremes under the A2 high emission scenario might intensify into the future across Greater Sydney.

4.4.4 Is the magnitude of annual maxima of sub-daily rainfall events increasing?

The mean of the annual maxima of rainfall for 1-hour, 3-hour, 6-hour and 12-hour durations was estimated for the historical (1990-2009), the near-term (2020-2039) and the long-term (2060-2079) periods in the three model simulations. Then, the ratio of the annual maxima was estimated using Eq. 4.1 for the entire Greater Sydney domain.

Figure 4.5 illustrates the ratio of the annual maxima between the mean of the annual maxima at sub-daily durations for the near-term future period and for the historical period for R1, R2 and R3. In the figure, areas in white indicate no significant changes in the ratio of the means, with either underestimation or overestimation no greater than 10%, whereas blue areas indicate there was an increase and red areas a decrease, respectively.

When the ratio of the annual maxima was analysed for the near-term future, it was found that:

- The ratio in R1 showed an increase over the north continental area by up to 60% and a decrease in the north and south parts in the ocean by up to 30%. For long durations and especially over the central coast there were no significant changes.
- The ratio in R2 mostly decreased by up to 50% over the south coast and ocean areas and increased by 60% over inland areas, particularly for longer durations.
- R3 presented the greatest changes in the ratio along the coastline with a decrease up to 60% and a little increase of up to 50% over the north inland.

The results indicate that the main changes in the ratio of the annual maxima for the near-term future showed an overall increase in most north inland areas (blue areas), whereas there is an decrease over the south and central coast areas (red areas). In fact, the main increase in the intensity of the annual maxima over inland areas was found in R1 particularly for short durations, while the main reduction over coastal and sea areas was noticeable in R2 particularly for all durations.

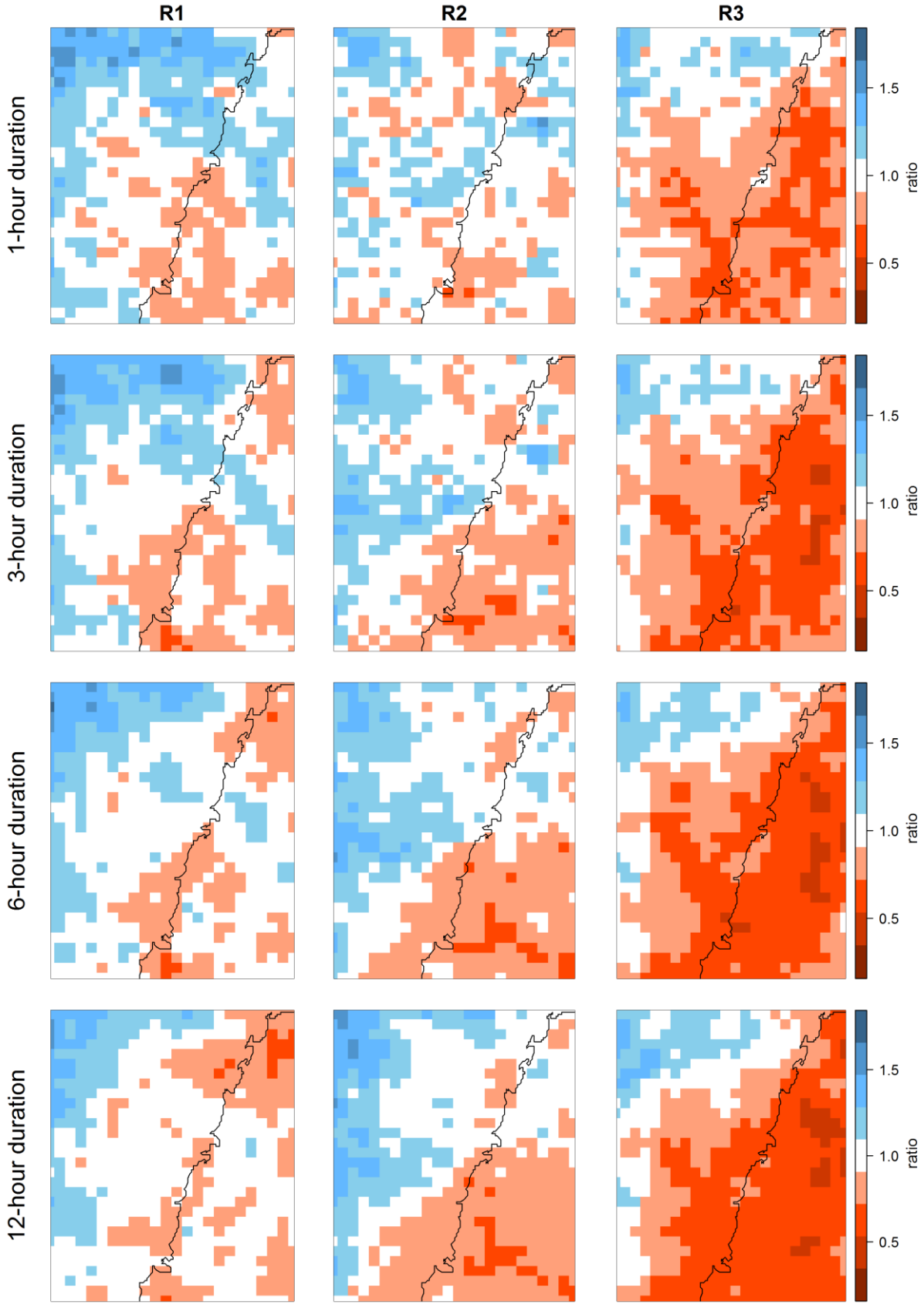

Figure 4.5 **Ratio between the mean of the annual maxima at sub-daily durations for the near-term future (2020-2039) period and for the historical period for R1, R2 and R3 simulations over Greater Sydney. Ratios in white colour indicate no significant changes (no greater than 10% of the historical values), ratios in blue colour indicate increases, while ratios in red colour indicate decreases.**

Figure 4.6 shows the ratio of the annual maxima for the long-term future period which was estimated in the same way as the ratio for the near-term future in R1, R2 and R3 simulations for the entire Greater Sydney domain.

When the ratio of the annual maxima was analysed for the long-term future, it was found that:

- The ratio in R1 increased by up to 60% over inland areas, particularly at hourly duration, and decreased by up to 30% along the coastline for 12-hour duration.
- The ratio in R2 increased by up to 50% over inland areas and slightly decreased over the sea up to 20%.
- R3 presented the greatest changes in the ratio along the coastline, with decreases up to 50% and increases up to 40% over inland, particularly in the north.

The overall results in the ratio of the annual maxima showed an increase in most north inland areas (blue areas) and a decrease over coast areas (red areas). R1 and R2 projected mainly increases of the ratio while R3 indicated the greatest decreases.

Findings from the R1, R2 and R3 simulations from both future periods (Figure 4.5 and Figure 4.6) projected an increase in the mean annual maxima in north inland areas and also a reduction in the intensity of the annual maxima along the coastline and ocean parts which became more evident for longer durations. However, the reduction is more evident for the near-term period in comparison with the long-term period in simulations.

In addition, the ratio of the annual maxima for the 1 in 10-year rainfall event was estimated and the results are showed on Supplementary Figure 1 and Supplementary Figure 2 in the Appendix. The ratios of the annual maxima for the near-term and long-term future indicated similar results that for the annual maxima, with reductions along the coastline and ocean parts and increases over north inland parts.

Future projections of the annual maxima from the three RCMs indicated mainly increases over inland areas and increases along the coast but these projections should be carefully considered before model outputs are used for developing future climate change projections.

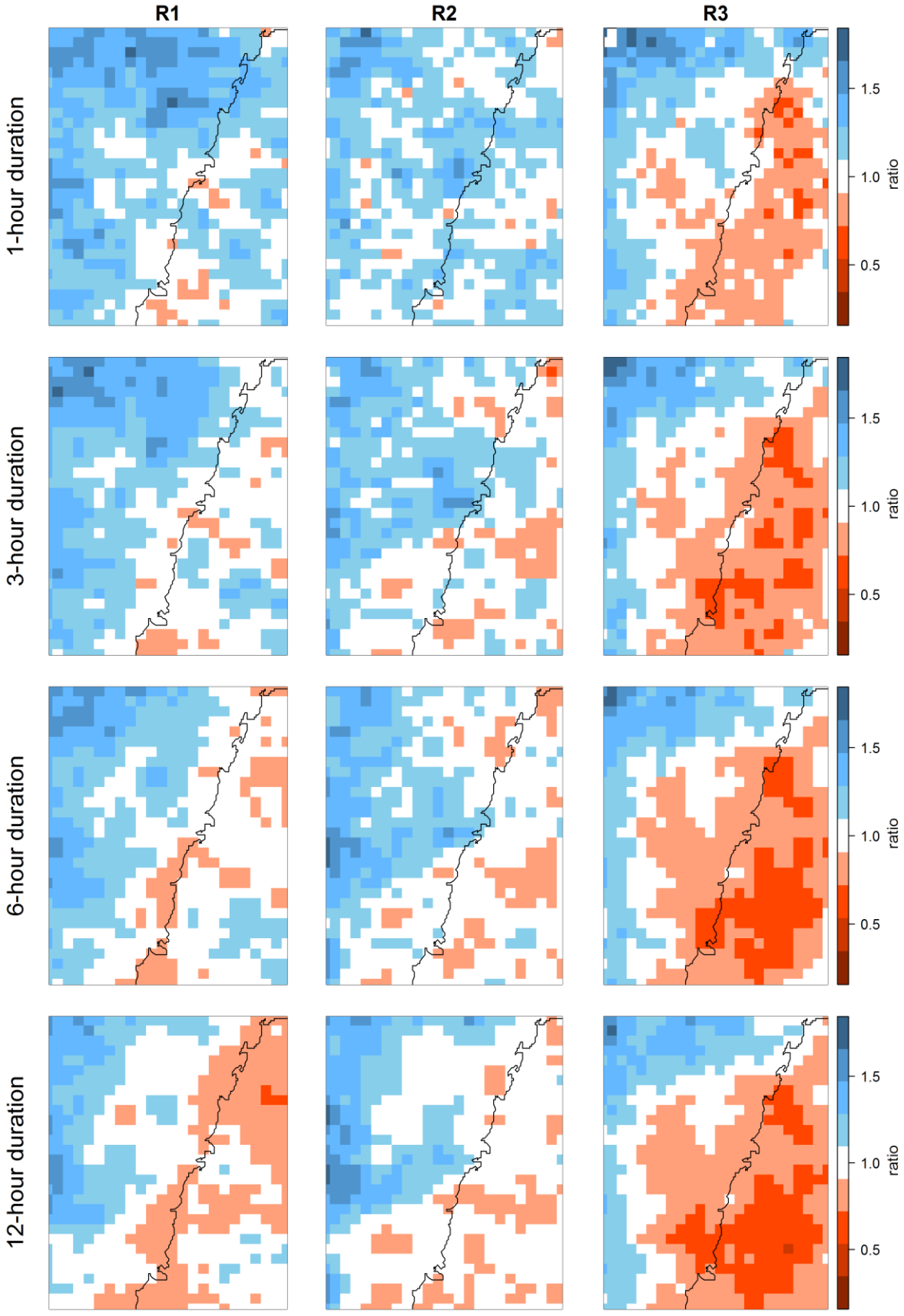

Figure 4.6 **Ratio between the mean of the annual maxima at sub-daily durations for the long-term future (2060-2079) period and for the historical period for R1, R2 and R3 simulations over Greater Sydney. Ratios in white colour indicate no significant changes (no greater than 10% of historical values), ratios in blue colour indicate increases, while ratios in red colour indicate decreases.**

4.5 Discussion

4.5.1 Using the past to model the future

In the practical field of water resources planning and design, the terms *stationarity* and *non-stationarity* implied different assumptions for predicting changes, particularly when considering future climate change (Lins and Cohn, 2011). Features of future events are commonly assumed to resemble past conditions (i.e. stationarity), and this assumption underpins most models used in the water resources planning and design context. Even in climate impact assessments, stationarity assumptions are commonly made; for example, hydrological models calibrated to the historical climate are assumed to be appropriate for future rainfall-runoff predictions (e.g. Westra et al., 2014a), and statistical downscaling models are often developed under the assumption that historical relationships between rainfall and the atmospheric predictors will remain valid in the future. However, when the assumption of stationarity proves to be invalid over time, it is necessary to adapt to the changes and adjust the models to reflect emerging scenarios.

The relationship between sub-daily rainfall extremes and mean temperature provides an example of circumstances that can be used to identify whether a historical relationship will be valid under future projections involving RCMs. Figure 4.7 presents a conceptual understanding of four possible scenarios of the scaling relationship for future climate model projections when stationarity cannot be assumed:

Scenario 1. In the first scenario, stationarity is assumed, providing a baseline scaling relationship in which future projections of weather behaviour match the simulation based on historical data.

Scenario 2. In the second scenario, the scaling relationship in future projections is extended along the same curve as in the first scenario, but for higher temperatures. Therefore, the historical assumption is partially stable under specific temperature ranges but overall is characterised by non-stationarity.

Scenario 3. In the third scenario, the scaling relationship in future projections is displaced from the historical simulation and demonstrates non-stationarity in terms of the historical assumption.

Scenario 4. The scaling relationship in future projections is completely changed from the historical simulation in the fourth scenario. The scenario is characterised by non-stationarity.

Alternative scenarios in which projections of future rainfall extremes are developed using only atmospheric temperature as a predictor were explored for model simulations for the near-term and long-term future and then compared to the historical period as shown in Figure 4.8 and Figure 4.9. This can provide insight into the validity of the stationarity or non-stationary of the observed temperature scaling of short-duration rainfall extremes over Greater Sydney, explored in the following section.

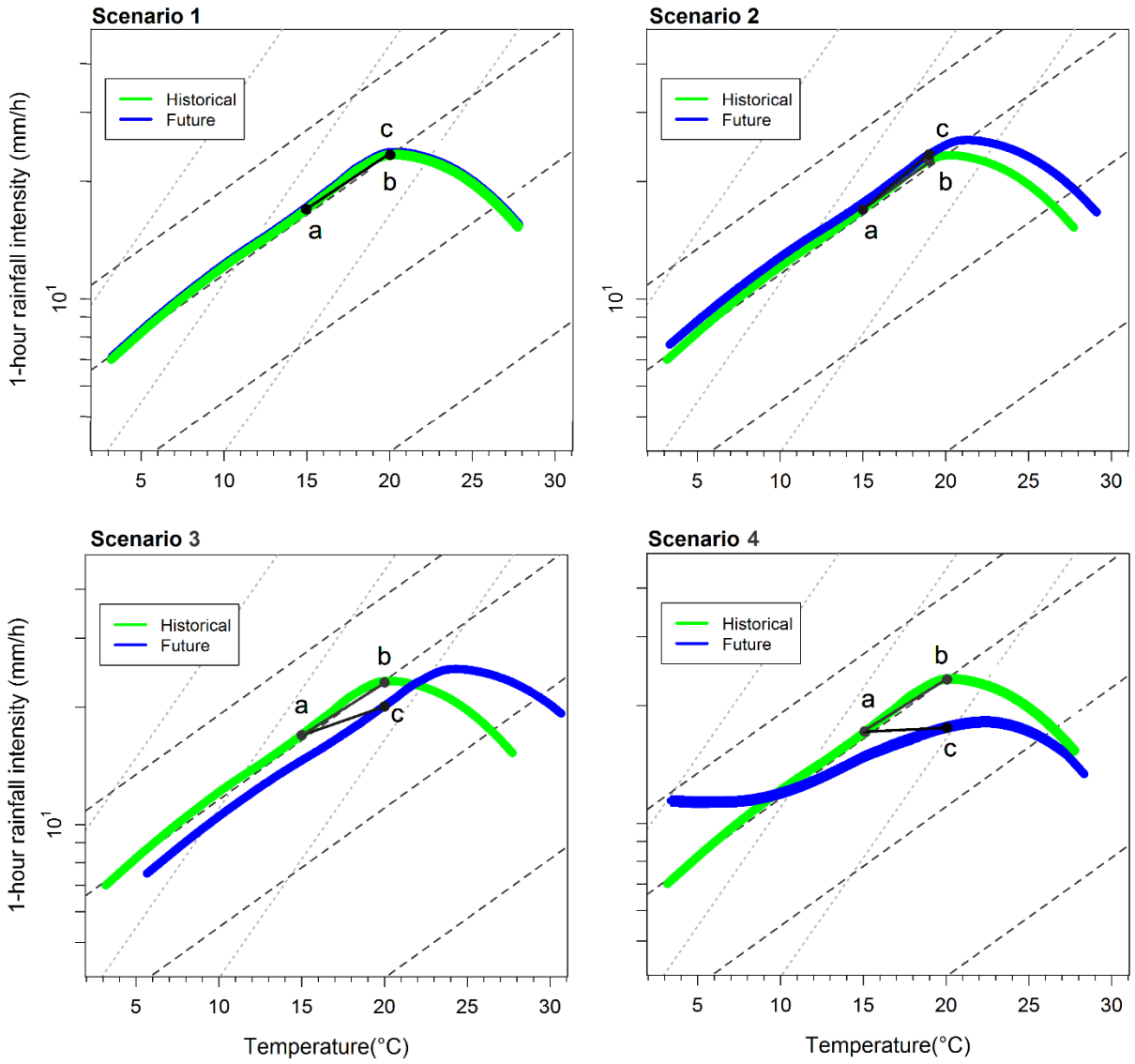

Figure 4.7 **Conceptual understanding of the intensification of hourly rainfall extremes with future warmer temperatures. The historical period (green curve) in model simulations is compared to the future period (blue curve) in observations to validate whether the relationship is stationary (left panel) or non-stationary (right panel) under future climate conditions.**

4.5.2 Projecting future rainfall extremes using atmospheric temperature

Stationary scaling relationship in simulations. Suppose that the historical period in simulations (green curve) approximates the C-C rate for temperatures up to 20°C. If a temperature increase of 4°C is projected in a future (long-term) warmer climate, the temperature rise will lead to an increase in the intensity of rainfall extremes at a rate of ~7% per 1°C along the scaling. For example, rainfall intensity for a temperature of 15°C (point *a*) is projected to increase following a scaling rate close to the C-C rate after a 4°C temperature increase (point *b*).

The stationarity assumption of the historical scaling relationship is illustrated in Figure 4.7, Scenario 1. The long-term future period in simulations indicates a scaling relationship (blue curve) that is exactly the same as the curve for the historical period and which also approximates the C-C for temperatures up to 20°C. In this scenario, the intensity of rainfall extremes associated with a 4°C rise in temperature, from point *a* to point *c* in the figure, is expected to approximate the C-C rate.

Non-stationary scaling relationship in simulations. A future increase of 4°C in temperature is expected to lead to a rise in rainfall intensity in accordance with the C-C rate (going from point *a* to point *b*). In contrast, future projections in the simulation (blue curve) are either displaced (Scenarios 2 or 3) or completely changed (Scenario 4) from the historical period. Although the scaling rate along the projected curve follows the C-C rate, the increase in temperature means that the curve will deviate from the historical record. For instance, the intensity of rainfall at a given temperature (point *a* in the historical period) will increase from point *a* to point *c* following a scaling rate much lower than the C-C.

These hypothetical scenarios for future projections of the scaling relationship were investigated for both the 99^{th} (Figure 4.8) and 99.9^{th} (Figure 4.9) percentiles of hourly rainfall intensity in R1 under the A2 emission scenario of future climate change. Figure 4.8 shows the scaling relationship between the 99^{th} percentile of hourly rainfall intensity with mean temperature for the historical period (light blue curve), the near-term future (medium blue curve) and the long-term future (dark blue curve) periods in simulations.

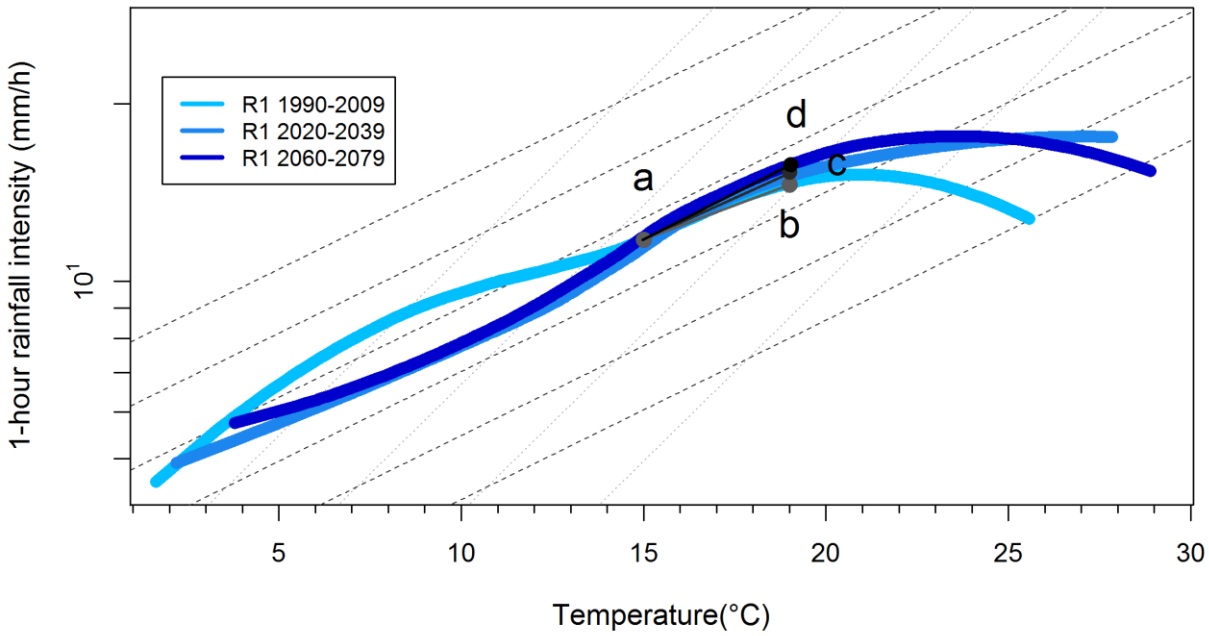

Figure 4.8 **The temperature scaling using the 99th percentiles of hourly rainfall for the historical assumption (light blue curve), the near-future period (medium blue curve) and the long-term future projection in R1. The segments a- c and a- d are used to determine the validity of the historical assumption of the segment a-b for future projections.**

Considering a given temperature of 15°C and a future increase of 4°C in temperature, the intensity of rainfall in point *a* to point *b* will increase by a scaling rate of approximately the C-C. Similar scaling rates were also found in future simulations where the intensity of rainfall from point *a* to point *c* or from point *a* to point *d* approximated to the C-C rate. The stationarity assumption of the C-C scaling rate was only found within the temperature range 15°C-19°C (similar to Scenario 1), while for lower temperatures the scaling relationship was much lower than the C-C rate. Figure 4.9 showed the historical assumption of the scaling relationship using the 99.9th percentile of hourly rainfall (light blue curve). Considering again a temperature of 15°C and a future increase of 4°C in temperature, the intensity of rainfall from point *a* to point *b* will increase at approximately the C-C rate.

In contrast, a future increase of 4°C in temperature might increase the intensity of rainfall with a lower scaling rate than the C-C. For example, the rate of the increase in intensity of rainfall from point *a* to point *b* differed from the rate projected from point *a* to point *c* and from point *a* to point *d*. Higher and lower temperature ranges projected different scaling rates for each future period. These tended to be lower than the scaling rates in the historical period.

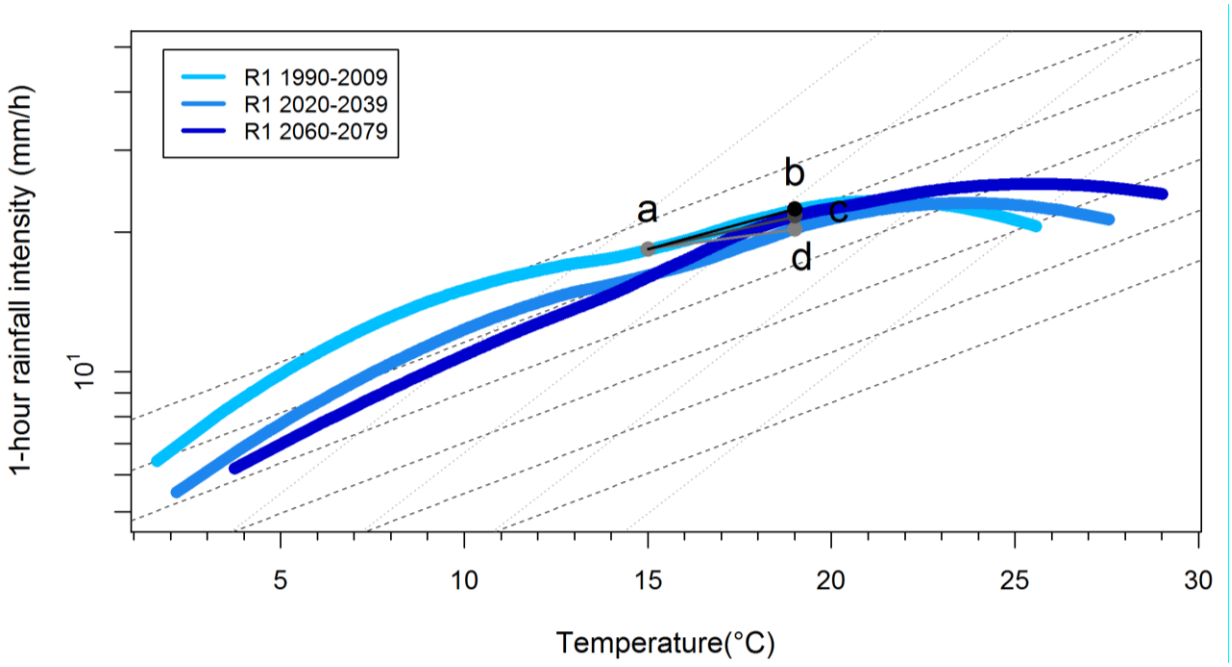

Figure 4.9 **The temperature scaling using the 99.9th percentiles of hourly rainfall for the historical assumption (light blue curve), the near-future period (medium blue curve) and the long-term future projection in R1. The segments a- c and a- d are used to determine the validity of the historical assumption of the segment a-b for future projections.**

Despite the fact that future projections in model simulations indicate a scaling relationship close to the C-C, the validity of the scaling relationship for future projections (based on the historical period simulations) indicates an overall pattern of change that must be considered for future projections.

4.6 Summary and conclusions

Simulations for the near-term and long-term future projections in three RCMs were used to identify future potential changes in sub-daily rainfall extreme events under the A2 high emission scenario of climate change for Greater Sydney.

A summary of the main findings is presented below:

- Assuming that the model simulations during the historical period (1990-2009) were a valid baseline, near-term projections (2020-2039) show a similar number of grid cells exhibiting increases compared to decreases over land for all durations, although with significant differences between the models. In contrast, for longer-term projections (2060-2079), more grid cells exhibited increases over land for all durations, with some grid cells showing increases of 50% or more relative to the historical period. Results also indicate a marked decrease of the annual maxima for the coast and over the ocean. This reduction was more evident during the near-term future than the long-term future, mainly in R3.

- The diurnal cycle of hourly rainfall extremes in both future simulated periods for three RCMs indicated no significant changes in the future. The diurnal cycle exhibited an overall late afternoon peak that agreed with results found during the simulations of the historical period as well as with results from observations discussed in the previous chapter.
- The main changes for future climate conditions were identified in the seasonality of occurrences of sub-daily rainfall extremes, which became more frequent in summer with a large increase in the number of extreme events, while winter experienced a dramatic decrease that was most evident in the simulations of the near-term future. Given that summer rainfall is often dominated by convective activity, the results suggest that sub-daily rainfall extremes over Greater Sydney will be increasingly influenced by summer convective rainfall as temperatures increase.
- Future projections in the RCMs suggested that the intensity of rainfall extremes at hourly durations would increase in a manner consistent with the C-C rate. For hourly durations, temperature scaling rates closely followed the C-C rate with a rate of between 4.3%/°C and 6.3% /°C, depending on the model, for temperatures up to 25°C. However, the intensity estimated for the 99^{th} and the 99.9^{th} percentiles of rainfall was significantly lower than observations.

These results contribute to the evidence for potential future changes of sub-daily rainfall extremes in conditions of future climate change in Greater Sydney, considering the A2 emission scenario of climate change.

Chapter 5. Summary and conclusions

5.1 Thesis outcomes

This dissertation presents a strategy to evaluate the capacity of RCMs to reproduce the statistics of sub-daily rainfall extremes, as well as some of the relevant physical processes related to such extreme events. The strategy was used to evaluate three different physics parameterisations of the 10-km resolution WRF model (R1, R2 and R3) over the Greater Sydney region during 1990-2009. Moreover, likely future changes in sub-daily rainfall extremes using the three RCMs were investigated for two future periods: 2020-2039 and 2060-2079. The main outcomes are summarised in turn below:

5.1.1 Evaluation of the three different configurations of the WRF model

The specific results included:

- The observed rainfall extreme events were associated with convective rainfall for short durations; whereas for long durations, the rainfall extremes were stratiform. Therefore, sub-daily rainfall extremes over the region exhibited strong diurnal and seasonal variability.
- The diurnal cycle of rainfall extremes was overall well reproduced by the three RCMs, showing a late evening peak in agreement with the observations, although a 3-hour delay in the timing of the maxima was found in R3 (Figure 3.4).
- The seasonality of rainfall extremes was better captured for 1-hour and 3-hour durations. The maximum number of extreme events occurred in the summer months and the minimum in the winter months, especially in R1. For long rainfall durations, the seasonality was reproduced successfully by the three RCMs for the summer months. However, they failed to reproduce the increased occurrence of rainfall extremes during the winter months (Figure 3.5).
- The thermodynamical concept of the intensification of rainfall extremes with atmospheric temperature was consistent with the C-C scaling rate for 1-hour and 3-hour durations and for temperatures up to 23°C. Scaling rates like the C-C rate were also reported in the observations and in previous studies over the region; however, the intensity of rainfall extremes during the scaling in simulations was lower than in the observations (Figure 3.6 and Figure 3.7).
- Differences in the three RCMs were mostly attributed to the three selected parameterisations in the WRF model, particularly for the convective and boundary layer schemes that are very important for representing convection processes associated with sub-daily rainfall extremes (Table 3.1).

The statistics of sub-daily rainfall extremes include the mean of the annual maxima of rainfall and the 1 in 10-year rainfall event for 1-hour, 3-hour, 6-hour and 12-hour durations. The specific results included:

- R1 and R3 performed better in terms of modelling the rainfall depth over coastal parts, whereas R2 produced better results over the inland from 3- to 6-hour durations when compared with the observations at 69 sites across the Greater Sydney region. The observed rainfall depths of sub-daily rainfall extremes were mainly underestimated for short durations and overestimated for longer durations by the three RCMs. R1 performed better over inland areas; whereas R3 performed better along the coastline (Figure 3.9).
- Q-Q plots of the annual maxima constructed for six selected sites across the Greater Sydney region showed that R3 performed better over low-elevation coastal areas and short durations; whereas R2 performed better over inland areas and for most sub-daily durations (Figure 3.10).
- The trend of the annual maxima was overall overestimated by the RCMs, especially along the coast and for long durations (e.g. 6-hour and 12-hour). R1 (for short rainfall durations) and R3 (for long rainfall durations) partially captured the trend of the annual maxima over inland and some coastal areas (Figure 3.12).

Overall, the results indicate that the three RCMs reasonably reproduced some relevant physical processes of sub-daily rainfall extremes over Greater Sydney. Moreover, the intensification of hourly rainfall extremes with temperatures up to 23°C was also captured by the RCMs, which provides confidence in their ability to project future changes. Therefore, R1, R2 and R3 are recommended for investigating future changes in sub-daily rainfall extremes.

5.1.2 Future projections

Future changes in sub-daily rainfall extremes under the A2 high emission scenario of the IPCC were investigated for the 2020-2039 and the 2060-2079 periods in R1, R2 and R3 and compared with the historical record (1990-2009) from the Greater Sydney region. The specific results included:

- The influence of future climate change in the diurnal cycle of rainfall extremes showed no significant changes in the shape and timing of the peak of extreme rainfall occurrence (Figure 4.1).
- Future projections showed significant changes in the seasonality of sub-daily rainfall extremes. Sub-daily rainfall extremes are expected to increase in summer and dramatically decrease in winter (Figure 4.2).
- The future intensification of sub-daily rainfall extremes (considering both the 99^{th} and 99.9^{th} percentile of rainfall) associated with temperature rise approximated the C-C scaling rate for temperatures up to 25°C. However, the historical scaling relationship for hourly durations suggested that the historical relationship is not maintained in future projections because the intensity of rainfall is expected to change by a different scaling rate due to the rise in temperatures. Future projections must therefore consider the non-stationarity of the temperature scaling relationship (Figure 4.3 and Figure 4.4).
- The intensity of sub-daily rainfall extremes is expected to increase in the future over some land areas and decrease over coastal and ocean areas (Figures 4.5 and Figure 4.6).

The results presented in this thesis therefore provide significant information on the nature of likely future changes of sub-daily rainfall extremes in the greater Sydney region as a result of anthropogenic climate change.

5.2 Research contributions

High resolution climate models such as RCMs will remain the primary tool for investigating the influence of future global warming on climate, particularly at regional and local scales where most extreme events take place. Therefore, it is of great importance to evaluate their reliability in realistically simulating sub-daily rainfall extremes.

Commonly used metrics of model evaluation based on direct measures of the difference observed and modelled rainfall extremes provides only limited insight into whether the model simulates the correct physical processes; therefore, this research provides a framework for evaluating the skill of

RCMs to simulate sub-daily rainfall extremes based on metrics that characterized physical underlying processes that lead to the occurrence of such extremes.

Chapter 2 provided a detailed review of the current knowledge of changes in sub-daily rainfall extremes and their potential intensifications due to climate warming, the role of climate model (especially RCMs) in representing the relationships between local-scale thermodynamic effects, large-scale atmospheric circulation, and sub-daily extreme rainfall intensity.

Chapter 3 developed a strategy to evaluate the performance of RCMs to capturing sub-daily rainfall extremes. This is the first time that a large set of metrics characterising physical processes was implemented for evaluate different feature of sub-daily rainfall extremes over Greater Sydney.

Chapter 4 provided climate modelling evidence for potential changes attributed to emission of GHGs under the A2 high emission scenario. This contributed to the knowledge for future likely increases in the intensity of rainfall extremes over Greater Sydney, Australia, as projected for the end of the 21st century.

The findings in this study showed an overall reasonable match between model simulations with the observations that increase the confidence for the use of the specific RCMs for further applications, such as in the development of future projections in sub-daily rainfall extremes over Greater Sydney, although bias correction will be required to improve main differences found in the annual maxima at different durations.

5.3 Limitations

The generalisability of results in this research was subject to the following limitations:

Limitations in observations. The availability, quality and record length in observations represented the primarily limitation to evaluate physical relationships in RCMs. A total of 69 observational records were selected based on considering the criteria 90% of completeness and record length from 1990-2009. Because of the sparseness of observations, it was not possible to develop a gridded sub-daily rainfall product for direct comparison with WRF. The 10 km resolution of the WRF model is relatively small and this facilitates comparison with point observations, however, it is possible that there exist biases when comparing extreme rainfall amounts between point and gridded data. Issues

related to comparisons between point-based observations and grids are less likely to be important for comparisons of the diurnal cycle, seasonal cycle and temperature scaling relationships.

Limitations in the RCMs. RCMs are highly dependent on the selection of physics parametrizations, particularly the convective and boundary layer schemes required for the configurations of the WRF model. For instance, this dependency influenced the timing response in the model in reaching the maximum intensity of rainfall. For future projections, the results described herein were strongly dependent on the lateral boundary provided by the MIROC-GCM and future GHGs forcings supplied by the A2 high emission scenario.

Limitations in very high resolution climate models. The benefit of a very high resolution climate model, such as a convective-permitting model is a better representation of spatial and temporal scales relevant to sub-daily rainfall extremes. However, most studies using these types of models were derived from singular models and/or short simulated periods (less than 10 years), as a consequence of the very high computational cost. Therefore, short climate records are not sufficient to understand the climate change signal and involved feedbacks that are used in climate model evaluation.

Limitations in the evaluation metrics. The evaluation of sub-daily rainfall extremes is limited by the availability of relevant atmospheric weather variables to better understand the physical processes associated to sub-daily rainfall extremes. Most observations are obtained from ground-based systems that are not able to provide information about cloud processes and cloud feedbacks, such as convective available potential energy (CAPE) and convective cloud cover which are relevant to atmospheric instability and convective cloud formation that will ultimately lead to the occurrence of rainfall extremes. Nevertheless, it is likely that the ground-based data provides useful proxies most of the relevant physical processes relevant to the generation of rainfall extremes.

5.4 Recommendation in the use of evaluation approach for future studies

The strategy of climate model evaluation based on the use of physically meaningful metrics can be applied to any climate model (GCM, RCM or convective-permitting model) that investigates sub-daily rainfall extremes, considering the follow recommendations:

- High-quality observational data with long-continuous records must be available. Observational data is primarily needed for establishing the relationships to be included in the evaluation of

the climate model in order to provide an adequate representation of the relevant physical processes.

- The spatial and temporal resolution of model outputs must be comparable with the resolution in observations. For RCMs, model simulations are considered consistent and comparable with observations for point locations when the spatial resolution is no higher than 20 km and temporal sub-daily resolution such as hourly outputs.
- Particularly for future projections, the time-slice of climate model outputs must be long enough to suggest that the results are representative of likely changes under future climate.
- The strategy of evaluation implemented in this research can be extended by considering multiple outputs, multiple models and ensembles as well as longer realizations in the climate model rather than selecting only one model that performs best.

5.5 Future research

It is recommended that further research be undertaken in the following areas:

- Improve the representation of local storm dynamics (e.g cloud and moisture processes) and their interaction with large-scale atmospheric circulation in regional climate models.
- Differentiate the type of rainfall extremes (e.g. convective and large-scale stratiform rainfall) that might cause changes in the rainfall extreme pattern and may also influence the scaling relationship between hourly rainfall extremes and surface temperature. Further research needs to examine more closely the decline of the temperature scaling of sub-daily rainfall extremes for temperatures higher than 25°C and which seems to be associated with the availability of the atmospheric moisture content and/or the transport of atmospheric moisture.
- Investigate the ways in which moisture availability constrains the intensification of rainfall extremes in conjunction with higher temperature ranges. Further research is needed to examine more closely the decline of the temperature scaling of sub-daily rainfall extremes for temperatures higher than 25°C which seems to be associated with the availability of the atmospheric moisture content and/or the transport of atmospheric moisture.
- The selection of future GHGs emission scenarios and/or the generation of new representative concentration pathways (RCPs) is required to investigate future change in sub-daily rainfall extremes.

References

ADB, A. D. B., 2014: Northern Flood-Damaged Infrastructure Emergency Rehabilitation Project. Asian Developement Bank.

Ahern, M. , R. S. Kovats , P. Wilkinson , R. Few, and F. Matthies, (2005), Global Health Impacts of Floods: Epidemiologic Evidence, *Epidemiologic Reviews*, 27(1), 36-46, doi: 10.1093/epirev/mxi004.

Ai-Juan, B. , L. Chang-Hai, and L. Xiao-Dong, (2008), Diurnal variation of summer rainfall over the Tibetan Plateau and its neighboring regions revealed by TRMM Multi-satellite Precipitation Analysis.

Alexander, L. V. , X. Zhang , T. C. Peterson , J. Caesar , B. Gleason , A. M. G. Klein Tank , M. Haylock , D. Collins , B. Trewin , F. Rahimzadeh , A. Tagipour , K. Rupa Kumar , J. Revadekar , G. Griffiths , L. Vincent , D. B. Stephenson , J. Burn , E. Aguilar , M. Brunet , M. Taylor , M. New , P. Zhai , M. Rusticucci, and J. L. Vazquez-Aguirre, (2006), Global observed changes in daily climate extremes of temperature and precipitation, *Journal of Geophysical Research: Atmospheres*, 111(D5), D05109, doi: 10.1029/2005JD006290.

Alfieri, L., and J. Thielen, (2015), A European precipitation index for extreme rain-storm and flash flood early warning, *Meteorological Applications*, 22(1), 3-13, doi: 10.1002/met.1328.

Allan, R. , C. Liu , M. Zahn , D. Lavers , E. Koukouvagias, and A. Bodas-Salcedo, (2014), Physically Consistent Responses of the Global Atmospheric Hydrological Cycle in Models and Observations, *Surveys in Geophysics*, 35(3), 533-552, doi: 10.1007/s10712-012-9213-z.

Allan, R. P., and B. J. Soden, (2008), Atmospheric Warming and the Amplification of Precipitation Extremes, *Science*, 321(5895), 1481-1484, doi: 10.1126/science.1160787.

Allen, M. R., and W. J. Ingram, (2002), Constraints on future changes in climate and the hydrologic cycle, *Nature*, 419(6903), 224-232.

Aon, cited 2014: Impact Forecasting. [Available online at http://thoughtleadership.aonbenfield.com/Pages/home.aspx?reportcategory=impact%20forecasting.]

Argueso, D. , J. P. Evans, and L. Fita, (2013), Precipitation bias correction of very high resolution regional climate models, *HESSD*, 10(6), doi: 10.5194/hessd-10-8145-2013.

Attema, J. J. , J. M. Loriaux, and G. Lenderink, (2014), Extreme precipitation response to climate perturbations in an atmospheric mesoscale model, *Environmental Research Letters*, 9(1), 014003 (014012 pp.)-014003 (014012 pp.), doi: 10.1088/1748-9326/9/1/014003.

Benestad, R. E., (2010), Downscaling precipitation extremes, *Theoretical & Applied Climatology*, 100(1/2), 1-21, doi: 10.1007/s00704-009-0158-1.

Beniston, M. , D. Stephenson , O. Christensen , C. T. Ferro , C. Frei , S. Goyette , K. Halsnaes , T. Holt , K. Jylhä , B. Koffi , J. Palutikof , R. Schöll , T. Semmler, and K. Woth, (2007), Future extreme events in European climate: an exploration of regional climate model projections, *Climatic Change*, 81(1), 71-95, doi: 10.1007/s10584-006-9226-z.

Berg, P. , C. Moseley, and J. O. Haerter, (2013), Strong increase in convective precipitation in response to higher temperatures, *Nature Geosci*, 6(3), 181-185, doi: 10.1038/ngeo1731.

Berne, A. , G. Delrieu , J.-D. Creutin, and C. Obled, (2004), Temporal and spatial resolution of rainfall measurements required for urban hydrology, *Journal of Hydrology*, 299(3–4), 166-179.

Betts, A. K., and M. J. Miller, (1993), The Betts-Miller scheme. Chapter 9 in "The Representation of Cumulus Convection in Numerical Models of the Atmosphere", *Amer. Meteor. Soc., Meteor.*(46), 107-121.

Beuchat, X. , B. Schaefli , M. Soutter, and A. Mermoud, (2011), Toward a robust method for subdaily rainfall downscaling from daily data, *Water Resources Research*, 47(9), W09524, doi: 10.1029/2010WR010342.

Buonomo, E. , R. Jones , C. Huntingford, and J. Hannaford, (2007), On the robustness of changes in extreme precipitation over Europe from two high resolution climate change simulations, *Quarterly Journal of the Royal Meteorological Society*, 133(622), 65-81, doi: 10.1002/qj.13.

Carbone, R. E., and J. D. Tuttle, (2008), Rainfall Occurrence in the U.S. Warm Season: The Diurnal Cycle*, *Journal of Climate*, 21(16), 4132-4146, doi: 10.1175/2008JCLI2275.1.

Chan, S. , E. Kendon , H. Fowler , S. Blenkinsop , C. T. Ferro, and D. Stephenson, (2013), Does increasing the spatial resolution of a regional climate model improve the simulated daily precipitation?, *Climate Dynamics*, 41(5-6), 1475-1495, doi: 10.1007/s00382-012-1568-9.

Chan, S. C. , E. J. Kendon , H. J. Fowler , S. Blenkinsop , N. M. Roberts, and C. A. T. Ferro, (2014), The Value of High-Resolution Met Office Regional Climate Models in the Simulation of Multihourly Precipitation Extremes, *Journal of Climate*, 27(16), 6155-6174, doi: 10.1175/JCLI-D-13-00723.1.

Chen, C.-T., and T. Knutson, (2008), On the Verification and Comparison of Extreme Rainfall Indices from Climate Models, *Journal of Climate*, 21(7), 1605-1621, doi: 10.1175/2007JCLI1494.1.

Chen, D. , C. Achberger , T. Ou , U. Postgård , A. Walther, and Y. Liao, (2015), Projecting Future Local Precipitation and Its Extremes for Sweden, *Geografiska Annaler: Series A, Physical Geography*, 97(1), 25-39, doi: 10.1111/geoa.12084.

Chou, C., and C.-W. Lan, (2011), Changes in the Annual Range of Precipitation under Global Warming, *Journal of Climate*, 25(1), 222-235, doi: 10.1175/JCLI-D-11-00097.1.

Chou, C. , J. C. H. Chiang , C.-W. Lan , C.-H. Chung , Y.-C. Liao, and C.-J. Lee, (2013), Increase in the range between wet and dry season precipitation, *Nature Geosci*, 6(4), 263-267.

Christensen, J. H., and O. B. Christensen, (2003), Climate modelling: Severe summertime flooding in Europe, *Nature*, 421(6925), 805-806.

Coles, S. G., 2001: *An Introduction to Statistical Modelling of Extreme Values.*

Conrad, W., and S. Ashish, (2015), Climate change: Hot storms bring big rainfall swings, *Nature*, 522(7555), 130-131, doi: 10.1038/522130d.

Coumou, D., and S. Rahmstorf, (2012), A decade of weather extremes, *Nature Clim. Change*, 2(7), 491-496.

da Rocha, R. P. , C. A. Morales , S. V. Cuadra, and T. Ambrizzi, (2009), Precipitation diurnal cycle and summer climatology assessment over South America: An evaluation of Regional Climate Model version 3 simulations, *Journal of Geophysical Research: Atmospheres*, 114(D10), n/a-n/a, doi: 10.1029/2008JD010212.

Dai, A., (2006), Precipitation Characteristics in Eighteen Coupled Climate Models, *Journal of Climate*, 19(18), 4605-4630, doi: 10.1175/JCLI3884.1.

Dai, A., (2011), Drought under global warming: a review, *Wiley Interdisciplinary Reviews: Climate Change*, 2(1), 45-65, doi: 10.1002/wcc.81.

Dai, A., and K. E. Trenberth, (2004), The Diurnal Cycle and Its Depiction in the Community Climate System Model, *Journal of Climate*, 17(5), 930-951.

Di Luca, A. , R. de Elía, and R. Laprise, (2012), Potential for added value in precipitation simulated by high-resolution nested Regional Climate Models and observations, *Climate Dynamics*, 38(5-6), 1229-1247, doi: 10.1007/s00382-011-1068-3.

Donat, M. G. , L. V. Alexander , H. Yang , I. Durre , R. Vose , R. J. H. Dunn , K. M. Willett , E. Aguilar , M. Brunet , J. Caesar , B. Hewitson , C. Jack , A. M. G. Klein Tank , A. C. Kruger , J. Marengo , T. C. Peterson , M. Renom , C. Oria Rojas , M. Rusticucci , J. Salinger , A. S. Elrayah , S. S. Sekele , A. K. Srivastava , B. Trewin , C. Villarroel , L. A. Vincent , P. Zhai , X. Zhang, and S. Kitching, (2013), Updated analyses of temperature and precipitation extreme indices since the beginning of the twentieth century: The HadEX2 dataset, *Journal of Geophysical Research: Atmospheres*, 118(5), 2098-2118, doi: 10.1002/jgrd.50150.

Durman, C. F. , J. M. Gregory , D. C. Hassell , R. G. Jones, and J. M. Murphy, (2001), A comparison of extreme European daily precipitation simulated by a global and a regional climate model for present and future climates, *Quarterly Journal of the Royal Meteorological Society*, 127(573), 1005-1015, doi: 10.1002/qj.49712757316.

Evans, J. , M. Ekström, and F. Ji, (2012), Evaluating the performance of a WRF physics ensemble over South-East Australia, *Climate Dynamics*, 39(6), 1241-1258, doi: 10.1007/s00382-011-1244-5.

Evans, J. P., and M. F. McCabe, (2010), Regional climate simulation over Australia's Murray-Darling basin: A multitemporal assessment, *Journal of Geophysical Research: Atmospheres*, 115(D14), D14114, doi: 10.1029/2010JD013816.

Evans, J. P., and S. Westra, (2012), Investigating the Mechanisms of Diurnal Rainfall Variability Using a Regional Climate Model, *Journal of Climate*, 25(20), 7232-7247, doi: Doi 10.1175/Jcli-D-11-00616.1.

Evans, J. P., and F. Ji, 2012: Choosing GCMs, NARCliM Technical Note 1, Sydney, Australia.

Evans, J. P., and M. F. McCabe, (2013), Effect of model resolution on a regional climate model simulation over southeast Australia, *Climate Research*, 56(2), 131-145, doi: 10.3354/cr01151.

Evans, J. P. , M. Ekström, and F. Ji, (2011), Evaluating the performance of a WRF physics ensemble over South-East Australia, *Climate Dynamics*, 39(6), 1241-1258, doi: 10.1007/s00382-011-1244-5.

Evans, J. P. , F. Ji , C. Lee , P. Smith , D. Argüeso, and L. Fita, (2014), Design of a regional climate modelling projection ensemble experiment – NARCliM, *Geosci. Model Dev.*, 7(2), 621-629, doi: 10.5194/gmd-7-621-2014.

Fowler, H. J., and C. G. Kilsby, (2003), Implications of changes in seasonal and annual extreme rainfall, *Geophysical Research Letters*, 30(13), 1720, doi: 10.1029/2003GL017327.

Fowler, H. J., and M. Ekström, (2009), Multi-model ensemble estimates of climate change impacts on UK seasonal precipitation extremes, *International Journal of Climatology*, 29(3), 385-416, doi: 10.1002/joc.1827.

Fowler, H. J. , S. Blenkinsop, and C. Tebaldi, (2007), Linking climate change modelling to impacts studies: recent advances in downscaling techniques for hydrological modelling, *International Journal of Climatology*, 27(12), 1547-1578, doi: 10.1002/joc.1556.

Fowler, H. J. , M. Ekström , C. G. Kilsby, and P. D. Jones, (2005), New estimates of future changes in extreme rainfall across the UK using regional climate model integrations. 1. Assessment of control climate, *Journal of Hydrology*, 300(1–4), 212-233.

Frei, C. , R. Schöll , S. Fukutome , J. Schmidli, and P. L. Vidale, (2006), Future change of precipitation extremes in Europe: Intercomparison of scenarios from regional climate models, *Journal of Geophysical Research: Atmospheres*, 111(D6), D06105, doi: 10.1029/2005JD005965.

Frei, C. , J. H. Christensen , M. Déqué , D. Jacob , R. G. Jones, and P. L. Vidale, (2003), Daily precipitation statistics in regional climate models: Evaluation and intercomparison for the European Alps, *Journal of Geophysical Research: Atmospheres*, 108(D3), n/a-n/a, doi: 10.1029/2002JD002287.

Fujibe, F., (2013), Clausius–Clapeyron-like relationship in multidecadal changes of extreme short-term precipitation and temperature in Japan, *Atmospheric Science Letters*, 14(3), 127-132, doi: 10.1002/asl2.428.

Gleckler, P. J. , K. E. Taylor, and C. Doutriaux, (2008), Performance metrics for climate models, *Journal of Geophysical Research: Atmospheres*, 113(D6), D06104, doi: 10.1029/2007JD008972.

Gregersen, I. B. , H. J. D. Sørup , H. Madsen , D. Rosbjerg , P. S. Mikkelsen , K. Arnbjerg-Nielsen , I. B. Gregersen , H. J. D. Sørup , H. Madsen , D. Rosbjerg , P. S. Mikkelsen, and K. Arnbjerg-Nielsen, (2013), Assessing future climatic changes of rainfall extremes at small spatio-temporal scales, *Climatic Change*, 118(3-4), 783-797, doi: 10.1007/s10584-012-0669-0.

Groisman, P. Y. , R. W. Knight, and T. R. Karl, (2001), Heavy Precipitation and High Streamflow in the Contiguous United States: Trends in the Twentieth Century, *Bulletin of the American Meteorological Society*, 82(2), 219-246, doi: 10.1175/1520-0477(2001)082<0219:HPAHSI>2.3.CO;2.

Groisman, P. Y. , R. W. Knight, and T. R. Karl, (2012), Changes in Intense Precipitation over the Central United States, *Journal of Hydrometeorology*, 13(1), 47-66, doi: 10.1175/JHM-D-11-039.1.

Groisman, P. Y. , R. W. Knight , D. R. Easterling , T. R. Karl , G. C. Hegerl, and V. N. Razuvaev, (2005), Trends in Intense Precipitation in the Climate Record, *Journal of Climate*, 18(9), 1326-1350, doi: 10.1175/JCLI3339.1.

Gutowski, W. J. , S. G. Decker , R. A. Donavon , Z. Pan , R. W. Arritt, and E. S. Takle, (2003), Temporal–Spatial Scales of Observed and Simulated Precipitation in Central U.S. Climate, *Journal of Climate*, 16(22), 3841-3847, doi: 10.1175/1520-0442(2003)016<3841:TSOOAS>2.0.CO;2.

Gutowski, W. J. , R. W. Arritt , S. Kawazoe , D. M. Flory , E. S. Takle , S. Biner , D. Caya , R. G. Jones , R. Laprise , L. R. Leung , L. O. Mearns , W. Moufouma-Okia , A. M. B. Nunes , Y. Qian , J. O. Roads , L. C. Sloan, and M. A. Snyder, (2010), Regional Extreme Monthly Precipitation Simulated by NARCCAP RCMs, *Journal of Hydrometeorology*, 11(6), 1373-1379, doi: 10.1175/2010JHM1297.1.

Haerter, J. O., and P. Berg, (2009), Unexpected rise in extreme precipitation caused by a shift in rain type?, *Nature Geosci*, 2(6), 372-373.

Hand, W. H. , N. I. Fox, and C. G. Collier, (2004), A study of twentieth-century extreme rainfall events in the United Kingdom with implications for forecasting, *Meteorological Applications*, 11(1), 15-31, doi: 10.1017/S1350482703001117.

Hanel, M., and T. A. Buishand, (2010), On the value of hourly precipitation extremes in regional climate model simulations, *Journal of Hydrology*, 393(3–4), 265-273.

Harding, K. J., and P. K. Snyder, (2014), Examining future changes in the character of Central U.S. warm-season precipitation using dynamical downscaling, *Journal of Geophysical Research: Atmospheres*, 119(23), 2014JD022575, doi: 10.1002/2014JD022575.

Harding, K. J., and P. K. Snyder, (2015), Using dynamical downscaling to examine mechanisms contributing to the intensification of Central U.S. heavy rainfall

events, *Journal of Geophysical Research: Atmospheres*, 120(7), 2754-2772, doi: 10.1002/2014JD022819.

Hardwick Jones, R. , S. Westra, and A. Sharma, (2010), Observed relationships between extreme sub-daily precipitation, surface temperature, and relative humidity, *Geophysical Research Letters*, 37(22), L22805, doi: 10.1029/2010GL045081.

Hartmann, D. L. , A. M. G. K. Tank , M. Rusticucci , L. V. Alexander , S. Brönnimann , Y. Charabi , F.J. Dentener , E.J. Dlugokencky , D.R. Easterling , A. Kaplan , B.J. Soden , P.W. Thorne , M. Wild, and P.M. Zhai, 2013: Observations: Atmosphere and Surface., Contribution of Working Group I to the Fifth Assessment Report of the Intergovernmental Panel on Climate Change Cambridge, United Kingdom and New York, NY, USA, 159–254 pp.

Haylock, M. R. , G. C. Cawley , C. Harpham , R. L. Wilby, and C. M. Goodess, (2006), Downscaling heavy precipitation over the United Kingdom: a comparison of dynamical and statistical methods and their future scenarios, *International Journal of Climatology*, 26(10), 1397-1415, doi: 10.1002/joc.1318.

Hitchens, N. M. , R. J. Trapp , M. E. Baldwin, and A. Gluhovsky, (2010), Characterizing Subdiurnal Extreme Precipitation in the Midwestern United States, *Journal of Hydrometeorology*, 11(1), 211-218, doi: 10.1175/2009JHM1129.1.

Hohenegger C. , P. Brockhaus, and C. Schaer, (2008), Towards climate simulations at cloud-resolving scales, *Meteorol. Z*, 17(4), 383-394.

Holtanová, E. , J. Mikšovský , J. Kalvová , P. Pišoft, and M. Motl, (2012), Performance of ENSEMBLES regional climate models over Central Europe using various metrics, *Theoretical and Applied Climatology*, 108(3-4), 463-470, doi: 10.1007/s00704-011-0542-5.

Hong, S.-Y. , Y. Noh, and J. Dudhia, (2006), A New Vertical Diffusion Package with an Explicit Treatment of Entrainment Processes, *Monthly Weather Review*, 134(9), 2318-2341, doi: 10.1175/MWR3199.1.

Horsham, (2003), DO WE NEED TO CONSIDER FLOODS RARER THAN 1% AEP?, *HEALTHY Floodplains WEALTHY Future*.

Hurkmans, R. , W. Terink , R. Uijlenhoet , P. Torfs , D. Jacob, and P. A. Troch, (2010), Changes in streamflow dynamics in the rhine basin under three high-resolution regional climate scenarios, *J. Clim.*, 23(3), 679.

INSW, I. N. S. W., 2012: 2012 State Infrastructure Strategy: First things first. Infrastructure, Ed., 53.

IPCC, 2012: *Managing the Risks of Extreme Events and Disasters to Advance Climate Change Adaptation.* Cambridge University Press, 582 pp pp.

IPCC, 2013: Climate Change 2013: The Physical Science Basis *Contribution of Working Group I to the Fifth Assessment Report of the Intergovernmental Panel on Climate Change [Stocker, T.F., D. Qin, G.-K. Plattner, M. Tignor, S.K. Allen, J. Boschung, A. Nauels, Y. Xia, V. Bex and P.M. Midgley (eds.)].* 1535.

Jakob, D. , D. J. Karoly, and A. Seed, (2011a), Non-stationarity in daily and sub-daily intense rainfall – Part 2: Regional assessment for sites in south-east Australia, *Nat. Hazards Earth Syst. Sci.*, 11(8), 2273-2284, doi: 10.5194/nhess-11-2273-2011.

Jakob, D. , D. J. Karoly, and A. Seed, (2011b), Non-stationarity in daily and sub-daily intense rainfall – Part 1: Sydney, Australia, *Nat. Hazards Earth Syst. Sci.*, 11(8), 2263-2271, doi: 10.5194/nhess-11-2263-2011.

Janjić, Z. I., (1994), The Step-Mountain Eta Coordinate Model: Further Developments of the Convection, Viscous Sublayer, and Turbulence Closure Schemes, *Monthly Weather Review*, 122(5), 927-945, doi: 10.1175/1520-0493(1994)122<0927:TSMECM>2.0.CO;2.

Jeong, J.-H. , A. Walther , G. Nikulin , D. Chen, and C. Jones, (2011), Diurnal cycle of precipitation amount and frequency in Sweden: observation versus model simulation, *Tellus A*, 63(4).

Johnson, F., and A. Sharma, (2011), Accounting for interannual variability: A comparison of options for water resources climate change impact assessments, *Water Resources Research*, 47(4), W04508, doi: 10.1029/2010WR009272.

Kain, J. S., (2004), The Kain–Fritsch Convective Parameterization: An Update, *Journal of Applied Meteorology*, 43(1), 170-181, doi: 10.1175/1520-0450(2004)043<0170:TKCPAU>2.0.CO;2.

Kang, I.-S. , Y.-M. Yang, and W.-K. Tao, (2014), GCMs with implicit and explicit representation of cloud microphysics for simulation of extreme precipitation frequency, *Climate Dynamics*, 1-11, doi: 10.1007/s00382-014-2376-1.

Kao, S.-C., and A. R. Ganguly, (2011), Intensity, duration, and frequency of precipitation extremes under 21st-century warming scenarios, *Journal of Geophysical Research: Atmospheres*, 116(D16), n/a-n/a, doi: 10.1029/2010JD015529.

Kendon, E. J. , D. P. Rowell , R. G. Jones, and E. Buonomo, (2008), Robustness of Future Changes in Local Precipitation Extremes, *Journal of Climate*, 21(17), 4280-4297, doi: 10.1175/2008JCLI2082.1.

Kendon, E. J. , N. M. Roberts , C. A. Senior, and M. J. Roberts, (2012), Realism of Rainfall in a Very High-Resolution Regional Climate Model, *Journal of Climate*, 25(17), 5791-5806, doi: 10.1175/JCLI-D-11-00562.1.

Kendon, E. J. , N. M. Roberts , H. J. Fowler , M. J. Roberts , S. C. Chan, and C. A. Senior, (2014), Heavier summer downpours with climate change revealed by weather forecast resolution model, *Nature Clim. Change*, 4(7), 570-576, doi: 10.1038/nclimate2258.

Kharin, V. V. , F. W. Zwiers , X. Zhang, and G. C. Hegerl, (2013), Changes in Temperature and Precipitation Extremes in the IPCC Ensemble of Global Coupled Model Simulations, *Journal of Climate*, 20(8), 1419-1444, doi: 10.1175/JCLI4066.1.

Kitoh, A. , H. Endo , K. Krishna Kumar , I. F. A. Cavalcanti , P. Goswami, and T. Zhou, (2013), Monsoons in a changing world: A regional perspective in a global context, *Journal of Geophysical Research: Atmospheres*, 118(8), 3053-3065, doi: 10.1002/jgrd.50258.

Kotlyakov, V. M. , L. V. Desinov , S. V. Dolgov , N. I. Koronkevich , E. A. Likhacheva , A. N. Makkaveev , A. A. Medvedev, and V. A. Rudakov, (2013), Flooding of July 6–7, 2012, in the town of Krymsk, *Reg. Res. Russ.*, 3(1), 32-39, doi: 10.1134/S2079970513010061.

Kunkel, K. E. , T. R. Karl , D. R. Easterling , K. Redmond , J. Young , X. Yin, and P. Hennon, (2013), Probable maximum precipitation and climate change, *Geophysical Research Letters*, 40(7), 1402-1408, doi: 10.1002/grl.50334.

Lenderink, G., and E. van Meijgaard, (2008), Increase in hourly precipitation extremes beyond expectations from temperature changes, *Nature Geosci*, 1(8), 511-514.

Lenderink, G., and E. Van Meijgaard, (2010), Linking increases in hourly precipitation extremes to atmospheric temperature and moisture changes, *Environmental Research Letters*, 5(2).

Lenderink, G. , H. Y. Mok , T. C. Lee, and G. J. van Oldenborgh, (2011), Scaling and trends of hourly precipitation extremes in two different climate zones – Hong Kong and the Netherlands, *HESSD*, 8(3), 4701-4719, doi: 10.5194/hessd-8-4701-2011.

Leonard, M. , S. Westra , A. Phatak , M. Lambert , B. van den Hurk , K. McInnes , J. Risbey , S. Schuster , D. Jakob, and M. Stafford-Smith, (2014), A compound

event framework for understanding extreme impacts, *Wiley Interdisciplinary Reviews: Climate Change*, 5(1), 113-128, doi: 10.1002/wcc.252.

Li, F. , D. Rosa , W. D. Collins, and M. F. Wehner, (2012), “Super-parameterization”: A better way to simulate regional extreme precipitation?, *Journal of Advances in Modeling Earth Systems*, 4(2), M04002, doi: 10.1029/2011MS000106.

Li, J. , R. Yu, and T. Zhou, (2008), Seasonal Variation of the Diurnal Cycle of Rainfall in Southern Contiguous China, *Journal of Climate*, 21(22), 6036-6043, doi: 10.1175/2008JCLI2188.1.

Lins, H. F., and T. A. Cohn, (2011), Stationarity: Wanted Dead or Alive?1, *JAWRA Journal of the American Water Resources Association*, 47(3), 475-480, doi: 10.1111/j.1752-1688.2011.00542.x.

Loriaux, J. M. , G. Lenderink , S. R. De Roode, and A. P. Siebesma, (2013), Understanding Convective Extreme Precipitation Scaling Using Observations and an Entraining Plume Model, *Journal of the Atmospheric Sciences*, doi: 10.1175/JAS-D-12-0317.1.

Maraun, D. , H. W. Rust, and T. J. Osborn, (2009), The annual cycle of heavy precipitation across the United Kingdom: a model based on extreme value statistics, *International Journal of Climatology*, 29(12), 1731-1744, doi: 10.1002/joc.1811.

Maraun, D. , T. Osborn, and H. Rust, (2011), The influence of synoptic airflow on UK daily precipitation extremes. Part I: Observed spatio-temporal relationships, *Climate Dynamics*, 36(1-2), 261-275, doi: 10.1007/s00382-009-0710-9.

Maraun, D. , F. Wetterhall , A. M. Ireson , R. E. Chandler , E. J. Kendon , M. Widmann , S. Brienen , H. W. Rust , T. Sauter , M. Themeßl , V. K. C. Venema , K. P. Chun , C. M. Goodess , R. G. Jones , C. Onof , M. Vrac, and I. Thiele-Eich, (2010), Precipitation downscaling under climate change: Recent developments to bridge the gap between dynamical models and the end user, *Reviews of Geophysics*, 48(3), RG3003, doi: 10.1029/2009RG000314.

Mellor, G. L., and T. Yamada, (1982), Development of a turbulence closure model for geophysical fluid problems, *Reviews of Geophysics*, 20(4), 851-875, doi: 10.1029/RG020i004p00851.

Min, S.-K. , X. Zhang , F. W. Zwiers, and G. C. Hegerl, (2011), Human contribution to more-intense precipitation extremes, *Nature*, 470(7334), 378-381.

Mishra, V., and D. P. Lettenmaier, (2011), Climatic trends in major U.S. urban areas, 1950–2009, *Geophysical Research Letters*, 38(16), L16401, doi: 10.1029/2011GL048255.

Mishra, V. , F. Dominguez, and D. P. Lettenmaier, (2012a), Urban precipitation extremes: How reliable are regional climate models?, *Geophysical Research Letters*, 39(3), L03407, doi: 10.1029/2011GL050658.

Mishra, V. , J. M. Wallace, and D. P. Lettenmaier, (2012b), Relationship between hourly extreme precipitation and local air temperature in the United States, *Geophysical Research Letters*, 39(16), L16403, doi: 10.1029/2012GL052790.

Mishra, V. , D. Kumar , A. R. Ganguly , J. Sanjay , M. Mujumdar , R. Krishnan, and R. D. Shah, (2014), Reliability of regional and global climate models to simulate precipitation extremes over India, *Journal of Geophysical Research: Atmospheres*, 119(15), 9301-9323, doi: 10.1002/2014JD021636.

Moberg, A. , P. D. Jones , D. Lister , A. Walther , M. Brunet , J. Jacobeit , L. V. Alexander , P. M. Della-Marta , J. Luterbacher , P. Yiou , D. Chen , A. M. G. Klein Tank , O. Saladié , J. Sigró , E. Aguilar , H. Alexandersson , C. Almarza , I. Auer , M. Barriendos , M. Begert , H. Bergström , R. Böhm , C. J. Butler , J. Caesar , A. Drebs , D. Founda , F.-W. Gerstengarbe , G. Micela , M. Maugeri , H. Österle , K. Pandzic , M. Petrakis , L. Srnec , R. Tolasz , H. Tuomenvirta , P. C. Werner ,

H. Linderholm , A. Philipp , H. Wanner, and E. Xoplaki, (2006), Indices for daily temperature and precipitation extremes in Europe analyzed for the period 1901–2000, *Journal of Geophysical Research: Atmospheres*, 111(D22), D22106, doi: 10.1029/2006JD007103.

Muller, C. J. , P. A. O'Gorman, and L. E. Back, (2011), Intensification of Precipitation Extremes with Warming in a Cloud-Resolving Model, *Journal of Climate*, 24(11), 2784-2800, doi: 10.1175/2011JCLI3876.1.

National Weather Service, cited 2014: Oklahoma and Arkansas Severe Weather Awareness Week. [Available online at http://www.srh.noaa.gov/tsa/?n=swaw-thunderstorm-safety.]

Nesbitt, S. W., and E. J. Zipser, (2003), The Diurnal Cycle of Rainfall and Convective Intensity according to Three Years of TRMM Measurements, *Journal of Climate*, 16(10), 1456-1475, doi: 10.1175/1520-0442-16.10.1456.

Ngongondo, C. , C.-Y. Xu , L. Tallaksen , B. Alemaw, and T. Chirwa, (2011), Regional frequency analysis of rainfall extremes in Southern Malawi using the index rainfall and L-moments approaches, *Stoch Environ Res Ris Assess*, 25(7), 939-955, doi: 10.1007/s00477-011-0480-x.

Nguyen, V. T. V. , N. Desramaut, and T.-D. Nguyen, (2010), Optimal rainfall temporal patterns for urban drainage design in the context of climate change *Water Science & Technology*, 62(5), 1170–1176.

Nicholls, N., and L. Alexander, (2007), Has the climate become more variable or extreme? Progress 1992-2006, *Progress in Physical Geography*, 31(1), 77-87, doi: 10.1177/0309133307073885.

NOAA, N. O. a. A. A., cited 2014: Flood Hazards. [Available online at http://www.floodsafety.noaa.gov/hazards.shtml.]

O'Gorman, P. A., and T. Schneider, (2009), The physical basis for increases in precipitation extremes in simulations of 21st-century climate change, *Proceedings of the National Academy of Sciences*, 106(35), 14773-14777, doi: 10.1073/pnas.0907610106.

O'Gorman, P., (2015), Precipitation Extremes Under Climate Change, *Curr Clim Change Rep*, 1(2), 49-59, doi: 10.1007/s40641-015-0009-3.

O'Gorman, P. A., and T. Schneider, (2009), Scaling of Precipitation Extremes over a Wide Range of Climates Simulated with an Idealized GCM, *Journal of Climate*, 22(21), 5676-5685, doi: 10.1175/2009JCLI2701.1.

O'Gorman, P. A., and C. J. Muller, (2010), How closely do changes in surface and column water vapor follow Clausius–Clapeyron scaling in climate change simulations?, *Environmental Research Letters*, 5(2), 025207.

Olsson, J. , U. Willén, and A. Kawamura, (2012), Downscaling extreme short-term regional climate model precipitation for urban hydrological applications, *Hydrol. Res*, doi: 10.2166/nh.2012.135.

Prein, A. F. , G. J. Holland , R. M. Rasmussen , J. Done , K. Ikeda , M. P. Clark, and C. H. Liu, (2013), Importance of Regional Climate Model Grid Spacing for the Simulation of Heavy Precipitation in the Colorado Headwaters, *Journal of Climate*, 26(13), 4848-4857, doi: 10.1175/JCLI-D-12-00727.1.

Randall, D. A. , R. A. Wood , S. Bony , R. Colman , T. Fichefet , J. Fyfe , V. Kattsov , A. Pitman , J. Shukla , J. Srinivasan , R. J. Stouffer , A. Sumi, and K. E. Taylor, 2007: Climate Models and Their Evaluation. In: Climate Change 2007: The Physical Science Basis. Contribution of Working Group I to the Fourth Assessment Report of the Intergovernmental Panel on Climate Change, Cambridge, United Kingdom and New York, NY, USA.

Romps, D. M., (2010), Response of Tropical Precipitation to Global Warming, *Journal of the Atmospheric Sciences*, 68(1), 123-138, doi: 10.1175/2010JAS3542.1.

Ross, R. J., and W. P. Elliott, (2001), Radiosonde-Based Northern Hemisphere Tropospheric Water Vapor Trends, *Journal of Climate*, 14(7), 1602-1612, doi: 10.1175/1520-0442(2001)014<1602:RBNHTW>2.0.CO;2.

Saha, S. , S. Moorthi , H.-L. Pan , X. Wu , J. Wang , S. Nadiga , P. Tripp , R. Kistler , J. Woollen , D. Behringer , H. Liu , D. Stokes , R. Grumbine , G. Gayno , J. Wang , Y.-T. Hou , H.-Y. Chuang , H.-M. H. Juang , J. Sela , M. Iredell , R. Treadon , D. Kleist , P. Van Delst , D. Keyser , J. Derber , M. Ek , J. Meng , H. Wei , R. Yang , S. Lord , H. van den Dool , A. Kumar , W. Wang , C. Long , M. Chelliah , Y. Xue , B. Huang , J.-K. Schemm , W. Ebisuzaki , R. Lin , P. Xie , M. Chen , S. Zhou , W. Higgins , C.-Z. Zou , Q. Liu , Y. Chen , Y. Han , L. Cucurull , R. W. Reynolds , G. Rutledge, and M. Goldberg, 2010: NCEP Climate Forecast System Reanalysis (CFSR) 6-hourly Products, January 1979 to December 2010. Research Data Archive at the National Center for Atmospheric Research, Computational and Information Systems Laboratory, 10.5065/D69K487J.

Salathé, E., Jr. , L. R. Leung , Y. Qian, and Y. Zhang, (2010), Regional climate model projections for the State of Washington, *Climatic Change*, 102(1-2), 51-75, doi: 10.1007/s10584-010-9849-y.

Sato, T. , H. Miura , M. Satoh , Y. N. Takayabu, and Y. Wang, (2009), Diurnal Cycle of Precipitation in the Tropics Simulated in a Global Cloud-Resolving Model, *Journal of Climate*, 22(18), 4809-4826, doi: 10.1175/2009JCLI2890.1.

Schindler, A. , D. Maraun, and J. Luterbacher, (2012), Validation of the present day annual cycle in heavy precipitation over the British Islands simulated by 14 RCMs, *Journal of Geophysical Research: Atmospheres*, 117(D18), D18107, doi: 10.1029/2012JD017828.

Schlosser, C. A., and P. R. Houser, (2007), Assessing a Satellite-Era Perspective of the Global Water Cycle, *Journal of Climate*, 20(7), 1316-1338, doi: 10.1175/JCLI4057.1.

Seidel, D. J. , Q. Fu , W. J. Randel, and T. J. Reichler, (2008), Widening of the tropical belt in a changing climate, *Nature Geosci*, 1(1), 21-24.

Sillmann, J. , V. V. Kharin , F. W. Zwiers , X. Zhang, and D. Bronaugh, (2013), Climate extremes indices in the CMIP5 multimodel ensemble: Part 2. Future climate projections, *Journal of Geophysical Research: Atmospheres*, 118(6), 2473-2493, doi: 10.1002/jgrd.50188.

Simmons, A. J. , K. M. Willett , P. D. Jones , P. W. Thorne, and D. P. Dee, (2010), Low-frequency variations in surface atmospheric humidity, temperature, and precipitation: Inferences from reanalyses and monthly gridded observational data sets, *Journal of Geophysical Research: Atmospheres*, 115(D1), D01110, doi: 10.1029/2009JD012442.

Singh, M. S., and P. A. O'Gorman, (2014), Influence of microphysics on the scaling of precipitation extremes with temperature, *Geophysical Research Letters*, 41(16), 6037-6044, doi: 10.1002/2014GL061222.

Singleton, A., and R. Toumi, (2013), Super-Clausius–Clapeyron scaling of rainfall in a model squall line, *Quarterly Journal of the Royal Meteorological Society*, 139(671), 334-339, doi: 10.1002/qj.1919.

Skamarock, W., C. , J. B. Klemp , J. Dudhia , D. O. Gill , B. D.M. , M. G. Duda , X. Y. Huang , W. Wang, and P. J.G., 2008: A description of the Advanced Research WRF version 3TN- 4751STR, 113 pp.

Skansi, M. D. L. M. , M. Brunet , J. Sigró , E. Aguilar , J. A. Arevalo Groening , O. J. Bentancur , Y. R. Castellón Geier , R. L. Correa Amaya , H. Jácome , A. Malheiros Ramos , C. Oria Rojas , A. M. Pasten , S. Sallons Mitro , C. Villaroel Jiménez , R. Martínez , L. V. Alexander, and P. D. Jones, (2013), Warming and

wetting signals emerging from analysis of changes in climate extreme indices over South America, *Global and Planetary Change*, 100, 295-307.

Solomon, S. , D. Qin , M. Manning , Z. Chen , M. Marquis , K. Averyt , M. Tignor, and H. Miller, (2007), Summary for Policymakers. Climate Change 2007: The Physical Science Basis. Contribution of Working Group I to the Fourth Assessment Report of the Intergovernmental Panel on Climate Change, 18.

Speer, M. S. , P. Wiles, and A. Pepler, (2009), Low pressure systems off the New South Wales coast and associated hazardous weather: establishment of a database, *Australian Meteorological and Oceanographic Journal*, 58, 29-39.

Stensmyr, P. , M. Babister, and M. Retallick, 2014: Australian Rainfall & Runoff, Revision Projects, Australia.

Stephens, G. L. , T. L'Ecuyer , R. Forbes , A. Gettlemen , J.-C. Golaz , A. Bodas-Salcedo , K. Suzuki , P. Gabriel, and J. Haynes, (2010), Dreary state of precipitation in global models, *Journal of Geophysical Research: Atmospheres*, 115(D24), n/a-n/a, doi: 10.1029/2010JD014532.

Sun, Y. , S. Solomon , D. Aiguo, and R. W. Portmann, (2006), How Often Does It Rain?, *Journal of Climate*, 19(6), 916-934.

Sunyer, M. A. , H. J. D. Sorup , O. B. Christensen , H. Madsen , P. S. Rosberjeg, and K. Arnbjerg-Nielsen, (2013), On the importance of observational data properties when assessing regional climate model performance of extreme precipitation, *HESSD*, 10(6), doi: 10.5194/hessd-10-7003-2013.

Taylor, K. E. , R. J. Stouffer, and G. A. Meehl, (2011), An Overview of CMIP5 and the Experiment Design, *Bulletin of the American Meteorological Society*, 93(4), 485-498, doi: 10.1175/BAMS-D-11-00094.1.

Trenberth, K., (2012), Framing the way to relate climate extremes to climate change, *Climatic Change*, 115(2), 283-290, doi: 10.1007/s10584-012-0441-5.

Trenberth, K. E., (1999), Atmospheric Moisture Recycling: Role of Advection and Local Evaporation, *Journal of Climate*, 12(5), 1368-1381, doi: 10.1175/1520-0442(1999)012<1368:AMRROA>2.0.CO;2.

Trenberth, K. E., (2005), The Impact of Climate Change and Variability on Heavy Precipitation, Floods, and Droughts, *Encyclopedia of Hydrological Sciences*, doi: 10.1002/0470848944.hsa211.

Trenberth, K. E., (2011), Changes in precipitation with climate change, *Climate Research*, 47(1), 123-138, doi: 10.3354/cr00953.

Trenberth, K. E. , D. P. Stepaniak, and J. M. Caron, (2000), The Global Monsoon as Seen through the Divergent Atmospheric Circulation, *Journal of Climate*, 13(22), 3969-3993, doi: 10.1175/1520-0442(2000)013<3969:TGMAST>2.0.CO;2.

Trenberth, K. E. , A. Dai , R. M. Rasmussen, and D. B. Parsons, (2003), The Changing Character of Precipitation, *Bulletin of the American Meteorological Society*, 84(9), 1205-1217, doi: 10.1175/BAMS-84-9-1205.

Tripathi, O. P., and F. Dominguez, (2013), Effects of spatial resolution in the simulation of daily and subdaily precipitation in the southwestern US, *Journal of Geophysical Research: Atmospheres*, n/a-n/a, doi: 10.1002/jgrd.50590.

Utsumi, N. , S. Seto , S. Kanae , E. E. Maeda, and T. Oki, (2011), Does higher surface temperature intensify extreme precipitation?, *Geophysical Research Letters*, 38(16), L16708, doi: 10.1029/2011GL048426.

van den Besselaar, E. J. M. , A. M. G. Klein Tank, and T. A. Buishand, (2013), Trends in European precipitation extremes over 1951–2010, *International Journal of Climatology*, 33(12), 2682-2689, doi: 10.1002/joc.3619.

van den Honert, R. C., and J. McAneney, (2011), The 2011 Brisbane Floods: Causes, Impacts and Implications, *Water*, 3(4), 1149-1173.

Walther, A. , J.-H. Jeong , G. Nikulin , C. Jones, and D. Chen, (2013), Evaluation of the warm season diurnal cycle of precipitation over Sweden simulated by the Rossby Centre regional climate model RCA3, *Atmospheric Research*, 119(0), 131-139.

Wang, B. , H.-J. Kim , K. Kikuchi, and A. Kitoh, (2011), Diagnostic metrics for evaluation of annual and diurnal cycles, *Climate Dynamics*, 37(5/6), 941-955, doi: 10.1007/s00382-010-0877-0.

Wehner, M. , R. Smith , G. Bala, and P. Duffy, (2010), The effect of horizontal resolution on simulation of very extreme US precipitation events in a global atmosphere model, *Climate Dynamics*, 34(2-3), 241-247, doi: 10.1007/s00382-009-0656-y.

Westra, S., and S. A. Sisson, (2011), Detection of non-stationarity in precipitation extremes using a max-stable process model, *Journal of Hydrology*, 406(1–2), 119-128.

Westra, S. , L. V. Alexander, and F. W. Zwiers, (2013), Global Increasing Trends in Annual Maximum Daily Precipitation, *Journal of Climate*, 26(11), 3904-3918, doi: 10.1175/JCLI-D-12-00502.1.

Westra, S. , M. Thyer , M. Leonard , D. Kavetski, and M. Lambert, (2014a), A strategy for diagnosing and interpreting hydrological model nonstationarity, *Water Resources Research*, 50(6), 5090-5113, doi: 10.1002/2013WR014719.

Westra, S. , H. J. Fowler , J. P. Evans , L. V. Alexander , P. Berg , F. Johnson , E. J. Kendon , G. Lenderink, and N. M. Roberts, (2014b), Future changes to the intensity and frequency of short-duration extreme rainfall, *Reviews of Geophysics*, 2014RG000464, doi: 10.1002/2014RG000464.

Wibig, J. , D. Maraun , R. Benestad , E. Kjellström , P. Lorenz, and O. B. Christensen, 2015: Projected Change—Models and Methodology. *Second Assessment of Climate Change for the Baltic Sea Basin*, B. I. I. A. T. The, Ed., Springer International Publishing, 189-215.

Willems, P. , K. Arnbjerg-Nielsen , J. Olsson, and V. T. V. Nguyen, (2012), Climate change impact assessment on urban rainfall extremes and urban drainage: Methods and shortcomings, *Atmospheric Research*, 103(0), 106-118.

WMO, 2009: *Manual for Estimation of Probable Maximum Precipitation.* 3rd ed.

Zhang, X. , L. Alexander , G. C. Hegerl , P. Jones , A. K. Tank , T. C. Peterson , B. Trewin, and F. W. Zwiers, (2011), Indices for monitoring changes in extremes based on daily temperature and precipitation data, *Wiley Interdisciplinary Reviews: Climate Change*, 2(6), 851-870, doi: 10.1002/wcc.147.

Zheng, F. , S. Westra, and M. Leonard, (2015), Opposing local precipitation extremes, *Nature Clim. Change*, 5(5), 389-390, doi: 10.1038/nclimate2579.

Zolina, O. , C. Simmer , A. Kapala , P. Shabanov , P. Becker , H. Mächel , S. Gulev, and P. Groisman, (2013), Precipitation Variability and Extremes in Central Europe: New View from STAMMEX Results, *Bulletin of the American Meteorological Society*, 95(7), 995-1002, doi: 10.1175/BAMS-D-12-00134.1.

Appendices

Appendix 1 – Supplementary figures

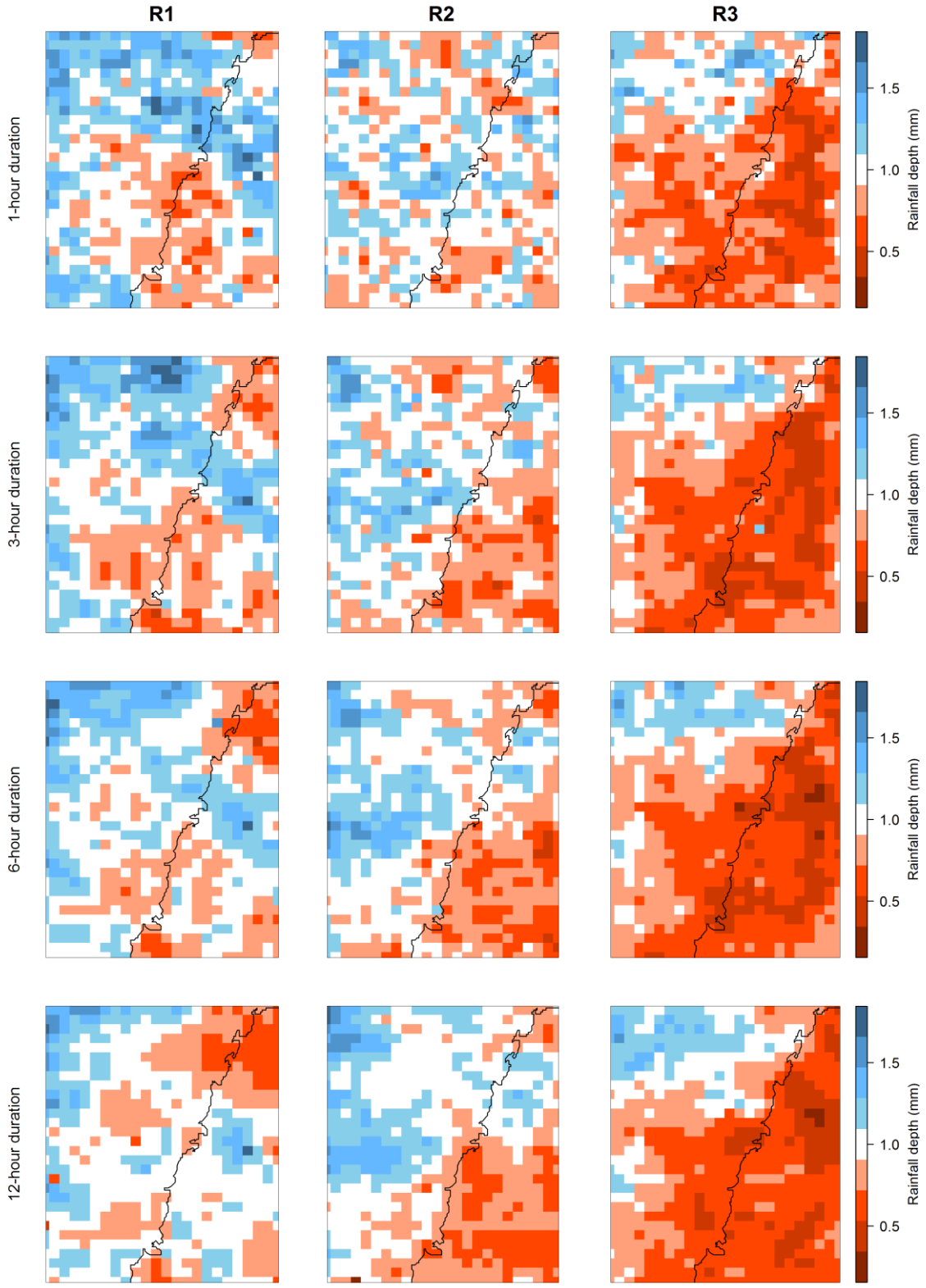

Supplementary Figure 1 **Ratio between the 1 in 10-year rainfall event at sub-daily durations for the near-term future (2020-2039) period and for the historical period for R1, R2 and R3 simulations over Greater Sydney.**

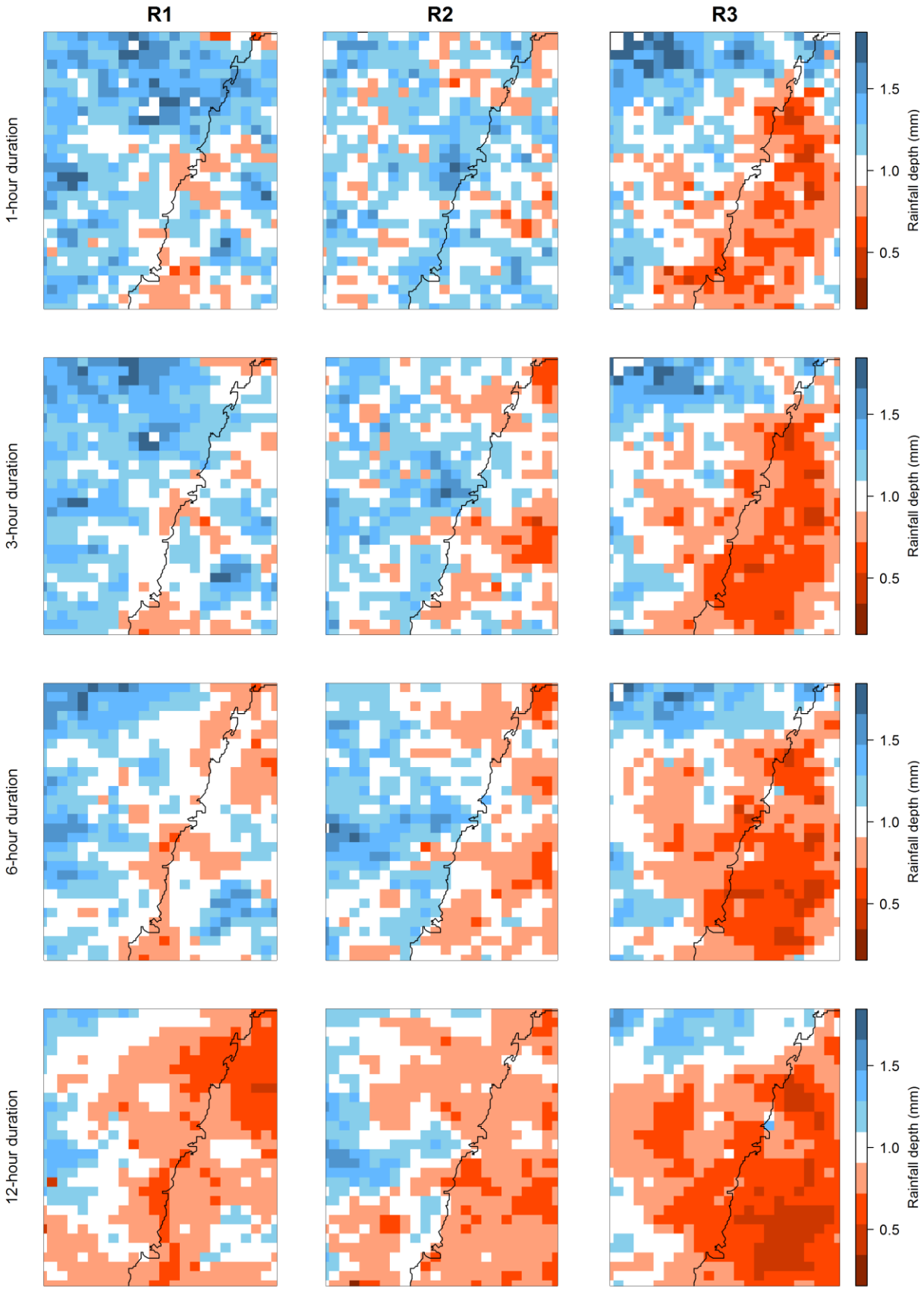

Supplementary Figure 2 **Ratio between the 1 in 10-year rainfall event at sub-daily durations for the near-term future (2060-2079) period and for the historical period for R1, R2 and R3 simulations over Greater Sydney.**

Appendix 2 – Supplementary figures

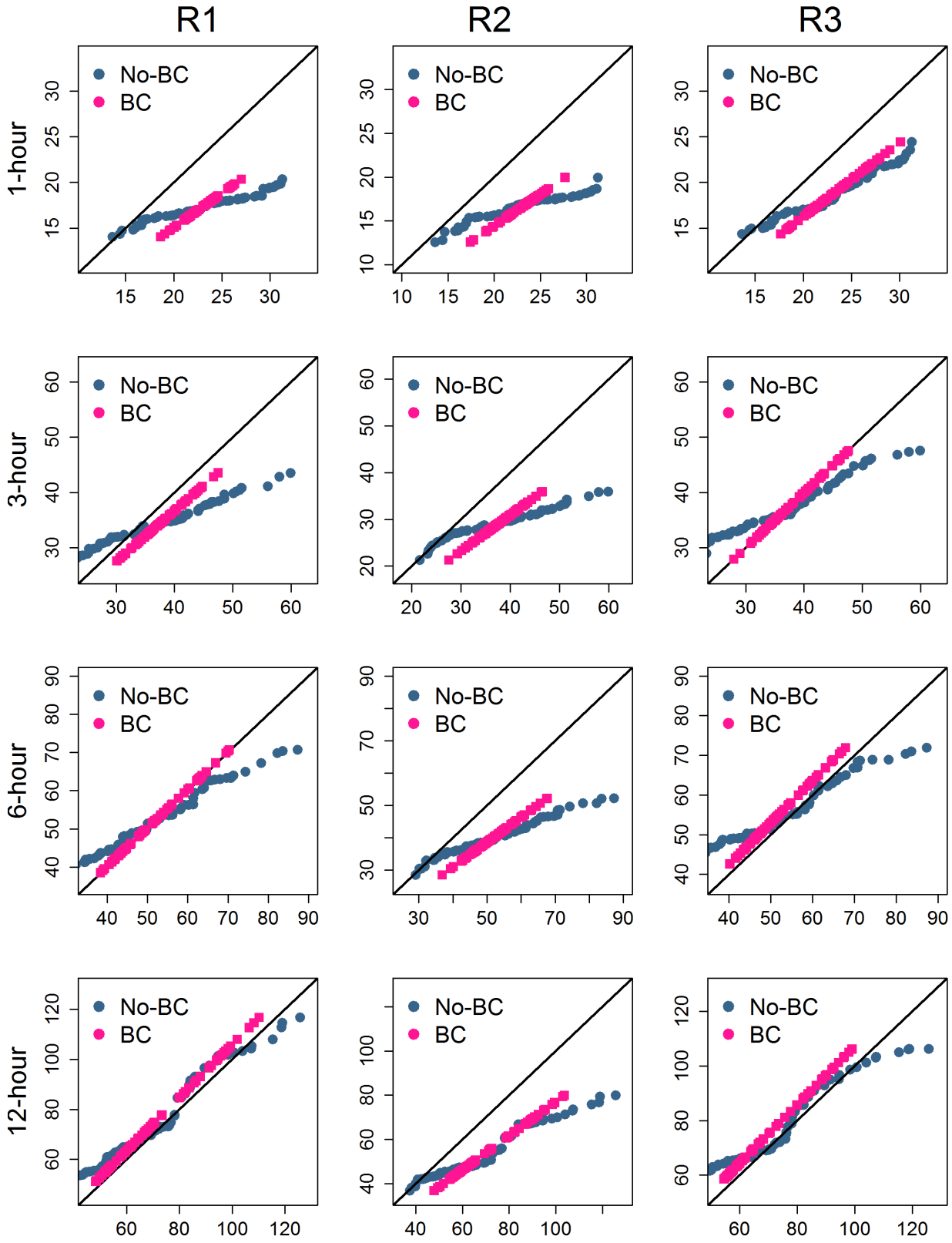

Supplementary Figure 3 **Quantile-quantile plots comparing the 1 in 2 year rainfall extreme events at 69 locations across the Greater Sydney region. Model outputs were compared with the observations (No BC) and then bias corrected (BC).**

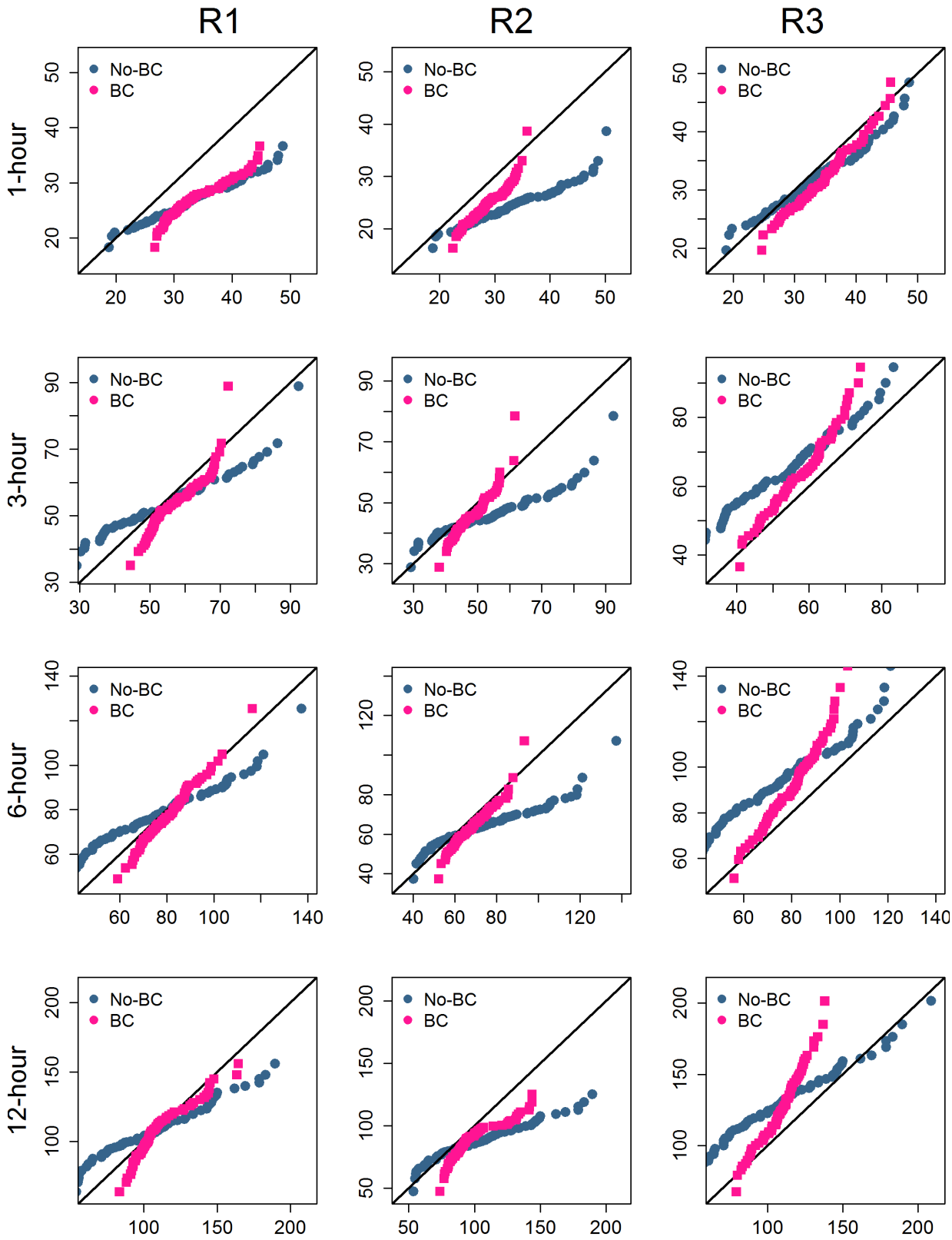

Supplementary Figure 4 **Quantile-quantile plots comparing the 1 in 10 year rainfall extreme events using the fitted GEV at 69 locations across the Greater Sydney region. Model outputs were compared with the observations (No BC) and then bias corrected (BC).**

Appendix 3 – The spatial configuration of atmospheric variables associated with the 10 most extreme rainfall events

Composite maps of weather variables associated with the most extreme precipitation events were constructed based on the work by Mishra et al. (2012b). Synoptic composite maps of the MSLP and 10-metre wind fields were built for the Greater Sydney region, based on the magnitude of the 10 most extreme rainfall events during 1990-2009 at Sydney Airport (-33.9465, 151.1731) weather station.

In observations, composite maps were made using the NCEP CFSR data sets. The spatial resolution in model simulations and CFSR (grid spatial resolution of 0.5° latitude x 0.5° longitude) datasets were interpolated using the R software package *akima* (http://www.r-project.org) to ensure consistency.

Synoptic composites of MSLP and wind (u and v components) fields associated with these extreme events were constructed in the R software by calculating the arithmetic mean of the variables for each grid point, as follows:

$$V_{ext} = \frac{\sum_{t=1}^{n} v_t}{n} \qquad \text{(Eq. S1)}$$

where V_{ext} is the mean magnitude of the variable (i.e. MSLP or wind speed) for each grid-point in both CSFR and RCM data from t=1 to n=10 (number of the most extreme events).

Finally, composite maps that associated the 10 most extreme rainfall events were constructed and compared between the reanalysis data (considered as observations) and model outputs.

Is the composite map of pressure and wind fields associated with the most extreme rainfall events in the observations and model simulations similar?

Daily maximum rainfall was used to identify the 10 most extreme rainfall events for the Sydney Airport weather location for both observations and model simulations during 1990-2009.

The dates and rainfall depths corresponding to the 10 most extreme rainfall events for both the OBS and RCMS are presented in the Supplementary Table 1. Most extreme events in the OBS occurred during summer months (DJFM) but less often in the RCM simulations. The lowest rainfall depth was registered in the observations (76.4 mm/day); whereas the highest in R3 (194.16 mm/day). The magnitude of daily maxima was mainly overestimated by R3 and overestimated by R1.

Supplementary Table 1 Rainfall depths and dates associated with the 10 most rainfall extreme for Sydney Airport location during the period 1990-2009.

No. events	the OBS		R1		R2		R3	
	date	rainfall depth	date	rainfall depth	date	rainfall depth	date	rainfall depth
1	1990-02-02	154	1991-01-17	102.88	1991-06-07	84	1996-02-16	102.17
2	1990-02-04	125.4	1995-06-05	94.78	1998-06-30	150	1996-05-19	146.13
3	1991-06-10	149.2	1996-02-15	102.57	1999-02-28	104.80	1997-05-22	112.66
4	1992-02-09	188.9	1996-08-31	99.83	2000-11-01	94.65	1998-07-25	169.86
5	1995-09-25	153.6	1998-01-28	106.45	2005-06-28	123.72	2000-11-04	122.52
6	1998-04-10	88.6	1999-04-02	98.17	2005-06-29	153.33	2001-02-05	114.62
7	2001-01-31	116.6	2000-02-22	111.25	2007-11-09	95.68	2001-02-06	157.94
8	2002-02-04	140	2005-04-15	105.92	2008-06-04	108.85	2005-06-29	147
9	2003-05-13	96.4	2007-06-16	93.68	2009-02-15	147.70	2008-05-27	130.24
10	2008-02-04	76.4	2007-11-30	121.91	2009-08-12	82.41	2009-02-03	194.16

The 10 selected days associated with the occurrence of the daily maxima of rainfall at the Sydney Airport weather location were used to construct a synoptic composite of the MSLP and 10-metre wind fields over the domain of Greater Sydney.

Supplementary Figure 5 illustrates the mean magnitude of MSLP (in mb) and 10-metre wind speed (in m/s), along with the direction vector associated with the 10 most extreme rainfall events at Sydney Airport for (a) the CFSR reanalysis data, (b) R1, (c) R2 and (d) R3 model simulations over Greater Sydney.

Results from reanalysis datasets indicated a mean sea-level pressure pattern with a relatively low pressure (1000 mb) centre over the northeast part, along with a predominant southwest wind direction over the upper and central coast of Greater Sydney.

When comparing with composites from R1, R2 and R3, it was found:

- Composite maps from R1, R2 and R3 were consistent with the low pressure patterns found in observations, although the three RCMs tend to underestimate the magnitude of the MSLP magnitude, in particular R3.
- The magnitude and direction of winds was partially captured by the RCMs. Along the coastline, R2 and R3 were able to reproduce the direction of winds but the magnitude was underestimated.
- The magnitude of the MSLP was mainly underestimated by the three RCMs. However, the presence of a relative lower MSLP system agreed with a previous study by Evans et al. (2012) which indicates that extremes events are associated with east coast low pressure systems.

Results also suggest that RCMs outputs partially simulated the composites of wind vectors, especially R1 and R2, along the northern and central part of the coast, but they underestimated the magnitude of the MSLP. In contrast, the main difference in the magnitude and direction of wind fields may be attributed to the spatial interpolation used. Both reanalysis and RCM simulations had different grid resolutions that may have an influence in capturing the predominant direction and magnitude of the wind over the region.

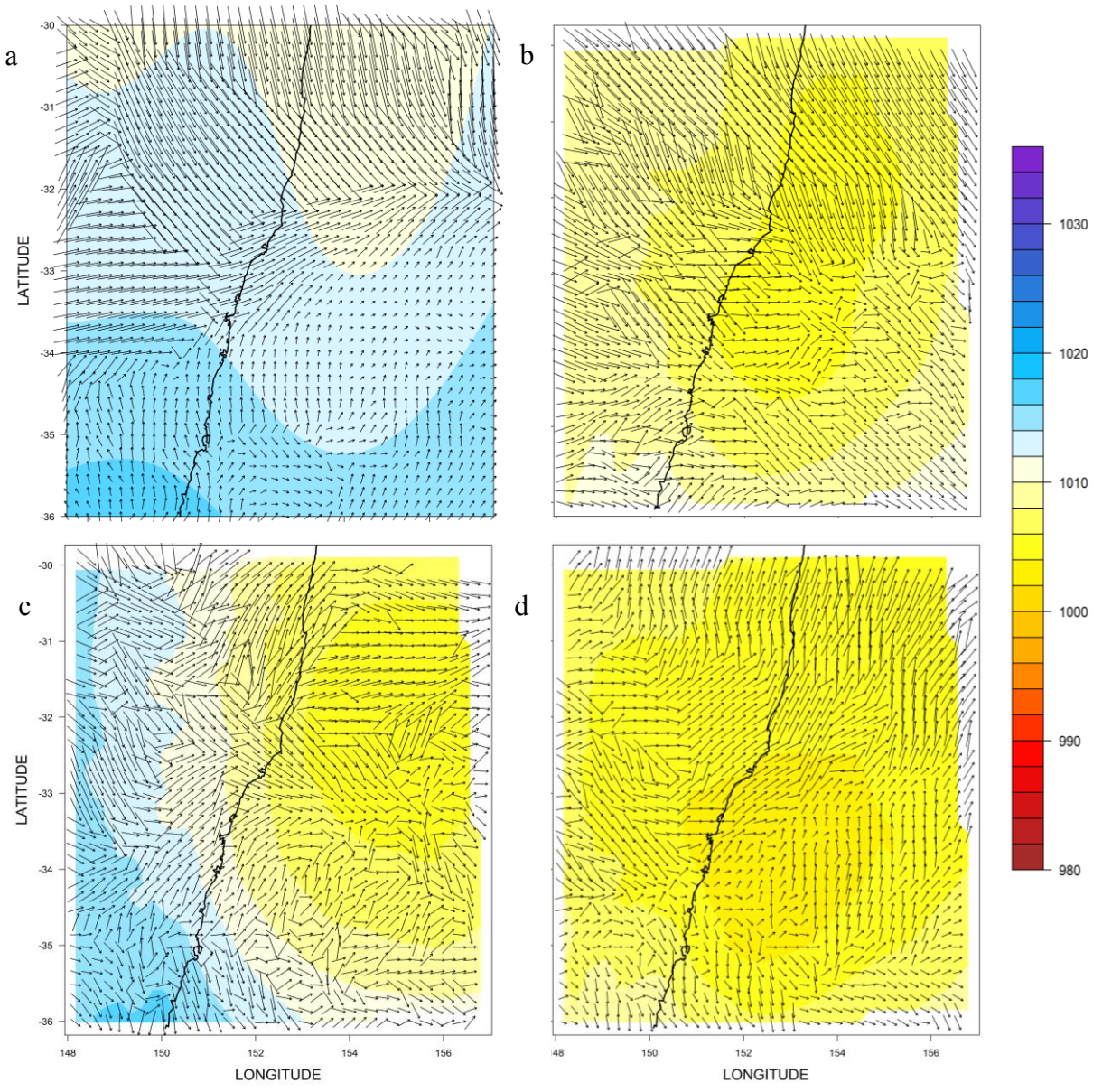

Supplementary Figure 5 **MSLP and 10-m wind composite maps associated with the 10 most extreme rainfall events were constructed from (a) CFSR reanalysis data, (b) R1, (c) R2 and (d) R3 simulations.**

Evaluating regional climate models simulations of sub-daily rainfall extremes

Statement of Authorship

Title of Paper	Evaluating regional climate models simulations of sub-daily rainfall extremes
Publication Status	☐ Published ☐ Accepted for Publication ☑ Submitted for Publication ☐ Publication Style
Publication Details	Cortes, V. E., Zheng, F., Evans, J., Lambert, M., Sharma A., & Westra S. Evaluating regional climate models for simulating sub-daily rainfall extremes. Journal of Climate Dynamics (submitted).

Principal Author

Name of Principal Author (Candidate)	Virginia Edith Cortés Hernández		
Contribution to the Paper	Obtained the data and performed in half of the analysis and wrote the first draft of the paper.		
Overall percentage (%)	40%		
Signature		Date	09/06/2015

Co-Author Contributions

By signing the Statement of Authorship, each author certifies that:

i. the candidate's stated contribution to the publication is accurate (as detailed above);
ii. permission is granted for the candidate in include the publication in the thesis; and
iii. the sum of all co-author contributions is equal to 100% less the candidate's stated contribution.

Name of Co-Author	Feifei Zheng		
Contribution to the Paper	Assist with coding, figures and data analysis, plus editing draft. (25%)		
Signature		Date	04/06/2015

Name of Co-Author	Jason Evans		
Contribution to the Paper	Ran the regional climate models that produced the data used. (10%)		
Signature		Date	29/5/2015

Name of Co-Author	Martin Lambert		
Contribution to the Paper	Assisting with supervision and discussions on research directions, discussion of results. (5%)		
Signature		Date	29/5/2015

Name of Co-Author	Ashish Sharma		
Contribution to the Paper	Assist with conceptual development and research direction. (5%)		
Signature		Date	12/06/2015

Name of Co-Author	Seth Westra		
Contribution to the Paper	Conceptual development, research direction, supervision and editing manuscript. (15%)		
Signature		Date	29/05/2015

Evaluating regional climate models simulations of sub-daily rainfall extremes

Virginia Edith Cortés Hernández, Feifei Zheng, Jason Evans,
Martin Lambert, Ashish Sharma and Seth Westra

Abstract: Sub-daily rainfall extremes are of significant societal interest, with implications for flash flood risk and the design of urban stormwater systems. It is increasingly recognised that extreme subdaily rainfall will intensify as a result of global temperature increases, with regional climate models (RCMs) representing one of the principal lines of evidence on the magnitude and spatiotemporal characteristics of these changes. To evaluate the ability of RCMs to simulate subdaily extremes, it is common to compare the simulated statistical characteristics of the extreme rainfall events with those from observational records. While such analyses are important, they provide insufficient insight into whether the RCM reproduces the correct underlying physical processes; in other words, whether the model "gets the right answers for the right reasons". This paper develops a range of metrics to assess the performance of RCMs in capturing the physical mechanisms that produce the rainfall extremes. These metrics include the diurnal and seasonal cycles, dependency between rainfall intensity and temperature, temporal scaling, and the spatial structure. We evaluate a high resolution RCM – the Weather Research Forecasting (WRF) model – over the Greater Sydney region, using three alternative parametrization schemes. The model shows consistency with the observations for most of the proposed metrics. Where differences exist, these are dependent on both the rainfall duration and model parameterization strategy. The use of physically meaningful performance metrics provide a significantly improved understanding of the model physics, which not only enhances the confidence in model simulations, but also paves the way for further model improvement.

Keywords: Regional climate models, climate model evaluation, sub-daily rainfall extremes, Weather Research Forecasting (WRF) model, Greater Sydney region.

1. Introduction

Extreme rainfall events are of significant societal concern due to their direct relationship with floods that can cause catastrophic impact on the environment and society (Hallegatte et al. 2013). Short-duration (sub-daily) extreme rainfall events can be particularly hazardous, as they can lead to flash floods that occur with little or no warning (Ahern et al. 2005). Understanding potential future changes to sub-daily rainfall in a future warmer climate is therefore critical to support urban planning policies and the design of flood protection infrastructure (IPCC 2013).

Global climate models (GCMs) are limited in their capacity to simulate the physical processes that cause short-duration extreme rainfall events. These models are run at coarse spatial scales (with typical grid sizes of 100km-300km) and have been used primarily to understand average rainfall patterns with long timescales (e.g. monthly or yearly) (IPCC 2013). At sub-daily timescales and when focusing on extremes, the model resolution and the necessity of using convection parameterisations to resolve sub-grid processes suggest that quantitative sub-daily rainfall projections from GCMs are unlikely to be reliable in the foreseeable future (Westra et al. 2014).

High resolution regional climate models (RCMs) therefore have been developed as the main tool for simulating future changes to sub-daily extreme rainfall. For instance, Beniston et al. (2007) used a RCM to simulate extreme rainfall events for Europe in future (2071-2100). Buonomo et al. (2007) investigated the robustness of changes in extreme rainfall over Europe from two high resolution RCMs. Furthermore, van Pelt et al. (2012) applied five bias-corrected RCM models to estimate the future changes of extreme rainfall in the Rhine basin. More recently, Kendon et al. (2014) projected hourly rainfall extremes for a region in the UK using a very high resolution RCM with 1.5 km grid spacing. Although each study focuses on sub-daily rainfall extremes, they differ substantially in terms of the models (and parameterisations) that were used, and their horizontal resolution.

Given the increasing reliance on RCMs to simulate future sub-daily extreme rainfall, it is natural to ask: How reliable are the extreme rainfall projections from these models? And which models and parameterisations most realistically reproduce the physical processes that cause extreme rainfall? In most cases, RCM performance is evaluated by comparing historical extreme rainfall statistics for various durations with those simulated by the model under historical greenhouse gas forcings (e.g. Kendon et al. 2014). While such analyses are important, they provide insufficient insight into whether the RCM reproduces the correct underlying physical processes that lead to the extreme rainfall events. In other words, focusing only on the extreme rainfall statistics themselves provides insufficient information to know whether the model “gets the right answers for the right reasons” (Kirchner 2006). Yet relatively little research has been undertaken to evaluate the RCMs’ ability in reproducing the physical mechanisms associated with sub-daily rainfall extremes (Westra et al. 2014).

Gaining deep insight into an RCM’s capacity to represent physical processes with regard to extreme rainfall can not only improve our confidence in their projections, but also can provide a pathway for further model improvement (Evans and Westra 2012). However, in the context of rainfall extremes, applications of this approach for model evaluation have been limited. For example, Lenderink and van Meijgaard (2008) applied a 25 km RCM to De Bilt, the Netherlands, for investigating the physical relationship between hourly rainfall extremes and temperature. Subsequently, Evans and Westra (2012) investigated a RCM’s utility in simulating 3-hour rainfall extremes using a measure of diurnal cycle, and Tripathi and

Dominguez (2013) evaluated the ability of a RCM in reproducing the spatial structure of observed 3-hour and 24-hour rainfall extremes in the Southwestern United States.

The aforementioned studies have made significant contributions in building knowledge for assessing RCMs' ability in terms of capturing the physical mechanisms associated with short-duration rainfall extremes. However, these previous studies focus on single measures of model performance, rather than provide a suite of diagnostic tools to assess whether the dominant physical processes leading to extreme rainfall are adequately captured. The present study develops a suite of physically meaningful metrics to assess the RCM's capacity in modelling sub-daily rainfall extremes. The metrics include the diurnal and seasonal cycles, dependency between extreme rainfall intensity and temperature, temporal scaling, and the spatial structure of extreme rainfall events.

The proposed metrics are used to evaluate the performance of a high resolution RCM-Weather Research Forecasting (WRF) with three different parametrization schemes in simulating sub-daily rainfall extremes for the Greater Sydney region from 1990 to 2009. The simulated rainfall is compared to observed rainfall from 69 sub-daily rainfall stations are from this region to enable a comparison with the simulated rainfall events over the common period (for details see Section 3). The timescales considered in the present study include 1-hour, 3-hour, 6-hour and 12-hour.

The remainder of the paper is presented as follows. Section 2 describes each proposed metric, and discusses how each metric can provide insight into the RCM's capacity to simulate specific processes. Section 3 presents the WRF model and the observational rainfall data from the Greater Sydney region, and Section 4 highlights the importance of understanding the RCM's ability to reproduce the physical mechanisms associated with rainfall extremes. The results of the proposed metrics applied to the Greater Sydney region as well as the relevant discussions are outlined in Section 5. Finally, Section 6 gives the conclusions of this study.

2. RCM evaluation metrics

The correct simulation of the statistical properties of extreme rainfall appears to be neither a necessary nor sufficient element for inclusion of the projections into climate impact studies. The lack of necessity is demonstrated by the widespread use of post-processing methods (commonly referred to as bias correction methods), in order to statistically correct RCM outputs to more closely match those of the observed data (Maraun 2013). However, even if the statistical properties of extreme rainfall are correctly represented, it does not necessarily mean that the physical processes that produced the extreme rainfall events are correct, which may be problematic when the model is used to predict future rainfall.

This paper describes a set of metrics that should be considered in addition to direct measures of the statistical properties of extreme rainfall, as a precursor to using a model to produce future projections of extreme rainfall. To this end, five metrics have been formulated that: (i) indicate whether the key rainfall-generating processes – including large-scale circulation and local-scale thermodynamic effects – are correctly simulated; and (ii) correspond to easily measureable quantities for which observational data is readily available. The metrics include the diurnal cycle, seasonal cycle, relationship between rainfall intensity and temperature, temporal scaling, and spatial distribution of the rainfall extremes (Table 1).

Table 1 Summary of the metrics

Metrics	Measure aspects of the climate models
Diurnal cycle	Can the model simulate rainfall extremes at the correct time of day?
Seasonal cycle	Whether the model can simulate rainfall extremes in the correct season?
Temperature scaling rate	Can the model capture the observed dependence between rainfall intensity and temperature?
Temporal scaling	Can the model reproduce the correct scaling relationships between different levels of aggregation?
Spatial structure	Are the model-simulated rainfall fields realistic?

2.1 Diurnal cycle

The diurnal cycle has previously been used to evaluate the performance of climate models in correctly representing the local storm dynamics that trigger rainfall extremes. For instance, Evans and Westra (2012) examined the diurnal cycle of 3-hour rainfall extremes simulated from a RCM over southeast Australia, and concluded that the amplitude of the diurnal cycle from the observations were reasonably reproduced by the RCM. Langhans et al. (2013) investigated the diurnal cycle of 3-hour extreme rainfall over the European Alps using a convection-parameterizing RCM and two cloud-resolving RCMs. They reported that the cloud-resolving RCMs showed good agreement with the observations in terms of diurnal evolution, although the convection-parameterizing RCM produced peaks of rainfall extremes that were too early, due to a too-early activation of deep convection.

The occurrences of extreme rainfall at time t=01:00, 02:00,…..,24:00 of day, denoted as $OD(t)$, can be expressed as

$$OD(t) = \sum_{i=1}^{n} I(T(E_i), t) \quad (1)$$

where $T(E_i)$ is the time of occurrence of the ith (i=1, 2,…,n) extreme rainfall event (E_i), and n is the total number of extreme events of a particular timescale (e.g., hourly). I is the indicator function:

$$I(T(E_i), t) = \begin{cases} 1 & T(E_i) = t \\ 0 & \text{otherwise} \end{cases} \quad (2)$$

The diurnal cycle is defined as the variation in $OD(t)$ with time, and is useful as a diagnostic measure as it can indicate the triggering mechanisms of the short-duration rainfall extremes (e.g., hourly) such as wind convergence, topographic lifting, land-sea breeze circulation and atmospheric pressure variations at the local scale (Dai and Trenberth 2004). For example, in the tropics the timing of maximum rainfall intensity is typically in the afternoon caused by the destabilization of the boundary layer. In contrast, the rainfall maxima may occur between

midnight and early morning at some land areas as a result of local effects such as complex terrain and sea-breeze circulations (Nesbitt and Zipser 2003).

Given the value of the diurnal cycle in revealing the underlying physical process, we adopted it as a metric to assess the RCM's performance in simulating hourly rainfall extremes. This metric directly evaluates whether the model can simulate hourly rainfall extremes at the correct time of day, and hence provide insight into model physics related with the convective process. While the diurnal cycle has been implemented in previous work (Evans and Westra 2012; Langhans et al. 2013), it was used to analyze the rainfall extremes with relatively longer durations (3-hour) compared to 1-hour timescale considered in the present study.

2.2 Seasonal cycle

The occurrences of extreme rainfall at different seasons (denoted as $OS(s)$) is defined analogously to the diurnal cycle as:

$$OS(s) = \sum_{i=1}^{n} I(S(E_i), s) \tag{3}$$

where $s \in \{\text{spring}, \text{summer}, \text{autumn}, \text{winter}\}$. The indicator function *I* is defined as the same as Equation (2), with $T(E_i)$ and *t* respectively replaced by $S(E_i)$ and *s*.

The seasonal cycle is a valuable metric for assessing the performance of climate models in characterizing the dominant synoptic meteorology of the rainfall extremes. For example, in the Sydney case study region, the convective rainfall extremes are more likely to occur in hot seasons (e.g., summer) with relatively short durations, whereas the stratiform extremes take place during seasons that are related with large-scale circulation patterns (e.g., frontal systems), typically with longer durations (Zheng et al. 2015). Therefore the shape of the seasonal cycle across different durations can indicate the roles of different climate drivers in producing rainfall extremes.

The use of the seasonal cycle to evaluate the performance of RCMs is not new. For example, Maraun et al. (2011) found that RCMs can reproduce the overall seasonal cycle of daily rainfall extremes, but cannot fully capture the amplitude. Subsequently, Schindler et al. (2012) evaluated the performance of 14 RCMs in simulating the annual cycle of daily extreme rainfall in the UK, and stated that most RCMs underestimated the observed peaks in summer. More recently, Zheng et al. (2015) showed that at the hourly duration in the Greater Sydney region, observed extreme rainfall was largely summer-dominated, whereas for longer durations the distribution was more evenly spread throughout the year. This latter result shows an important feature of the seasonal cycle: namely, that the seasonal cycle of extreme rainfall can strongly depend on the duration of the extreme rainfall event.

The seasonal cycle is used as a metric to evaluate the model's performance in correctly simulating rainfall extremes that are caused by different climate forcings. In contrast to its implementations using daily rainfall extremes in many previous studies, this paper applied this metric to sub-daily rainfall extremes ranging from 1-hour to 12-hour durations.

2.3 Relationship between rainfall intensity and temperature

A long-standing hypothesis regarding future changes to extreme rainfall is that extreme rainfall will scale in proportion to the moisture-holding capacity of the atmosphere, which based on the Clausius-Clapeyron relationship increases at a rate of approximately 7% per

degree (Trenberth et al. 2003). This hypothesis has become known as the 'Clausius-Clapeyron (CC) scaling hypothesis', and recently empirical and modelling studies have been conducted to assess whether and under which conditions the hypothesis holds (see Westra et al, 2014, for a detailed review).

Whereas at the global scale and for daily rainfall it has been shown that annual maximum daily rainfall has been increasing at a rate of between 5.9% and 7.7% per degree globally averaged atmospheric temperature (but with significant regional variations) (Westra et al, 2013), there is significant evidence that much higher scaling rates are possible for sub-daily rainfall. Lenderink and van Meijgaard (2008) examined a long time series of hourly rainfall in The Netherlands, and found rates double the CC scaling rate (14% per degree) for temperatures above 12°C. This has variously been attributed to latent heat release within the storm system, and a change from largely stratiform rainfall at lower temperatures to more convective rainfall at higher temperatures (e.g. see Berg et al, 2013). In contrast to these results, Hardwick-Jones et al (2010) found negative scaling rates at higher temperatures, particularly once temperatures exceeded 24°C. This latter result was attributed to potential moisture limitations at higher temperatures, although the explanations for this result as well as the future implications under a warming climate have yet to be explored in detail.

The complex set of physical mechanisms that collectively determine the relationship between extreme rainfall and atmospheric temperature make the temperature scaling relationship ideally suited as a diagnostic metric to assess the performance of climate models. The metric was formulated based on the method described in Lenderink and van Meijgaard (2008), in which:

i) the observed or simulated rainfall events (greater than 0.1 mm) with a particular duration (of say hourly) are paired with their corresponding mean daily temperature;

ii) the rainfall-temperature pairs are ranked based on the ascending order of the temperature;

iii) the sorted pairs are split into 12 bins such that each bin possesses the same number of events; and

iv) the 99th percentile of the rainfall events and the median temperature of each bin formed a dataset to enable a linear regression.

The slope of linear regression represents the CC scaling rate between the rainfall depth and temperature, and forms the basis of the comparison between modelling simulations and observations.

2.4 Temporal scaling

Previous studies have demonstrated rainfall patterns are often scale invariant, where the fluctuations in the field of interest at small scale and large scales are can be represented by a single scaling parameter (Lovejoy and Schertzer 1985). Following this physical behaviour, the presence of the invariant scale across different timescales in the rainfall field is expected due to the existence of the scale limits in their atmospheric forcings (Veneziano and Lepore 2012). There has been significant research on the temporal scaling relationships based on historical rainfall, focusing either on the scaling model developments or validation of their existence using observed rainfall data (Paschalis et al. 2013; Mandapaka and Qin 2014; Mascaro et al. 2014). In contrast, relatively little attention has been given to evaluate the climate models

using the temporal scaling relationships of the simulated rainfall extremes across different time resolutions.

The characterization of the statistical properties of extreme rainfall across a wide range of timescales (e.g., from daily to hourly) is an important part of the overall assessment of model performance. Such information is useful for developing and calibrating statistical downscaling tools that reproduce finer scales of rainfall properties from coarse predictions of RCMs. In the present study, the temporal scaling is proposed as a metric to assess whether the climate models can reproduce the observed scaling relationship between different levels of aggregations. More specifically, depths of observed and simulated rainfall extremes across different durations were converted to the percentages of their corresponding 24-hour rainfall amounts for each site, leading to a temporal scaling relationship that can be used to indicate model performance.

2.5 Spatial structure

The spatial properties of the observed rainfall extremes have been previously considered as a part of RCM evaluation studies. For example, Tripathi and Dominguez (2013) found that a 10 km resolution RCM was able to capture the main spatial structure of the 3-hour rainfall extremes in the southwestern US, whereas Wang and Kotamarthi (2014) applied a RCM to North America and observed that the model was capable of capturing the main features of the spatial patterns of the monthly rainfall.

The statistical properties of short-duration rainfall extremes are very different from those of rainfall averages or rainfall aggregated over long intervals (e.g. monthly or annual rainfall), and therefore a method is required that is specifically targeted towards modelling short-duration extreme events. Here, we use an approach drawn from spatial extreme value statistics (e.g. Schlather and Tawn 2003), by measuring how the intensity of extreme rainfall decays with distance.

The approach commences by considering extremal dependence between two sites via:

$$\Pr[Z(s_i) \le z, Z(s_j) \le z] = \exp\{-\frac{\eta(s_i - s_j)}{z}\} \qquad (4)$$

where $\eta(s_i - s_j)$ is the pairwise extremal coefficient between two sites s_i and s_j representing the dependence strength between these two sites (Schlather and Tawn 2003). The values of $\eta(\cdot)$ are bounded by (1,2). The case where $\eta(\cdot)$ = 1 corresponds to complete dependence, indicating that the sites s_i and s_j always simultaneously produce rainfall extremes; conversely, $\eta(\cdot)$ = 2 means complete independence.

The depth of the annual maximum rainfall at each site is described by the random variable $Z(s_i)$. Given that there are significant differences in the rainfall characteristics between different spatial locations as a result of orographic effects, coastal influences and so on (see Section 4), it is necessary to transform the rainfall at each location to a standard generalised extreme value distribution prior to conducting the dependence analysis. This is followed by the calculation of the joint cumulative probability of the combined rainfall depth at sites s_i

and s_j, as shown on the left hand size of Equation (4). Further details of the method are given in Schlather and Tawn (2003).

Finally, to obtain the overall dependence structure across the study domain, the values of $\eta(\cdot)$ are first estimated separately for each pair of locations s_i and s_j, totalling 2346 separate pairwise combinations amongst the 69 stations (or grid cells). These dependence values are then plotted against the spatial distance between each station pair, to obtain a measure of the overall spatial dependence within the study region. This plot forms the diagnostic plot to be used for RCM evaluation.

The approach is applied separately across multiple durations, since the spatial dependence for short-duration extremes is expected to be weaker than for longer timescales. This is because the short-duration extreme rainfall is most commonly caused by local-scale convective activity (Berg et al. 2013), while longer rainfall extremes (say daily) are associated with larger-scale meteorological conditions (Delworth and Zeng 2014). The complexities of the spatial structure as well as their underlying physical mechanisms provide another valuable metric to evaluate the performance of the climate models.

3. The regional climate model and the observed data

The Advanced Weather Research and Forecasting (WRF) model version 3.3 was used to demonstrate the model evaluation approach, with details of the model given in Skamarock et al. (2008). Three different WRF variants with varying physical schemes were run over the Greater Sydney region (Figure 1) from 1999 to 2009 with hourly resolution. These model variants are identically driven by the 6-hourly boundary conditions from the NCEP–NCAR reanalysis project (NNRP) (Kalnay et al. 1996) with an outer 50-km-resolution nest and an inner 10-km-resolution nest that covers the study region. Both nests used 30 vertical levels spaced closer together in the planetary boundary layer. The physical schemes used in these three WRF variants are outlined in Table 2. Many combinations of physics parameterizations have been tested over this region (Evans and McCabe 2010; Evans et al. 2012; Ji et al. 2014). The combinations given in Table 2 were chosen through a process that considered model performance and independence (Evans et al. 2013). These models were chosen as the regional climate models to be used within the NSW/ACT Regional Climate Modelling (NARCliM) project (Evans et al. 2014).

Table 2 Physical schemes of the three WRF variants

WRF variant	Planetary boundary layer scheme	Cumulus convection scheme	Cloud microphysics scheme	Short and long-wave radiation schemes
R1	Mellor-Yamada-Janjic/ Eta similarity	Kain-Fritsch	WRF Double Moment 5-class	Dudhia / Rapid Radiative Transfer Model
R2	Mellor-Yamada-Janjic /Eta similarity	Betts-Miller-Janjic	WRF Double Moment 5-class	Dudhia / Rapid Radiative Transfer Model
R3	Yonsei University / MM5 similarity	Kain-Fritsch	WRF Double Moment 5-class	NCAR Community Atmosphere

The most important parameterization for rainfall extremes that differs between the models is the cumulus convection scheme. Two criteria must be met to trigger the Kain-Fritsch (KF) scheme (Kain 2004). First, the temperature of an air parcel at its lifting condensation level (plus a small perturbation) must be greater than the environmental temperature at that level. Second, the parcel is released from this level with an initial vertical velocity and moves upward experiencing the effects of entrainment, detrainment and water loading. If the vertical velocity remains positive over a distance exceeding a threshold (typically 3-4km) then deep convection is activated. The scheme then increases the mass fluxes incrementally until the Convective Available Potential Energy (CAPE) is reduced by at least 90%.

The Betts-Miller-Janjić (BMJ) scheme (Janjić 1994) requires three conditions to trigger convection: at least some CAPE; convective cloud depth exceeding a threshold value; and moist soundings. This scheme does not explicitly produce a convective mass flux, instead it relaxes the atmosphere toward a set of reference equilibrium states using a time scale that depends on the “cloud efficiency”. This scheme is comparatively simple and computationally efficient, making it a good candidate for long climate simulations.

The planetary boundary layer scheme can also effect rainfall by changing the lower atmosphere, impacting the requirements to trigger the convection schemes. These parameterizations produce a well-mixed layer at the bottom of the atmosphere that is caused by the heating of the surface and hence has a strong diurnal cycle. The Mellor-Yamada-Janjić (MYJ) scheme (Janjić 1994) is a one dimensional prognostic turbulent kinetic energy scheme with local vertical mixing. The Yonsei University (YU) scheme (Hong et al. 2006) is a non-local-K scheme with an explicit entrainment layer and parabolic K profile in the unstable mixed layer. The two methods produce different growth rates and overall planetary boundary layer heights.

The WRF simulation results are compared to observed sub-daily rainfall at 69 subdaily rainfall sites with five-min resolution from the Greater Sydney, Australia (black solid points in Figure 1). The 1-hour, 3-hour, 6-hour and 12-hour annual maxima were used for analysis through accumulation based on the five-min rainfall records. To enable a reasonable comparison, each rainfall gauge was related with a grid point from the WRF model that had the minimum

spatial distance to this gauge. As such, 69 different grid points were determined to enable a comparative analysis against the observations.

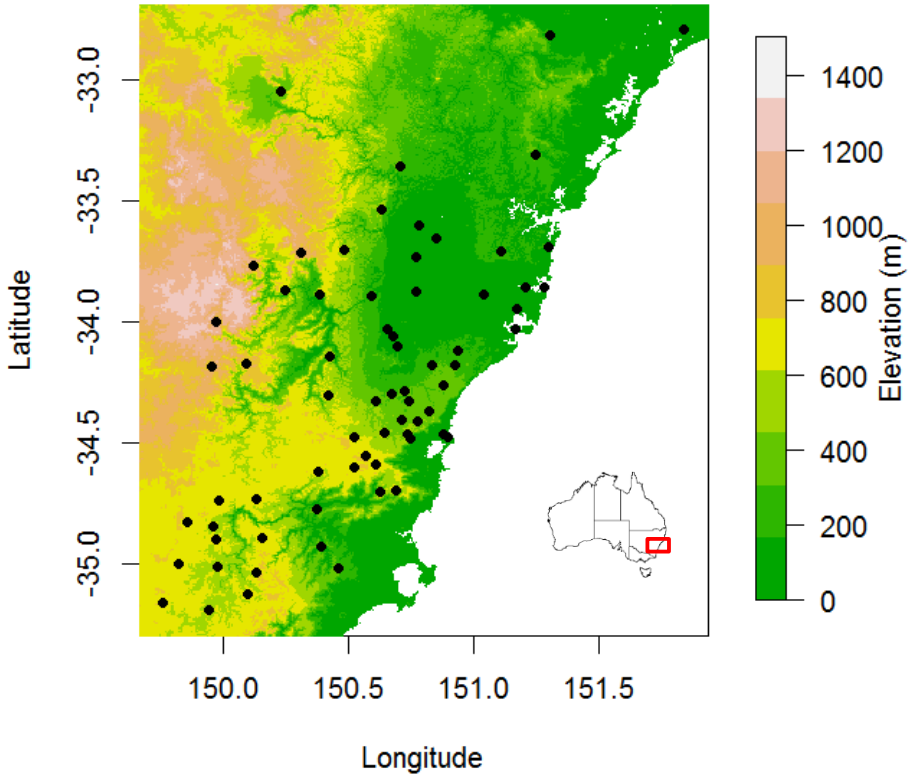

Figure 1: ***Spatial rainfall datasets (black solid dots) from the Greater Sydney region.***

4: Motivation of model evaluation using the physically-meaningful metrics

Figure 2 shows the mean of annual maximum rainfall intensity over the study domain for both observations and simulations, for durations from one to 12 hours. The observed rainfall intensities exhibit significant spatial variations for each duration, with generally higher rainfall intensity near the coast compared to further inland. The spatial gradient is high for all durations, with the rainfall intensity of the most intense stations being as much as three times higher than the rainfall intensity of the least intense stations.

The WRF results show significant differences with the observations, and between the different parameterisations (Table 2). For the 1-hour rainfall extremes, R1 appears to reasonably represent the observed rainfall intensity for gauges in the inland, while R3 shows better performance along the coastline. In contrast, R2 exhibited a significantly overall better performance compared to R1 and R3 for durations from 3-hour to 12-hour. None of the models entirely reproduce the observed rainfall intensity at all durations, with biases up to approximately 50% for some locations. Furthermore, the model does not appear to simulate

the magnitude of the spatial variability, with the difference between the most intense and least intense grid points being less than the observed data.

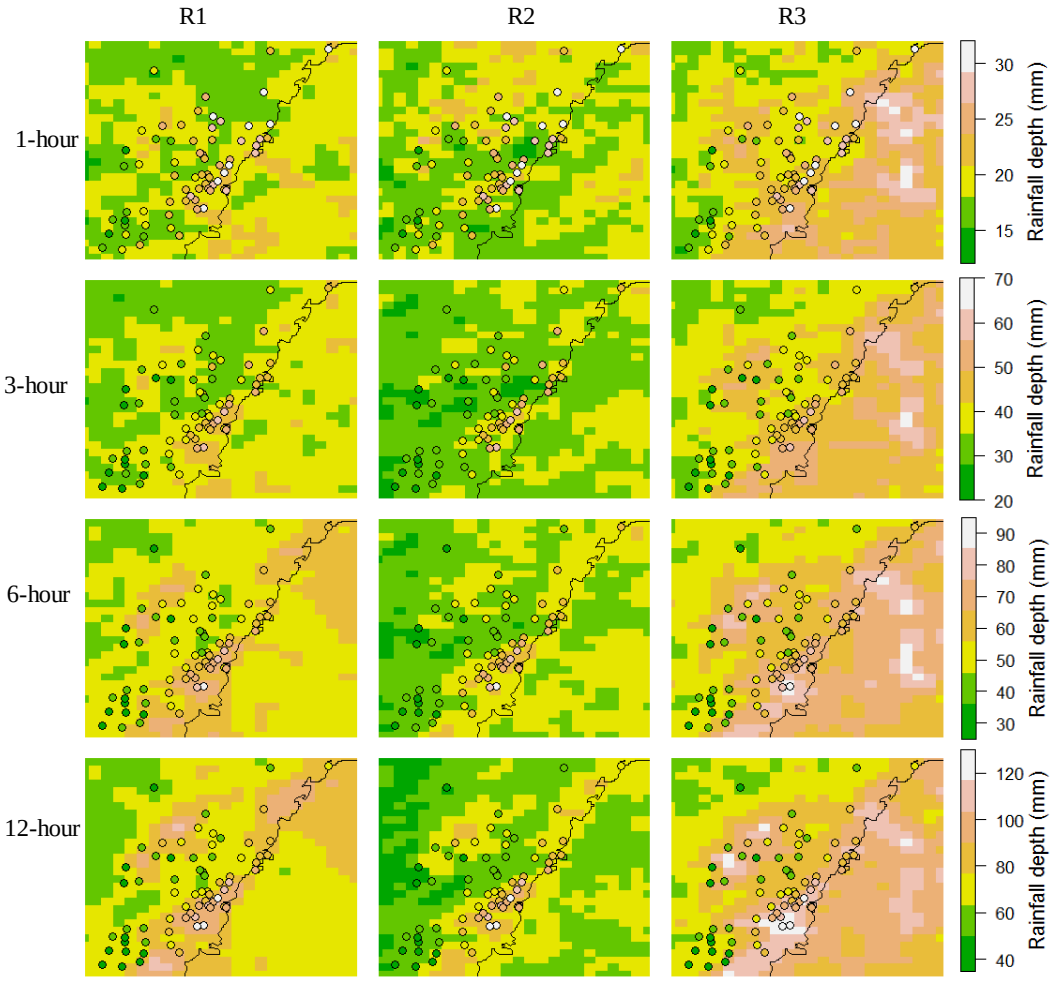

Figure 2: ***Spatial map of the average annual maximum rainfall intensity over the period from 1990-2009, with dots and shading representing observations and simulations, respectively.***

Based on the simulation results presented in Figure 2, it is clear that the models do not perfectly represent extremes across the full spatial domain for any duration. In such circumstances, it would be common to bias correct the RCM outputs to obtain a closer match with the observed data (Maraun 2013). However, prior to recommending such a course of action we ask: are the physical processes that lead to extreme rainfall represented with sufficient realism to support bias correction? This motivates the use of physically meaningful metrics covered in the next section.

5: Results and Discussion

4.1: Diurnal cycle

We examined the diurnal cycle using the 1-hour annual maxima from the WRF models and the observations. The number of extreme events occurring at each time of day was calculated for each rainfall gauge using Equation (1), and the occurrence statistics were then averaged across the 69 gauges (or the 69 grid points closest to the gauges for the WRF results) to

obtain a representative diurnal cycle over the study region. The results are shown in hourly increments for the observations and the three WRF variants (Figure 3).

There is a strong diurnal cycle in the occurrence of rainfall extremes for the observations, with a six-fold greater number of occurrences during the peak hour (4pm) relative to the hour with the fewest extremes (4am). Compared to the observations, all three WRF models exhibited overall similar patterns in the diurnal cycle, although the period with the greatest number of occurrences was between one and three hours later than the observations. This implies that the convection-parameterization schemes in Table 1 are unable to fully represent the physical processes that drive the deep convection (i.e. the activation of the convection scheme occurs too late) in the Great Sydney region.

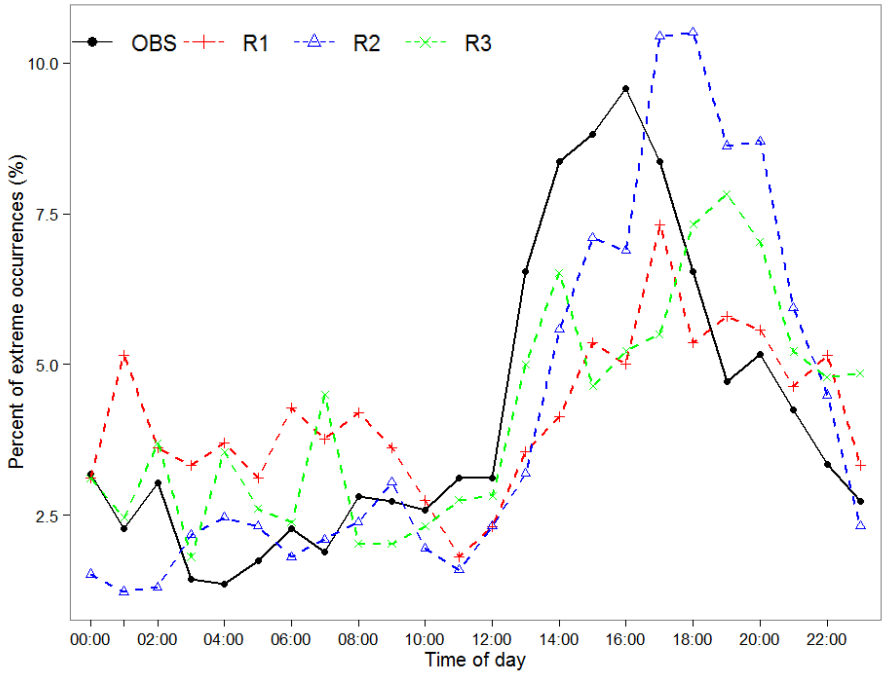

Figure 3: ***Results of diurnal cycle (OD(t)), with percent of extreme occurrences at each time of day averaged over 69 gauges.***

In addition to the delay in peak rainfall occurrence, simulations R1 and R3 also produced a larger number of morning extremes than observed. These extremes are generally driven by large-scale convergence, suggesting that the KF convection scheme (common to both simulations), once triggered by such convergence, produces extreme rainfall too frequently. Specifically, the extremes are produced by a combination of the convective scheme consuming the available CAPE, and the tendency for this scheme to produce unrealistically deep saturated layers thereby also activating the microphysics scheme rainfall (Glimore et al. 2015).

To gain further insight into the WRF's delay in the main peak as shown in Figure 3, we analyzed the statistics of starting time of the hourly annual maximum events. It was found that the three WRF models were able to reasonably reproduce the starting time of the rainfall extremes (not shown). This suggests that the WRF's delay in the peak hours is mainly caused by the delay in reaching the maximum hourly rainfall rate rather than the delay in the trigger time.

4.2: Seasonal cycle

The 1-hour, 3-hour, 6-hour and 12-hour annual maxima accumulated from the 69 gauges and co-located WRF grid points were considered to enable the seasonal cycle analysis, with results shown in Figure 4. The spring, summer, autumn and winter respectively corresponds to March-May, June-August, September-November, and December-February of the next year. The observations (black bars) showed strong seasonal cycles for all durations. For example, approximately 50% of 1-hour annual maximum rainfall events occurred in summer compared to only 7% in winter.

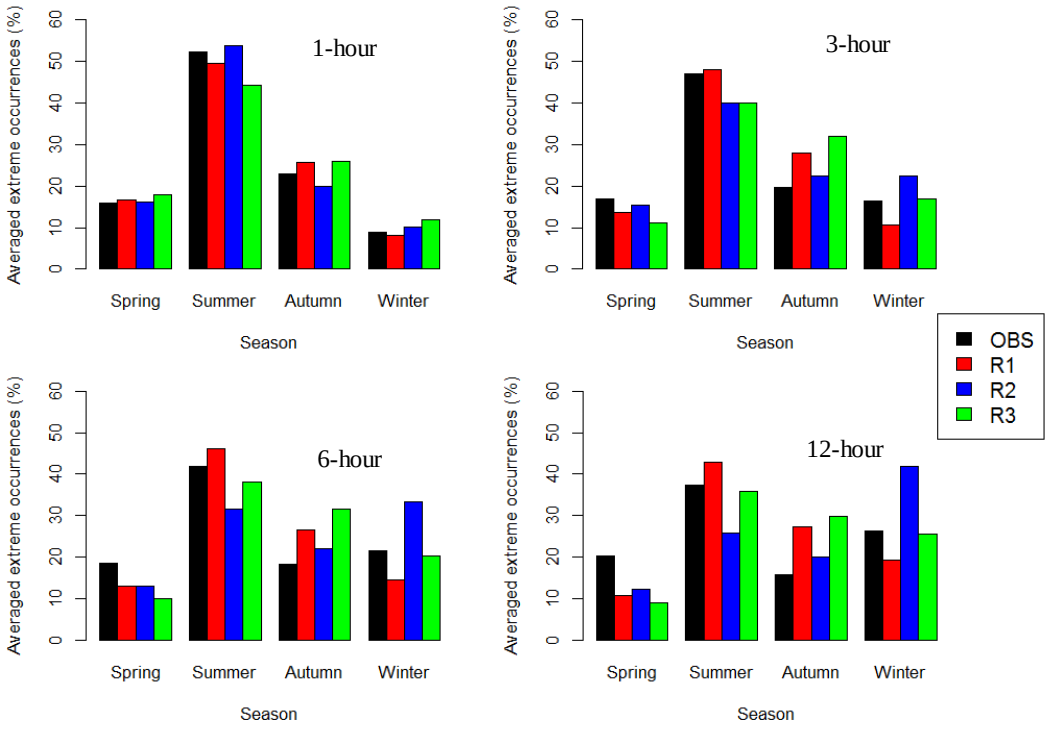

Figure 4: Results of seasonal cycle (OS(t)), with percent of extreme occurrence at each season of year averaged over 69 gauges.

The three WRF models were able to reproduce the observed seasonal cycle for the 1-hour duration extremes, but showed some biases for the longer durations. For durations of three hours or longer, the three WRF models consistently underestimated the extreme occurrences in spring, but overestimated events in autumn. For winter, the R1 and R2 simulations exhibited a lower and higher number of longer-duration extreme events, respectively, compared to the observations. In contrast, the R3 simulations yielded a good agreement with the observed events with longer timescales as shown in Figure 4. R1 outperformed the other two WRF variants in terms of reproducing the extreme events in summer for shorter durations (1-hour and 3-hour), while R3 became the better alternative for summer extremes with larger timescales.

The generally good performance in both the summer and winter for R1 and R3 for all durations suggests that the KF convective scheme, which is shared by these configurations, is able to generate extreme rainfall under both strongly thermally driven convective environments (summer) and convection driven largely by synoptic scale convergence (winter). The BMJ scheme used in R2, on the other hand, is able to do this for 1-hour rainfall extremes but becomes progressively more winter-dominated at longer durations. Hence, in thermally driven convective environments the BMJ scheme is often able to stabilize the atmospheric column more rapidly than the observations suggest. In contrast, in situations dominated by

synoptic convergence, the BMJ scheme is able to sustain extreme rainfall rates longer than the observations suggest.

The reason for differences between the model simulations and the observations in the transition seasons (spring and autumn) is less clear. During these seasons, there is a shift in climatology from largely convective events in summer to large-scale frontal systems in winter. There is some evidence that the dominant climatology is changing particular in autumn both for average rainfall (Delworth and Zeng, 2014) and for extremes (Zheng et al, 2015). The capacity of WRF to simulate these apparent changes in extremes is currently not known, and is difficult to assess for the present study because the period of analysis (i.e. 20 years) is unlikely to be sufficient to explore long-term trends. Further research is therefore needed on the capacity of WRF to simulate the apparent systematic changes over the transition seasons.

4.3: Dependence between rainfall intensity and temperature

As outlined in Section 2.3, we used the method described in Lenderink and van Meijgaard (2008) to calculate the temperature dependence from both the observational and simulated rainfall extremes for 1-hour, 3-hour, 6-hour and 12-hour durations. Figure 5 shows the results, with black dashed lines representing the result from each individual rainfall gauge and black solid line indicating the composite result. All the temperature dependence scaling from each grid of the three WRF variants are shown by the grey dashed lines and the composite results are given by the red (R1), blue (R2) and green (R3) solid lines.

It is seen from the observations that the temperature dependence scaling of the 1-hour rainfall extremes showed a good agreement with the empirical value of 7% per °C (orange dashed lines) for most of the temperature range considered, but this scaling rate decreased at the highest temperatures. The observations also show lower rates for longer timescales such as the 6 and 12-hour extremes. This observation matched well with the results in Hardwick

Jones et al. (2010), and does not show the super-CC scaling that has been found in other studies (e.g. Lenderink and van Meijgaard 2008).

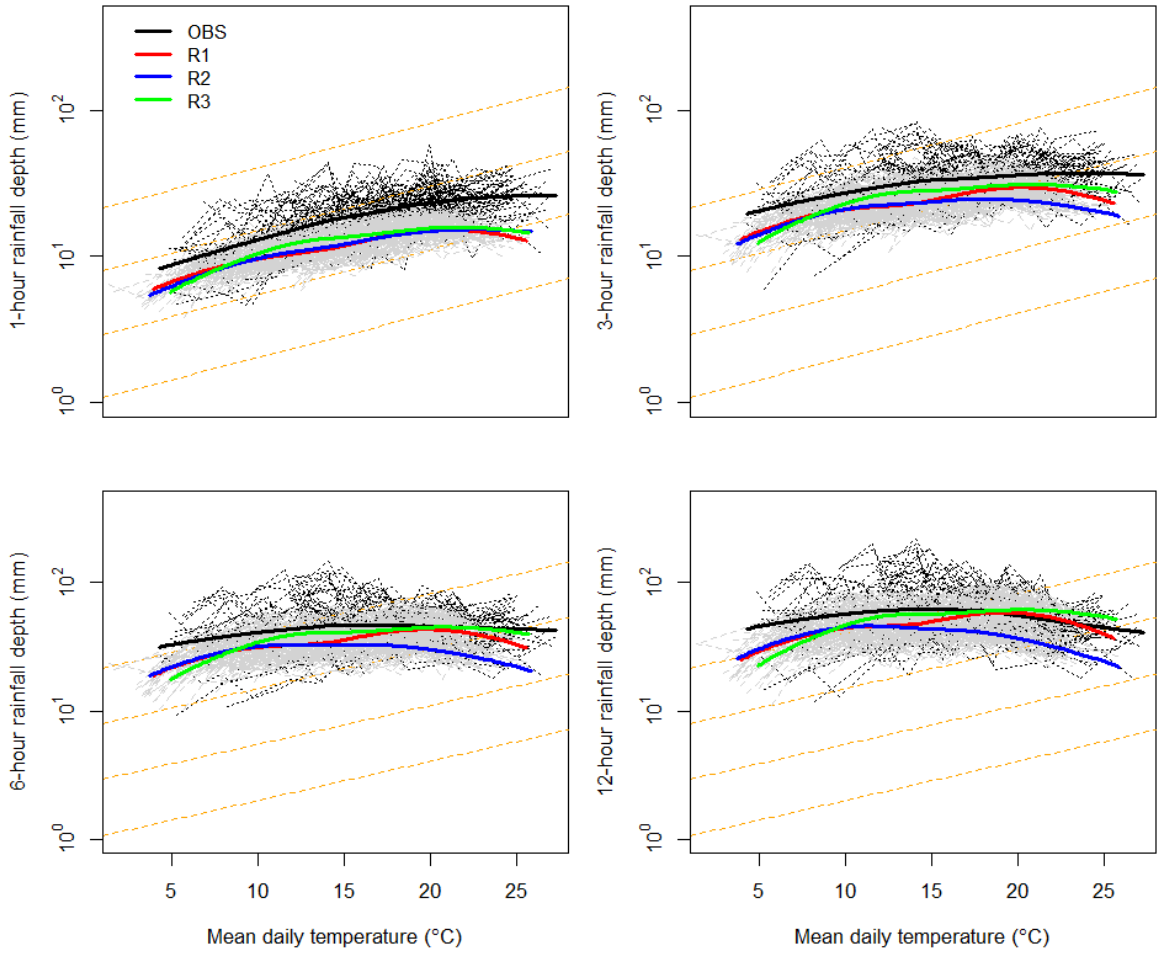

Figure 5: ***Results of temperature scaling rate from the observations (OBS) and three WRF models (R1, R2, and R3). The black and grey dashed lines respectively represent the temperature scaling rates from the rainfall gauges and the grid points of the three models. The solid lines are the composite temperature scaling rates and the orange dashed lines represents the CC scaling rate of 7% per °C.***

The simulated CC scaling rates exhibited a similar pattern across all durations with the observations. Furthermore, the level-off and decreases in the temperature scaling rates at higher temperatures were overall captured by the simulations. This demonstrates that the three WRF models with different parametrization schemes are all able to characterize the empirical relationship between rainfall intensity and temperature.

Despite reasonable consistency in terms of the scaling rates, the simulated rainfall intensity was consistently lower than the observed events across different temperatures. Interestingly, such an underestimation becomes more prominent for rainfall extremes with finer timescales. Given that the short-duration intensive rainfall is most commonly caused by local-scale convective activity (Berg et al. 2013), this bias can be either caused by the slight deviations in the spatial locations between the selected model grids and the rainfall gauges, or the models' insufficient convection depths. The WRF models can better reproduce the physical dependence between rainfall intensity and temperature for longer-duration events that are associated with larger-scale meteorological conditions (Delworth and Zeng 2014). It is worth noting that the modelled scatter (grey lines) produce a smaller spread than seen in the

observations, although his may at least partly be due to the comparison between point observations and grid point averages.

In comparing the relative performance of the three models, R1 and R3 yielded an overall better consistency with the observations than R2 in terms of the rainfall intensity, which is especially the case for longer-duration rainfall extremes such as 12-hour. This differentiation between models using convection schemes KF (R1, R3) and BMJ (R2) at high temperatures matches the seasonal result where R2 is found to produce fewer summer and more winter extreme events. However, R2 showed better agreement with the observations in terms of the mean temperature scaling rates, which will be further confirmed in Figure 6 below.

The spatial patterns of the mean temperature scaling rates were also considered for both the observations (dots) and simulations (background) as shown in Figure 6. The observations showed that the temperature scaling rates overall reduce when the rainfall duration increased, matching well with the results shown in Figure 5. Such a trend is well captured by R2, but not for R1 and R3.

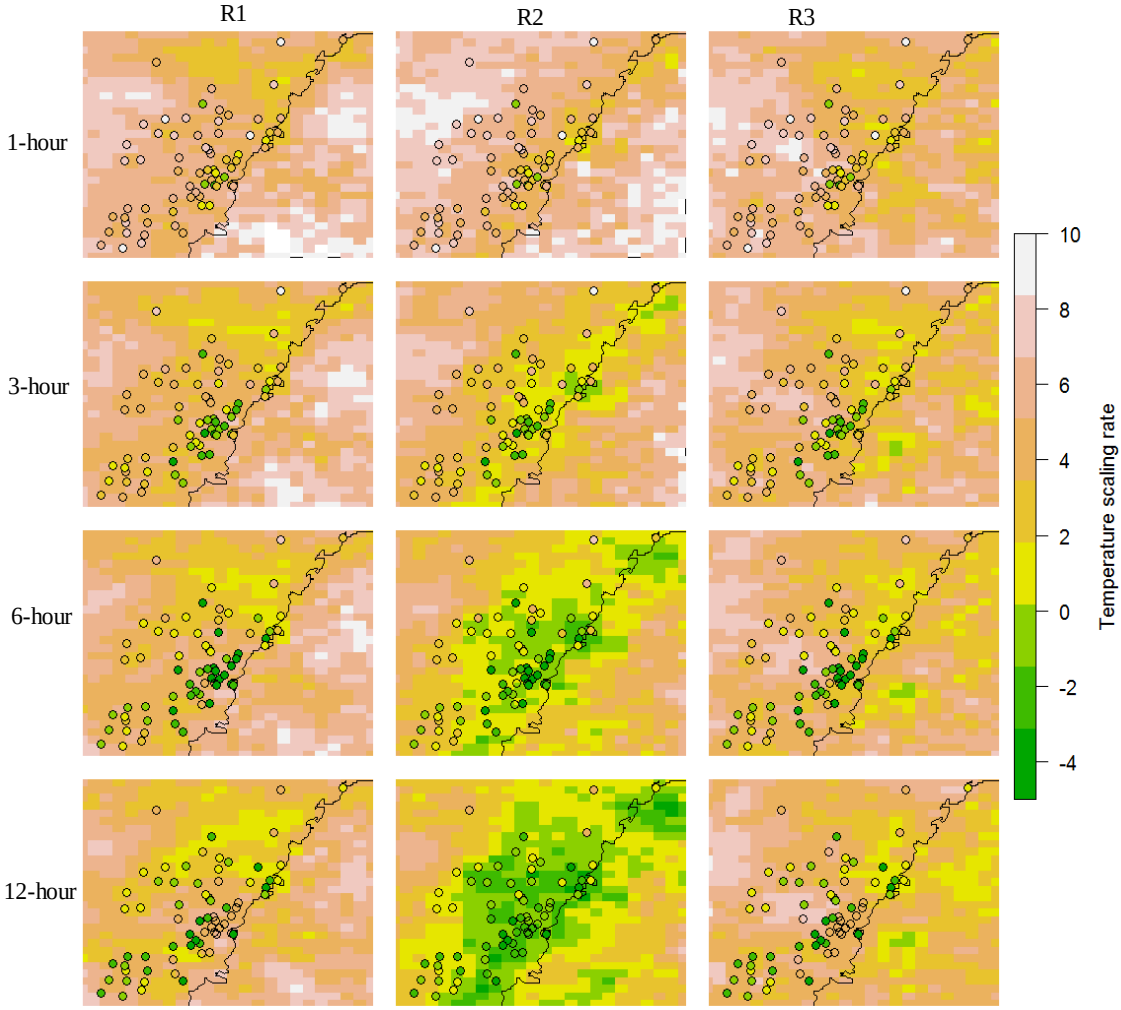

Figure 6: Spatial map of the temperature scaling rates, with dots and contours representing observations and simulations.

All the three WRF models yield a similar performance in simulating the spatial structure of the temperature scaling rates for the 1-hour rainfall extremes, which also exhibited a reasonable agreement with the observations. However, the models produced overall larger temperature scaling rates than the observed values for the 3-hour extremes in the coastline region. The most noteworthy difference between the three models is reflected by the simulations for the

12-hour rainfall extremes, where R2 shows a good agreement with the observations, whereas R1 and R3 significantly overestimate the temperature scaling rates overall.

4.4: Temporal scaling

The temporal scaling results are shown in Figure 7, where the rainfall depths of sub-daily extremes for each gauge are represented in terms of the percentages of the 24-hour rainfall amount (black dashed lines). The orange dashed line indicates the case where the rainfall is uniformly distributed within the 24 hours.

Compared to the observations, the three WRF models all yielded overall reasonable performance across different time resolutions, although their simulated distributions for relatively short-duration rainfall extremes were less intense relative to the 24 hour extremes. Another important result is that the temporal scaling of the WRF results is consistently less variable than to the observations. This is indicated by comparing the range of the temporal scaling results of the R1 simulations (red shaded region) across the 69 locations with those from the observations (grey shaded region). The temporal scaling ranges of R2 and R3 are similar to R1 (not shown).

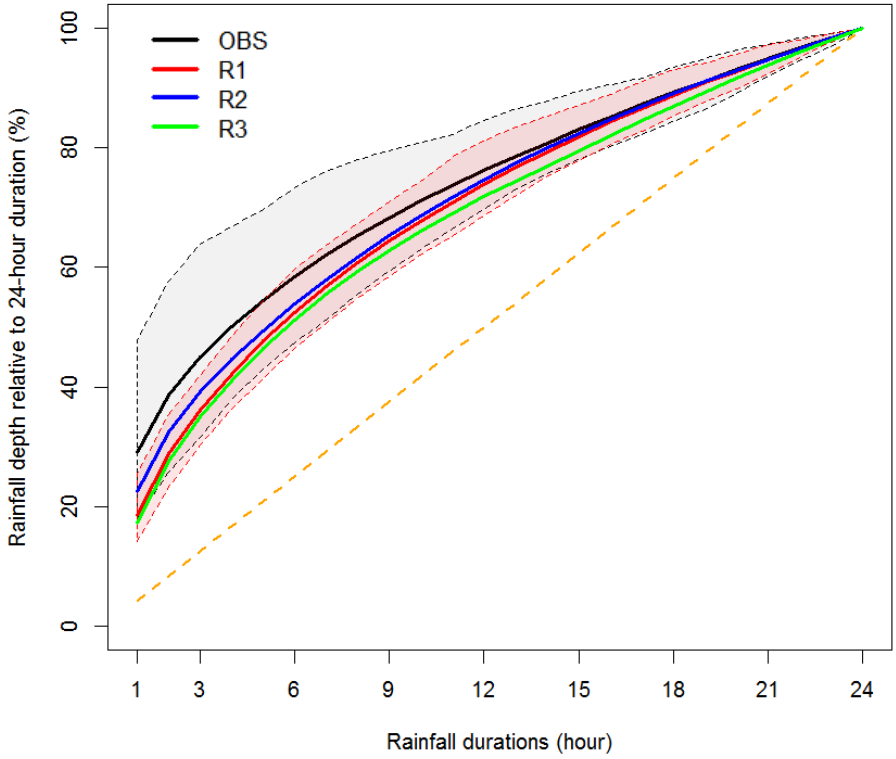

Figure 7: ***Results of temporal scaling rate from the observations (OBS) and three WRF models (R1, R2, and R3). The grey and light shaded region respectively represents the ranges of the observed results (69 gauges) and R1 simulations (69 grid points). The solid lines are the composite temporal scaling rates from the 69 gauges. The orange dashed line indicates the uniform temporal scaling rate.***

4.5: Spatial structure

Figure 8 shows the pairwise extremal coefficient $\eta(\cdot)$ estimates (Equation 4) from the observations (black circles) and R1 simulations (red "+") for 1-hour, 3-hour, 6-hour and 12-hour durations. As shown in this figure, the observed spatial dependence among the 1-hour rainfall extremes declined sharply after a very short distance, whereas the dependence

reduction among the 12-hour annual maxima was significantly more gradual, suggesting that the 12-hour rainfall extremes have an overall stronger spatial dependence compared to the 1-hour events. This is expected since the short-duration extremes are more likely to be driven by the local-scale convective activity, while the longer-duration events are associated with larger-scale meteorological forcings (Westra et al. 2014). Such a variation in spatial correlation as a function of duration was also overall captured by R1. The simulated spatial correlation from R1 is overall consistent with the observations, although it overestimated the correlation strength for locations with shorter distances, with biases being more significant for longer durations (e.g., 12-hour). R2 and R3 simulations are not shown due to their similarity with R1 results.

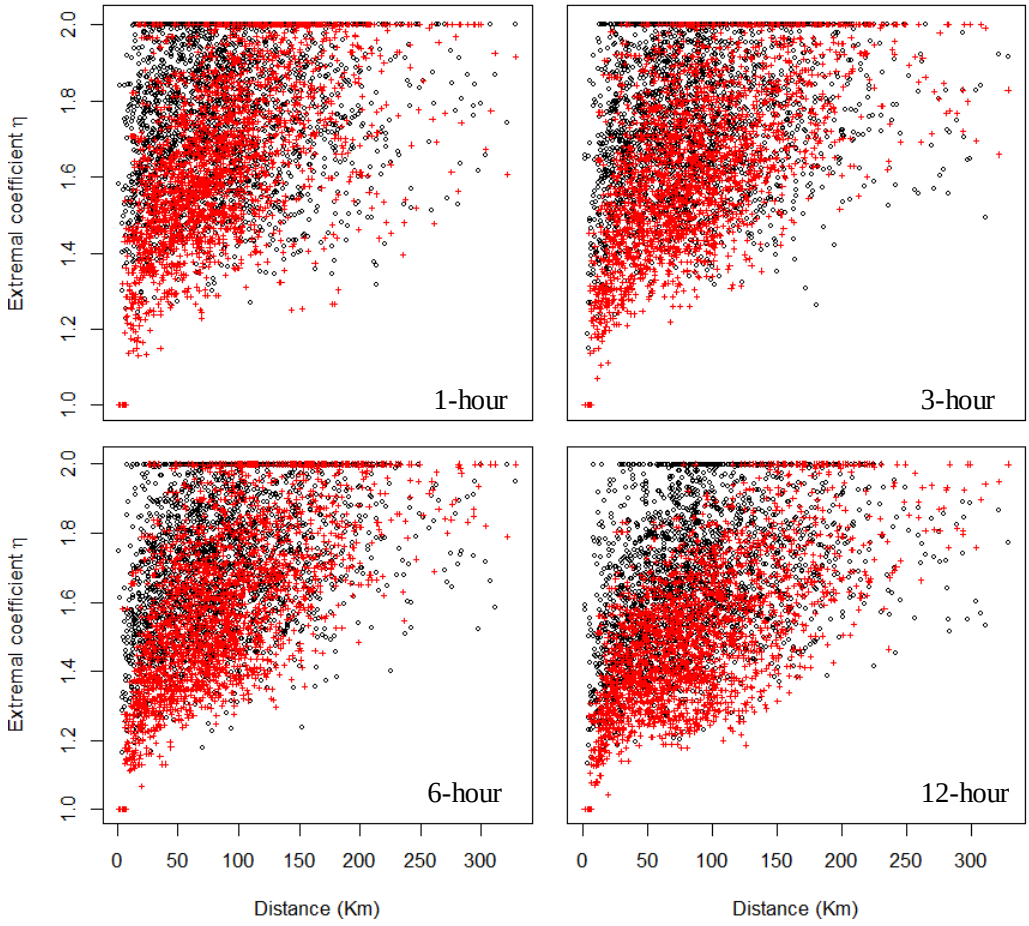

Figure 8: ***Spatial correlation versus distance for the observed annual maxima at 69 rainfall gauges (black circle) and for the 69 grid points from R1 (red '+').***

5: Conclusions

Research in the field of regional climate modelling for rainfall extremes has mainly focused either on the applications of RCMs, or on the evaluation of RCM-predicted rainfall intensities and frequencies using the observations. Few RCM evaluation studies have considered both the capacity of the RCM to simulate the extreme rainfall statistics as well as whether RCMs can reproduce the physical processes associated with the rainfall extremes at different timescales.

To this end, this study has developed five physically meaningful metrics to measure the RCM's behaviour. These metrics comprise the diurnal cycle, seasonality, relationship between intensity and temperature, temporal scaling, and the spatial structure of rainfall extremes, and collectively they provide a robust platform to evaluate the model's performance in

capturing the physical mechanisms behind the rainfall extremes. The WRF model with a 10 km grid spacing was used to demonstrate the utility of the proposed metrics. Three WRF variants with different parametrization schemes were run over the Greater Sydney region from 1990 to 2009, with simulations validated using data from 69 rain gauges.

The results of the analysis are summarised in Table 3. In general, the WRF models showed reasonable matches with the observations in terms of the overall physical processes, although they cannot entirely capture the relevant mechanisms. In particular, some biases were observed in the amplitudes of the diurnal and seasonal cycles compared to observations. The physical dependence between rainfall intensity and temperature was well reproduced by the WRF models, although the short-duration rainfall intensity was significantly underestimated.

Table 3 Summary of the measure metric results

Metrics	Regional climate models (R1, R2, R3)	
	Overall performance	Relative performance
Diurnal cycle	Successfully captures the diurnal cycle, but with delays in the peaks.	Models perform similarly
Seasonal cycle	Perform reasonably well for 1-hour extremes, but show amplitude biases for longer-durations.	R2 produces worst seasonal cycle for longer duration extremes
Temperature scaling rate	Exhibit good agreement with observations, although underestimate the rainfall intensity especially for short durations.	R1 and R3 perform better than R2 in rainfall intensity, but R2 is better in reproducing the mean temperature scaling rate
Temporal scaling	Shows reasonable consistency with observations, but with lower rainfall depths for short-durations.	R2 is better
Spatial structure	Can represent the overall spatial structure especially for the long-duration rainfall extremes and temperature scaling rates.	R2 is better

It is difficult to provide definitive guidance on the absolute model performance required (both in terms of the extreme rainfall statistics themselves and the other metrics discussed here) prior to recommending the use of model outputs for the development of future climate projections. In the case of the WRF results presented here, we suggest that the overall performance against all the metrics was sufficient to recommend the model for use in developing extreme rainfall projections in a future climate, although bias correction may be necessary given the differences in annual maximum rainfall discussed in the context of Figure 2. The lack of a clearly superior WRF parameterisation as shown in Table 3 suggest that it would be prudent to use all three models as part of an ensemble, rather than choose a single 'best' model.

The results presented above were specific to the case study region and the three WRF model parameterisations that were analysed. However, the general approach is suitable for adoption in similar studies of extreme rainfall. By providing a more comprehensive assessment of the performance of RCMs in simulating rainfall extremes, it becomes more likely that possible flaws in modelling will be exposed and used as part of a continual cycle of model improvement. This approach will not only improve the confidence that can be placed in model simulations, but will also build knowledge for improving the model representation, which will ultimately lead to higher quality projections of extreme rainfall.

References

Ahern M, Kovats RS, Wilkinson P, Few R ,Matthies F (2005) Global health impacts of floods: epidemiologic evidence. Epidemiological Reviews 27: 36-46.

Beniston M, Stephenson DB, Christensen OB, Ferro CAT, Frei C, Goyette S, Halsnaes K, Holt T, Jylha K, Koffi B, Palutikof JP, Scholl R, Semmler T ,Woth K (2007) Future extreme events in European climate: an exploration of regional climate model projections. Climatic Change 81: 71-95. doi: 10.1007/s10584-006-9226-z.

Berg P, Moseley C ,Haerter JO (2013) Strong increase in convective precipitation in response to higher temperatures. Nature Geoscience. doi: 10.1038/NGEO1731.

Buonomo E, Jones R, Huntingford C ,Hannaford J (2007) On the robustness of changes in extreme precipitation over Europe from two high resolution climate change simulations. Quarterly Journal of the Royal Meteorological Society 133(622): 65-81. doi: 10.1002/qj.13.

Dai A ,Trenberth KE (2004) The diurnal cycle and its depiction in the community climate system model. Journal of Climate 17: 930-951.

Delworth TL ,Zeng F (2014) Regional rainfall decline in Australia attributed to anthropogenic greenhouse gases and ozone levels. Nature Geosci 7(8): 583-587. doi: 10.1038/ngeo2201.

Evans JP, McCabe MF (2010) Regional climate simulation over Australia's Murray-Darling basin: A multitemporal assessment. Journal of Geophysical Research 115.

Evans J, Ekström M ,Ji F (2012) Evaluating the performance of a WRF physics ensemble over South-East Australia. Clim Dyn 39(6): 1241-1258. doi: 10.1007/s00382-011-1244-5.

Evans J, Westra S (2012) Investigating the Mechanisms of Diurnal Rainfall Variability using a Regional Climate Model. Journal of Climate 25(20): 7232-7247.

Evans JP, Ji F, Abramowitz G, Ekström M (2013) Optimally choosing small ensemble members to produce robust climate simulations. Environ Res Lett 8:044050. doi: 10.1088/1748-9326/8/4/044050.

Evans JP, Ji F, Lee C, et al (2014) Design of a regional climate modelling projection ensemble experiment – NARCliM. Geosci Model Dev 7:621–629. doi: 10.5194/gmd-7-621-2014.

Gilmore, J.B., J.P. Evans, S.C. Sherwood, M. Ekstrom and F. Ji (2015) Extreme Precipitation in WRF for the Newcastle East Coast Low of 2007. Submitted Theoretical and Applied Climatology.

Hallegatte S, Green C, Nicholls RJ ,Corfee-Morlot J (2013) Future flood losses in major coastal cities. Nature Climate Change 3(9): 802-806. doi: 10.1038/nclimate1979.

Hong SY, Noh Y, Dudhia J (2006) A new vertical diffusion package with an explicit treatment of entrainment processes. Mon Weather Rev 134:2318–2341.

Hardwick-Jones R, Westra S, Sharma A (2010) Observed relationships between extreme sub-daily precipitation, surface temperature and relative humidity. Geophysical Research Letters 37(L22805). doi: 10.1029/2010GL045081.

IPCC (2013) Intergovernmental Panel on Climate Change Special Report on Managing the Risks of Extreme Events and Disasters to Advance Climate Change Adaptation. In: Field CB, Barros V, Stocker TF, Qin D,

Dokken D, Ebi KL, Mastrandrea MD, Mach KJ, Plattner G-K, Allen SK, Tignor MMidgley PM (eds). Cambridge University Press, Cambridge, United Kingdom, and New York, NY, USA.

Janjic Z (1994) The step-mountain eta coordinate model: further developments of the convection, viscous sublayer, and turbulence closure schemes. Monthly Weather Review 122:927–945.

Ji F, Ekström M, Evans JP, Teng J (2014) Evaluating rainfall patterns using physics scheme ensembles from a regional atmospheric model. Theor Appl Climatol 115:297–304. doi: 10.1007/s00704-013-0904-2.

Kain JS (2004) The Kain - Fritsch convective parameterization: An update. Journal of Applied Meteorology 43:170–181.

Kalnay E, Kanamitsu M, Ristler R, Collins W, Deaven D, Gandin L, Iredell M, Saha S, White G, Woollen J, Zhu Y, Chelliah M, Ebisuzaki W, Higgins W, Janowiak J, Mo KC, Ropelewski C, Wang J, Leetmaa A, Reynolds

R, Jenne R ,Joseph D (1996) The NCEP/NCAR 40-year Reanalysis Project. Bulletin of the American Meteorological Society 77(3).

Kendon EJ, Roberts NM, Fowler HJ, Roberts MJ, Chan SC ,Senior CA (2014) Heavier summer downpours with climate change revealed by weather forecast resolution model. Nature Clim Change 4(7): 570-576. doi: 10.1038/nclimate2258.

Kirchner JW (2006) Getting the right answers for the right reasons: Linking measurements, analyses, and models to advance the science of hydrology. Water Resources Research 42(W03S04). doi: 10.1029/2005WR004362.

Langhans W, Schmidli J, Fuhrer O, Bieri S ,Schar C (2013) Long-term simulations of thermally driven flows and orographic convection at convection-parameterizing and cloud-resolving resolutions. Journal of Applied Meteorology and Climatology 52: 1490-1510.

Lenderink G, van Meijgaard E (2008) Increase in hourly precipitation extremes beyond expectations from temperature changes. Nature Geoscience 1: 511-514.

Lovejoy S, Mandelbrot B (1985) Fractal properties of rain, and a fractal model. Tellus A 37(3): 209-232.

Mandapaka P ,Qin X (2014) A large sample investigation of temporal scale-invariance in rainfall over the tropical urban island of Singapore. Theor Appl Climatol: 1-13. doi: 10.1007/s00704-014-1317-6.

Maraun D, Osborn T ,Rust H (2011) The influence of synoptic airflow on UK daily precipitation extremes. Part I: Observed spatio-temporal relationships. Clim Dyn 36(1-2): 261-275. doi: 10.1007/s00382-009-0710-9.

Maraun D (2013) Bias Correction, Quantile Mapping, and Downscaling: Revisiting the Inflation Issue. Journal of Climate 26(6): 2137-2143. doi: 10.1175/JCLI-D-12-00821.1.

Mascaro G, Vivoni ER, Gochis DJ, Watts CJ, Rodriguez JC (2014) Temporal Downscaling and Statistical Analysis of Rainfall across a Topographic Transect in Northwest Mexico. Journal of Applied Meteorology and Climatology 53(4): 910-927. doi: 10.1175/JAMC-D-13-0330.1

Nesbitt SW, Zipser EJ (2003) The diurnal cycle of rainfall and convective intensity according to three years of TRMM measurements. Journal of Climate 16: 1456-1475.

Paschalis A, Molnar P, Fatichi S ,Burlando P (2013) A stochastic model for high-resolution space-time precipitation simulation. Water Resources Research 49(12): 8400-8417. doi: 10.1002/2013WR014437.

Schlather M ,Tawn JA (2003) A dependence measure for multivariate and spatial extreme values: Properties and inference. Biometrika 90(1): 139-156. doi: 10.1093/biomet/90.1.139.

Schindler A, Maraun D ,Luterbacher J (2012) Validation of the present day annual cycle in heavy precipitation over the British Islands simulated by 14 RCMs. Journal of Geophysical Research: Atmospheres 117(D18): D18107. doi: 10.1029/2012JD017828.

Skamarock WC, Klemp JB, Dudhia J, Gill DO, Barker DM, Duda MG, Huang X-Y, Wang W ,Powers JG (2008) A description of the Advanced Research WRF Version 3. NCAR.

Trenberth KE, Dai A, Rasmussen RM, Parsons DB (2003) The changing character of precipitation. Bulletin of the American Meteorological Society 84: 1205-1217.

Tripathi OP, Dominguez F (2013) Effects of spatial resolution in the simulation of daily and subdaily precipitation in the southwestern US. Journal of Geophysical Research - Atmospheres 118(14): 7591-7605.

van Pelt SC, Beersma JJ, Buishand TA, van den Hurk BJJM ,Kabat P (2012) Future changes in extreme precipitation in the Rhine basin based on global and regional climate model simulations. Hydrol Earth Syst Sci 16(12): 4517-4530. doi: 10.5194/hess-16-4517-2012.

Veneziano D ,Lepore C (2012) The scaling of temporal rainfall. Water Resour Res 48(8): W08516. doi: 10.1029/2012wr012105.

Wang J ,Kotamarthi VR (2014) Downscaling with a nested regional climate model in near-surface fields over the contiguous United States. Journal of Geophysical Research: Atmospheres 119(14): 2014JD021696. doi: 10.1002/2014JD021696.

Westra S, Alexander LV ,Zwiers FW (2013) Global increasing trends in annual maximum daily precipitation Journal of Climate 26: 3904-3918. doi: 10.1175/JCLI-D-12-00502.1.

Westra S, Fowler HJ, Evans JP, Alexander LV, Berg P, Johnson F, Kendon EJ, Lenderink G, Roberts NM (2014) Future changes to the intensity and frequency of short-duration extreme rainfall. Reviews of Geophysics 52(3): 2014RG000464. doi: 10.1002/2014RG000464.

Zheng F, Westra S, Leonard M (2015) Opposing local precipitation extremes. Nature Clim Change 5(5): 389-390. doi: 10.1038/nclimate2579.